Design, development, and *in-vitro* evaluation of an intelligent photo-controlled transdermal therapeutic system

Inauguraldissertation

zur

Erlangung der Würde eines Doktors der Philosophie

vorgelegt der

Philosophisch-Naturwissenschaftlichen Fakultät

der Universität Basel

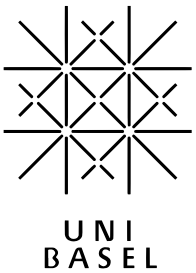

von

Jean-Baptiste Sauvet

aus Frankreich

Basel, 2016

Genehmigt von der Philosophisch-Naturwissenschaftlichen Fakultät

auf Antrag von

Prof. Dr. Wolfgang Meier

Prof. Dr. Michel Baudry

Basel, den 25. März 2014

Prof. Dr. Jörg Schibler
Dekan

Alvarium

Contents

Glossary

Ac_2O Acetic anhydride. 26, 27, 29, 72, 74, 82

AchEI anticholinesterase inhibitors. 4

ACN Acetonitrile. 74, 93

AcOH Acetic acid. 52, 72

AD Alzheimer's disease. 3, 4, 6

ADME absorption, distribution, metabolism and excretion. 4, 7, 10, 11

AS ammonia solution. 41, 47, 55, 68

aS adhesive support. 2, 106, 108, 109

ATTS ALTHERAS transdermal therapeutic system. 2, 11–13, 25, 66, 87, 105–109, 112, 113, 115, 119, 120, 132

BOP (Benzotriazol-1-yloxy) tris (dimethylamino) phosphonium hexafluorophosphate. 66

D_2O Deuterium oxide. 52

DBF Dibenzofulvene. 68–70, 74, 75, 81, 119

DBU 1,8-Diazabicyclo[5.4.0] undec -7-ene. 68, 69, 74–76

DCl Deuterium chloride. 39, 52

DDA degree of deacetylation. 39–41, 46, 52, 70

DIC *N,N'*-Diisopropylcarbodiimide. 73, 74, 82

DIPEA *N,N*-Diisopropylethylamine. 66–68, 71, 72, 74, 75, 81, 82

dM diffusion media. 12, 13, 72, 90, 92, 93, 95, 99, 100, 106–108, 112, 113, 134, 135

DMAP 4-Dimethylaminopyridine. 68, 73, 74, 82

DMF *N,N*-Dimethylformamide. 26–28, 67, 69, 72

DMSO Dimethyl sulfoxide. 23

DMSO-*d6* Deuterated dimethyl sulfoxide. 27, 29, 31, 124

DP degree of polymerization. 39, 40, 46, 70

EDTA Ethylenediaminetetraacetic acid. 93, 95

eS electronic support. 2, 106, 108, 114, 119

EtOAc Ethyl acetate. 27, 28, 30, 31

EtOH Ethanol. 41–43, 45–47, 54, 55

FDA Food and Drug Administration. 4, 6, 13, 38

FD-C Franz diffusion cell. 88–90, 93, 95, 119

FEM finite element method. 14, 48–51, 55, 57, 118

FID free induction decay. 39

Fmoc Fluorenylmethyloxycarbonyl. 25, 67, 69, 81, 119

GC Gas Chromatography. 27, 74, 93

GlcNAc *N*-acetylglucosamine. 38, 52

GlcNH glucosamine. 38, 39, 52, 132

Gly-Fmoc *N*-(9-Fluorenylmethoxy-carbonyl)glycine. 69, 74–76

HATU 1-[Bis(dimethylamino) methylene] -1H-1,2,3-triazolo [4,5-b] pyridinium-3-oxid hexafluorophosphate. 66

HBTU *N,N,N',N'*-Tetramethyl -*O* -(1H-benzotriazol-1-yl) uronium hexafluorophosphate. 66–68, 71, 74, 75, 81

HCl Hydrochloric acid. 27, 30, 31

HIV/AIDS Human Immunodeficiency Virus infection and Acquired Immune Deficiency Syndrome. 3, 93

HMPA Hexamethylphosphoramide. 66

HNO_3 Nitric acid. 26, 27, 29

HOBt 1-Hydroxybenzotriazole. 66–68, 71, 73–75, 81, 82

HPLC High Performance Liquid Chromatography. 27, 69, 73–75, 81, 88, 90, 93, 98

Ibu Ibuprofen. 82, 93

IR Infrared. 39

K_2CO_3 Potassium carbonate. 26–28

LA lactic acid solution. 40–42, 53, 55, 70, 132

LC-MS Liquid Chromatography — Mass Spectrometry. 27

LED Light Emitting Diode. 11, 108, 114

LPP lipid-protein-partitioning. 9

MeOH Methanol. 26, 27, 29, 30

mS medication support. 2, 13, 88, 106, 108, 109, 132

Na_2SO_4 Sodium sulfate. 27, 28, 30, 31

$NaBH_4$ Sodium borohydride. 26, 27, 30

NaCl Sodium chloride. 27, 28

NaH_2PO_4 Sodium phosphate monobasic. 93, 94

$NaH_2PO_4 \cdot 2H_2O$ Sodium phosphate dibasic dihydrate. 93, 94

NaOH Sodium hydroxide. 26, 27, 30, 31, 95

NH_3 Ammonia. 52

NLC nano-structured lipid carriers. 10

NMDA *N*-methyl-D-aspartate. 4

NMM *N*-Methylmorpholine. 66

NMP *N*-Methyl-2-pyrrolidone. 67–76, 81, 82

NMR Nuclear Magnetic Resonance. 23, 28, 29, 31, 39, 52, 124

NP nanoparticles. 10

OECD Organisation for Economic Co-operation and Development. 88

PDE partial differential equations. 99

PLGA poly (lactic-co-glycolic acid). 10, 120, 136, 137

PM peltier modules. 45, 51, 54, 120

PMSF Phenylmethanesulfonyl fluoride. 93, 95

***p*-NPCF** *p*-Nitrophenylchloroformate. 138

POMAP porous matrix producer. 14, 37, 42, 45, 48, 50, 51, 53, 54, 57, 71, 73, 118, 120, 132, 133

PVP polyvinylpyrrolidone. 13

R_c cooling rate. 42, 45, 49, 54, 57

RS receiving solution. 88, 90, 91, 93, 95, 99–101

SB-M Saarbrücken penetration model. 88

SC *stratum corneum*. 8–10, 95

SEM Scanning Electron Microscope. 43–48, 52, 55

SLN solid lipid nanoparticles. 10

TBTU *N,N,N',N'*-Tetramethyl -*O* -(benzotriazol-1-yl) uronium tetrafluoroborate. 66

TEA Triethylamine. 66

TFA Trifluoroacetic acid. 73

THF Tetrahydrofuran. 26, 27, 30

TIPS thermally induced phase separation. 39–42, 44–46, 48, 50, 51, 55, 68, 73, 118, 120

TMS Tetramethylsilane. 27, 28

TP transdermal patch. 6, 7, 12

TSP-*d4* Deuterated trimethylsilyl propanoic acid. 52

TTS transdermal therapeutic system. 2, 5, 6, 10, 11, 13, 38, 72, 88, 106–109, 112, 119

UV Ultraviolet. 13, 14, 23, 39, 66, 73, 74, 87–91, 93, 95, 99, 138

WHO World Health Organization. 3

Chapter 1

– Introduction –

Abstract: The aim of ALTHERAS (ALzheimer THERApeutic System) is the development of a drug delivery system to enable improvement in the individual medication of people suffering from Alzheimer's disease. Transdermal systems are particularly attractive as they represent a non-invasive and self regulated treatment. The goal is to create a system in which the drug is immobilized and released by a light induced cleavage. As a consequence, the project involves a multi-disciplinary approach, using suitable chemistry combined with pharmaceutical engineering, physics and nanotechnologies. The main objectives are the manufacturing of a pre-prototype through the identification of basic specifications and the obtaining of the proof of concept.

1.1 ALTHERAS: Presentation of the topic

This project aims in the creation of a transdermal therapeutic system (TTS) making possible on the same time automation and polymedication. Herein, the creation of the ALTHERAS transdermal therapeutic system (ATTS) is suggested.

The core of the project is the reversible immobilisation of a medication (drug, excipient, etc.) on a substrate and its release using a physical stimulus. The programmed control of the stimulus emission guarantees an automatic control of the administration, thus reducing the risk of patients forgetting. On the other hand, it complements favourably the use of drug combinations. In this project a new therapeutic system using the transdermal pathway is designed to independently control in time and in dose the release of drugs.

The ATTS involves the development of adapted materials, an electronic control unit implemented in the system, a source of stimulus to induce the release and a wireless data transfer module for individual programming by the doctor, clinician or by the patient. In practice, the ATTS is divided into three parts which are presented in figure 1.1.

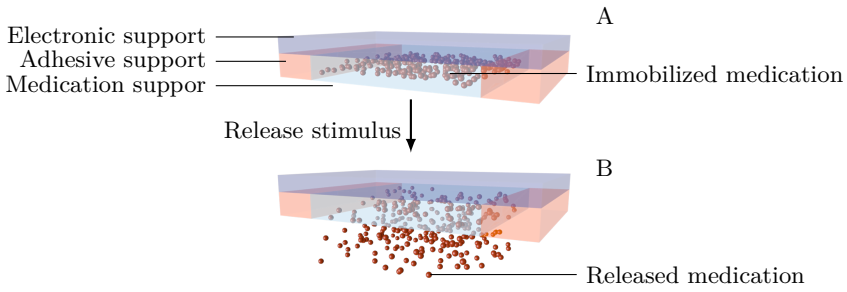

Figure 1.1: Principle of the ATTS
A: System OFF ; B: System ON

The electronic support (eS): which comports an energy supply unit, a programmable memory and a stimulus emitter ;

The medication support (mS): on which the medication is immobilized ;

The adhesive support (aS): which keeps the full system in contact with the skin.

1.2 Context

The use of smart apparatus able to manage and anticipate therapeutic needs of a patient is impressively growing [1]. On the same time, due to a better understanding of multi-factorial diseases, the discovery of drug cocktails is opening the way to individualized therapeutic treatments as specific drug interactions may be tuned depending on the patient.

By identifying drug combinations and associated synergistic effects, the pharmaceutical industry is looking to develop more efficient therapies to reduce doses and side effects. Moreover, the controlled release of such therapeutic molecules would implement the success of the therapy.

1.2.1 Chronic diseases

1.2.1.1 General remarks

Chronic diseases are characterised by a long therm and evolutive sickness, almost always associated with complications and invalidity. They represent the major cause of death and disability worldwide as they are considered to be responsible for almost 60% of all deaths and 43% of the world diseases. Furthermore, their impact in a long term of 10 years will rise the number of death to 73%. These pathologies include different categories:

Long-term mental disorders including depressive disorder, schizophrenia, Alzheimer's or Parkinson's disease, chronic pain ;

Rare diseases such as mucoviscidosis, drepanocytosis or myopathy ;

Persistent communicable diseases with HIV/AIDS or hepatitis ;

Others: chronic kidney disease, chronic bronchitis, asthma, cardiovascular diseases, cancers, diabetes, and multiple sclerosis.

The compliance refers to the following of treatment recommendations. Bad compliance accentuates the symptoms and can lead to grave consequences including over-dosage, sub-dosage, bad combinations or incorrect administration time. This phenomenon is particularly common in case of elder people as they tend to live isolated, take multiple medicines and have decreased dexterity.

A World Health Organization (WHO) study estimates that in developed countries only 50% of people suffering from chronic diseases follow treatment recommendations. The main identified obstacles include the complexity of modern medications, a non-understanding of the treatment, the side effects and the cost of medicines.

1.2.1.2 Case of Alzheimer's disease

Alzheimer's disease (AD) is a multifactorial degenerative disease which leads to a decline of cognitive capacities and memory [2]. The diagnosis remains difficult but symptoms are generally observed before the age of 60 years old. On the same time, the incidence increases significantly with age and represents the most frequent form of dementia in old people with almost 65% of cases.

Dementia generally includes a decrease of mental faculties, however AD is different as it evolves gradually and, in the first stage, seems to affect mainly the short term memory. It is a very complex and multi-factorial disease that involves a large amount of biological mechanisms and physiological functions in the brain. This could explain why it is so difficult to identify efficient medications despite of years of academic and pharmaceutical research.

The pharmaceutical market is currently dominated by 4 molecules (Figure 1.2) even if others are in pipelines. Among these drugs, three (Figures 1.2a, 1.2b and 1.2c) are anticholinesterase inhibitors (AchEI), meaning that they inhibits the activity of enzymes involved in acetylcholine degradation. The 4th molecule (Figure 1.2d) is a *N*-methyl-D-aspartate (NMDA) receptor antagonist as it inhibits the action of the NMDA receptor.

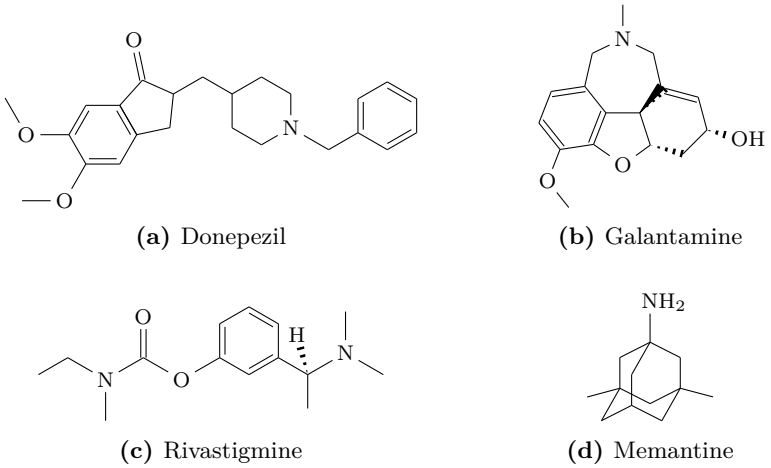

(a) Donepezil **(b)** Galantamine

(c) Rivastigmine **(d)** Memantine

Figure 1.2: Common molecules used for AD treatment

A recent and innovative strategy to treat AD consists in the development of drug combinations, acting simultaneously on different targeted sites or having synergistic effects. The goal is to increase clinical efficiency while reducing side effects. However, the major drawback when applying multiple drugs resides in the different pharmacokinetics of the drugs. As a consequence, the main challenge is to bring the proper amount of drug at the right place and right moment.

1.2.2 Drug delivery

1.2.2.1 General remarks

The drug delivery refers to the administering of a pharmaceutical compound to a patient. The pharmacokinetic properties such as absorption, distribution, metabolism and excretion (ADME) of active compounds are necessarily influenced by the route of administration.

The Food and Drug Administration (FDA) currently distinguishes more than 100 distinct ways to administer a drug. They can be divided into 4 main forms:

Topical delivery: epicutaneous, inhalation, enema, eyes drops, ears drops, intranasal, etc. ;

Enteral delivery: mouth or orally, gastric feeding, duodenal feeding tube, rectally, suppository, enema, etc. ;

Parenteral delivery: injection, infusion, intravenous, intraarterial, intramuscular, intracardiac, subcutaneous, intraosseous infusion, intradermal, intraperitoneal, transdermal, transmucosal, inhalational, etc. ;

Others: intraperitoneal, e.g. peritoneal dialysis, epidural, intrathecal.

Each of these formulations presents advantages and disadvantages, depending on the drug characteristics (molecular size, charge, etc.), on the patient (compliance, etc.) and on the type of disease. Common delivery systems suffer from restrictions such as burst release so the maintenance of blood therapeutic doses is challenging. Furthermore several medications such as peptides, proteins, antibodies, and gene based drugs cannot be delivered without a special attention from enzymatic or metabolic degradation.

Among drug delivery formulations, TTS are used for the administration of drug by its diffusion through the skin. They represent an appealing and non-invasive tool known to minimize the limitations allied with oral or parenteral administration as the medication reaches directly the blood stream. For these reasons, the transdermal pathway has become a well accepted drug delivery method.

1.2.2.2 Transdermal therapeutic systems

The historical use of plasters as medical devices can be tracked back up to the Egyptians which have developed formulations for cosmetic and therapeutic applications[3,4]. In recent years the knowledge of molecular and physical mechanisms involved in dermal release have been deeper understood, leading to the establishment of new TTS.

Modern TTS are used to deliver a specific dose of drug through the skin with a controlled kinetic. They implement traditional treatments, limited by poor oral bioavailability and severe side effects, and represents the most successful non-oral systemic drug delivery system[5].

The worldwide field of transdermal therapies is a fast growing market, estimated to two billion US dollars. By using TTS, the delivery of drugs having short half-lives presents better plasma profile and avoids the first-pass metabolism effect for drugs with poor oral bioavailability. In addition, they are a convenient delivery method with the potential of dose tuning by the patient[6].

TTS provide an adequate drug release from the formulation and at the same time allow good amount of drug to overcome the skin barrier, preventing unspecific cutaneous rush and drug inactivation[7]. They are formulated in different forms which present negative aspects such as skin irritation, manufacturing costs and aesthetic appearance[8,9,10]. Despite these features, they present the advantage to be non-invasive, easy to use and to successfully reduce side effects associated with oral administration[11].

Moreover, they can be used in situations requiring minimal patient cooperation[9]. Finally, in case of an accidental overdose, an effective disruption of administration is possible[12] by simply removing the support from the skin.

1.2.2.3 Transdermal patches

Among the TTS, the transdermal patch (TP) is an interesting alternative as it combines the advantages of classical TTS with an easy to use support. The first commercial TP, Transderm Scop® (scopolamine), was approved by the FDA in the 70's for sea sickness[1] and signed the beginning of acceptance of this method for modern commercial drug products[13].

From now, many TP are approved such as Trandate® (methylphenidate) for the treatment of attention deficit and hyperactivity disorder, Neupro® (rotigotine) for Parkinson's disease, Emsam® (selegiline) for depression and Durogesic® (fentanyl) for pain therapy[12]. In July 2007 the Exelon® patch (rivastigmine) was approved to treat moderate AD. This device constitutes an innovation in this therapy and in these days another TP using donepezil is under development[12,14].

The design of a TP can be divided into 4 traditional architectures which are reported in figure 1.3[14]. Some common features are present in each one, such as a backing layer and an adhesive that assures a good contact with the skin. Before applying a TP, a peelable layer is removed to expose the adhesive to the skin. This adhesive layer is placed on the skin applying a little pressure on the backing layer to make sure the patch is firmly in contact with the skin[15].

The simplest structure consists in a single layer "drug in adhesive" patch (Figure 1.3a). In this case, drug and potential excipient are directly dispersed into an adhesive matrix and the release depends only on the diffusion across the skin[14]. The multi layered version (Figure 1.3c) is based on the same principle. However, this one has two or more distinct adhesive layers separated by a membrane designed to modify the release rate.

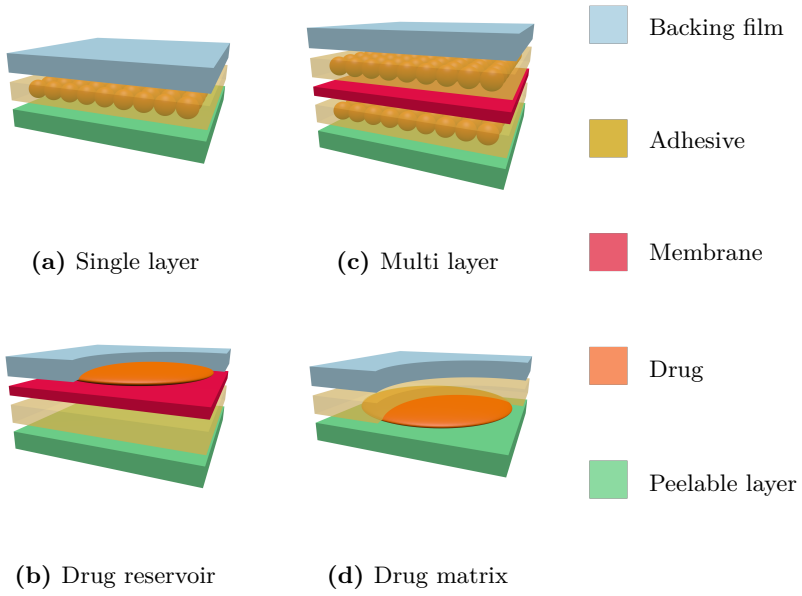

Figure 1.3: TP common structures

The "drug reservoir in adhesive" (Figure 1.3b) consists in the inclusion of a drug/excipient solution separated from the adhesive by a membrane. Finally, the last type of TP (Figure 1.3d) is an inclusion of a semi-solid drug/excipient matrix surrounded by the adhesive which forms a concentric configuration around this matrix.

1.2.2.4 Limitations of current drug delivery systems

1.2.2.4.a Polytherapies and drug combinations

Polytherapy consists in multiple medications treatments. Due to different ADME, drug-drug interactions and higher cost, the development of this kind of treatment is problematic. Other problems associated with polymedication include potential side effects induced by drug combinations and, in case of complicate polytherapies, a significant decrease of the compliance.

Even with an adapted posology, treatments requiring the taking of several drugs remain problematic. Three different cases can be distinguished:

No interaction between drugs: they act on different sites for different pathologies or not but with different mechanisms ;

Correlation of effects: one drug limits the side effects of the other one ;

Synergistic effects: the drugs combinations magnify the individual effects of the two molecules.

However, the precise control of multiple release from a single support is a new burgeoning field that presents challenges. This could explain current developments of drug delivery technologies.

1.2.2.4.b Personalized medicine

With the recent identification of drug combinations, a new parameter was introduced in the administration of drugs making the medication more complex. For pharmaceutical industries, even if it offers a potential market to personalized therapies, production problems limits its expansion. Indeed, customized handmade galenic prescriptions can sometime be produced by the pharmacist, but the common way to personalize a treatment remains the doctor prescription.

1.3 State of the art

1.3.1 The skin

The skin represents the largest and most easily accessible organ of the body with an average surface of approximately 2 m^2 [16]. It provides an efficient protection against environmental aggressions such as temperature changes, chemicals or pathogens. These features render the skin a strong barrier which hampers transdermal drug delivery [5,17]. This biological membrane consists of a multilayer of biological tissues having a complex organization with a wider variety of cell types than the brain.

The three main layers are the epidermis, the dermis and the hypodermis (Figure 1.4)[17]. The epidermis is composed out of 7 different layers. The most superficial, the *stratum corneum* (SC), or non viable epidermis, is responsible of drug absorption limitations.

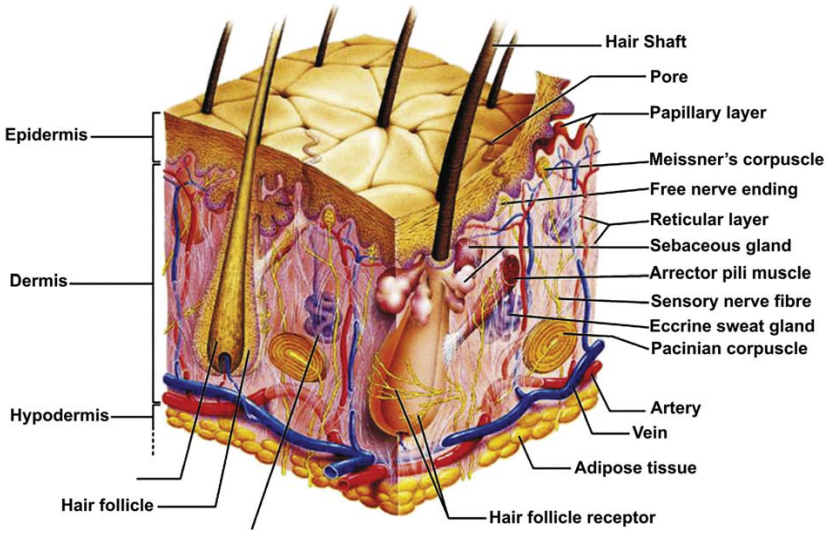

Figure 1.4: Anatomy of the skin

1.3.2 Drug adsorption through skin

SC possesses an average thickness from 10 to 20 µm. It consists of approximately 15 to 25 layers of cornified cells, the corneocytes, anchored in a mortar of highly organized intercellular lipids (Figure 1.5)[18]. Once applied on the skin, a drug either penetrates via transcellular route, alternately through the corneocytes and the lipid layers, or using intercellular routes along the tortuous pathways made by the lipid layers. A third minor way is also present, the appendageal route, in which the passage happens via sweat glands or follicular ducts[18].

Even if the intercellular route is considered as the most important transdermal absorption pathway for small substances[5], the corneocyte arrangement on the lipid matrix provides a highly tortuous diffusion pathway rendering the SC 1000 times less permeable to water compared to other biological membranes. This makes the total length of the entire pathway impressively long, around 500 µm, which is higher than the average of the SC thickness.

As a consequence, the transdermal absorption requires drugs having proper characteristics which allow it to cross the SC or an appropriate carrier able to deliver the drug[13,19]. Ideally, the molecular weight must be appropriate to facilitate the drug diffusion through the lipid bilayer but the permeation through the skin also depends on the ionization degree of the active molecule at physiological pH[19,20].

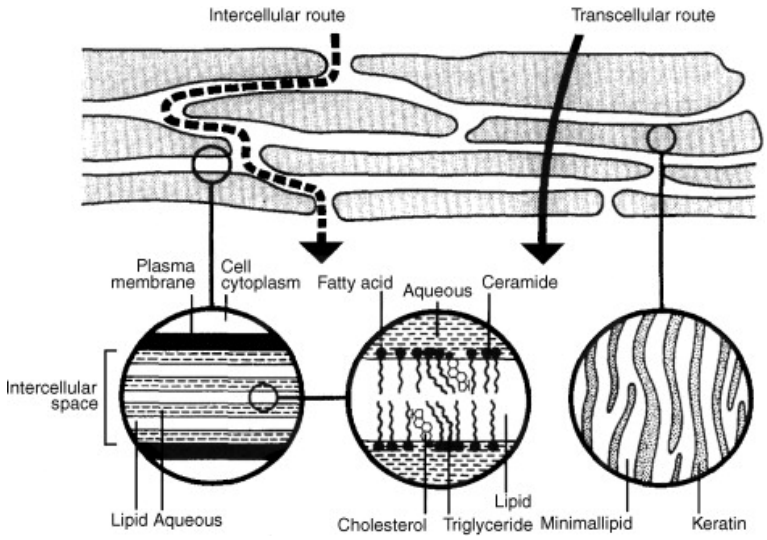

Figure 1.5: "Brick and Mortar" model of the skin organization

The SC is a selective barrier [17] having an important diffusional resistance due to complex interactions between lipid and protein components. As a matter of fact, the transdermal delivery of a large amount of drug remains problematic. Thus, approximately 10 mg of active can be daily delivered if the permeation is not enhanced [5]. In the last decade, researchers have been focused on developing new methods to enhance drug permeation across the skin. These methods can be separated in chemical, otherwise called passive, and physical, or active methods [9,17]. Furthermore, interesting combinations coupling physical/physical, chemical/physical methods exist and are well documented [21], as well as chemical/chemical methods [16].

1.3.2.1 Chemical or passive methods

Chemical permeation enhancers are substances able to promote the drug absorption through the skin by temporarily altering its permeability. Ideally, involved chemicals are non-toxic, non irritating and compatible with the drug [22]. According to the lipid-protein-partitioning (LPP) theory [7,23], which describes interactions between penetration enhancers and the SC, the three main mechanisms of enhancement are:

- Interactions with the intercellular lipids ;
- Interactions with the intracellular keratin ;
- Penetration of high amounts of enhancers resulting in an improved dissolving capacity of the barrier for drug.

Widely used classical enhancers [24] include molecules such as alcohols [25], acids amines and amides [4,26], esters, surfactants, terpenes, terpenoids and essential oils [11,27], sulfoxides [22,28], lipids and miscellaneous such as cyclodextrins [23,29], enzymes [22], drug mixtures [30] or simply water [31].

1.3.2.2 Physical or active methods

In addition to passive enhancement, the rates of transdermal transport can be increased using physical enhancement methods. These type of systems are able to increase the drug flux by either altering the skin barrier or providing driving force to the drug [1,17]. Recent advances in engineering and computing led to the production of small and powerful active TTS.

Examples include sonophoresis, using ultrasounds to induce SC lipid disruption [5,10,32] ; electroporation, creating temporary pores by short exposure to high voltage current [33,34] ; local thermal treatment, dilating skin pores [35] ; skin disruption by micro-needles or blades [18,36,37] ; high velocity particles propulsion [18] ; laser pressure wave [38] and iontophoresis, forcing drugs to diffuse by repulsion from an electrode [18,39].

1.3.2.3 Nanotechnology case

Over the past few decades, drug delivery systems have been improved by nanotechnologies with the use of drug nanocarriers [40,41,42] for diagnostics [43] or vaccines [44]. They are designed to prevent drug degradation [45] and uncontrolled interactions with unspecific targets. However, due to their features many risks remain unknown.

For this reason biocompatibility and biodegradability of the constituting materials are important requirements that have to be considered. Thus, only a limited number of biodegradable polymeric nanoparticles (NP) [46], solid lipid nanoparticles (SLN) [47,48], and nano-structured lipid carriers (NLC) have been studied in drug delivery systems. One of the most common polymer used nowadays for drug delivery is the poly (lactic-co-glycolic acid) (PLGA), which is biocompatible and biodegradable [10,49,50,51,52].

1.4 ALTHERAS: A technological breakthrough

1.4.1 Identification of main specifications

In order to face the disadvantages of multi therapies, two needs are identified:

Tool for polytherapy: Automatic management of multi drug release ;

Tool for chronotherapy: Automatic control of the time of administration.

Since ADME plays a major role in a therapy, the time control of drug release makes it possible to adapt a treatment to the patient needs. A tool allowing the delivery of a medicine at the right moment, even during sleeping time, would be a significant improvement. As a consequence, the drug delivery system designed can be programmed to release a molecule at specific times.

Ideally, the delivery device would be applied to the patient after its programming by the doctor. Moreover, the tool proposed is a real opportunity to allow the delivery of complex treatments and interactions do not have to be taken into account by the patient.

1.4.2 Proposals

The transdermal delivery remains one of the most convenient way to administer a drug for chronic disease. Simplicity of use, economical impact and personal tuning are the most evident achievement of this administration method. The main advantage of the ATTS is the possibility to tune the drug release. Therefore, the principal idea is the immobilization of pharmaceutical compounds on a support and the use of an external stimulus to release the molecules according to ADME. Once the drug is released, its absorption happens as for a normal TTS by simple diffusion of the molecule through the skin.

In reply to specifications, detailed technical proposals based on scientific literature, books, patents, etc. were studied. These proposals concern the chemistry and physics involved in the production, but also pharmaceutical engineering in close relation with electronics and programming.

1.4.2.1 Release stimulus

Different physical stimuli are able to trigger the release such as temperature changes, electric potential or electromagnetic signals. However, each method presents important disadvantages that can limit their potential uses:

Temperature change can induce the modification of a support, causing the release of entrapped molecule. However this option is limited to significant temperature changes leading to a possible degradation of the drug and risks for the patient. Moreover, the thermodegradation of the support does not fit the requirements ;

Electric potential to force the molecule migration, is already used today in iontopheretic TTS. An important issue in this approach is that the drug molecules have to be charged, which limits the number of suitable drugs. Moreover, the energy consumption remains an important parameter ;

Electromagnetic impulse is an interesting way to trigger a drug delivery without any of the disadvantages previously described. Using this method, the release of an immobilized medication would be induced by energy conversion of the electromagnetic signal. An optical approach, using light wavelengths, offers a clear advantage regarding its acceptance by the skin and the already existing embedded systems comporting LED technology.

1.4.2.2 The medication support

1.4.2.2.a Geometric considerations

According to the Richardson effect [53] applied to 3D structures, the surface to volume ratio of an object is inversely proportional to its size. For this reason, in order to reach high drug loading in a reduced volume, the covalent immobilization of the drug on small entities which are then embedded into a polymer matrix was considered. This method allows a high loading performance while reducing the complexity of the process by separating the drug immobilization from the embedding process.

Different possibilities emerge from this statement such as the immobilization on foil, micro-fibers, micro-particles or on a porous structure (Figure 1.6).

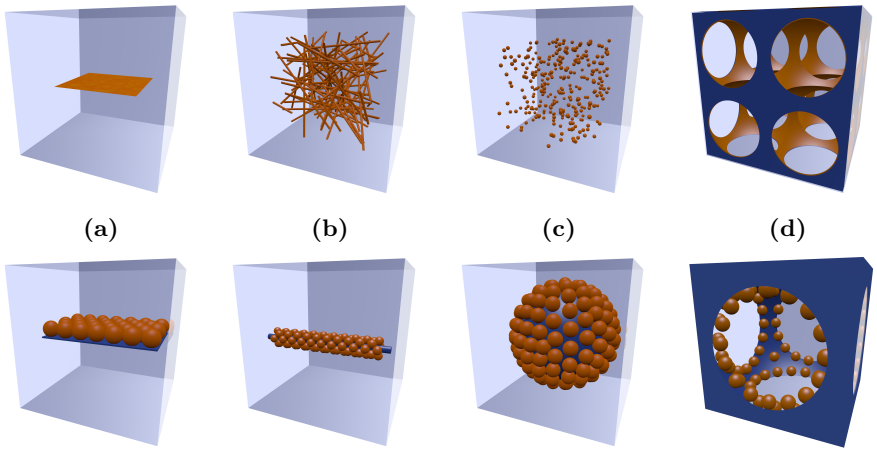

Figure 1.6: Possible designs for medication immobilization on support
General (up) and detailed (down) view.
(a) Foil support ; (b) Micro-fibre support ;
(c) Micro-particle support in polymer matrix ; (d) Porous structure matrix as support

As shown in design 1.6a, 1.6b and 1.6c, the use of a polymer matrix to fix the drug supports necessarily induces limitations for the diffusion of the active molecules. Indeed, in that case the polymer also serves as supporting structure for the TP, which means the use of a polymer having high viscosity η.

However, according to the Stokes-Einstein equation 1.1 the diffusion constant (D) for a molecule decreases with an increase of the media viscosity:

$$D = \frac{K_b\ T}{6\ \pi\ \eta\ r} \tag{1.1}$$

In a porous structure as in figure 1.6d, the scaffold plays the role of the supporting structure and immobilization support. In that case the drug diffusion is assured by a diffusion media (dM) which can be a liquid or a gel with low viscosity. This dM fills the porous structure and allows a fast diffusion. In this study, highly porous structures appeared as the best candidates for the design of the ATTS. In this manner, properties and porosity of the support are selectively tuned to control the release.

1.4.2.2.b Porous polymeric materials in TTS

The main challenge when producing a new TP lies in the design of a matrix. This is followed by the optimization of the drug loading, not only in terms of release properties, but also with respect to its physico-chemical properties, compatibility and stability with other components as well as with the skin [54].

General requirements of the polymer matrices are:

- Properties allowing fast diffusion of the drug ;
- Stability ;
- Easy manufacturing and fabrication ;
- Biocompatibility.

Common matrix materials include natural polymers such as cellulose derivatives [11,27,55], chitosan [56,57] or synthetic ones as povidone also commonly called polyvinylpyrrolidone (PVP) [6,11,58]. Hydrogel type porous systems in transdermal delivery [59,60] are advantageous as they overcome side effects such as skin irritation or problems associated with classical polymer matrix TTS by using a water based solution as dM. Different production methods and materials have been studied [61,62,63,64,65,66].

This study focused on the establishment of a chitosan porous matrix (ChipM) for controlled release. Chitosan scaffolds are particularly interesting as the final material is transparent, flexible [67] and allows an easy surface modification. Finally chitosan is approved by the FDA for drug delivery [68] and presents good characteristics regarding its biocompatibility [67] and antimicrobial activity [69].

1.5 Aim and outline of the thesis

Due to their ability to relieve the patient of treatment management by following pre-established care plans, the intelligent technologies are an interesting way to improve cares and compliance. On the same time, the introduction of mobile technology able to communicate recommendations and medication adjustments depending on the situation demands in real time is another possibility.

The aim of this work is the design of a medication support in which an active molecule is bound covalently to a support through a photocleavable linker. The active molecule is then released upon irradiation of the support by near UV light ($\lambda = 365$ nm). This type of delivery system is already described [70], but despite the complexity of the system, technical explanations suffer from a lack of data, rendering the production difficult. According to the claims of this patent, a process for the production of the ATTS was developed. The design comprehends:

A highly functionalized mS for drug immobilization, stable when surface modification is performed ;

A photolinker activated at $\lambda = 365$ nm and able to release proper amounts of medication without toxic residues ;

A suitable chemistry for mS surface modification, based on simple, high yield and established reactions ;

An in vitro study proving that the drug model is released trough human skin epidermis ;

A design proposal which renders easy the programming of the system and leading to almost infinite possibilities of drug cocktails.

The first part of the project consists in the identification of main specifications. This work takes into account different points of view such as the technologies for the production of the pre-prototype, the concordance with its use in the field of drug delivery and the economical point of view. The final step is the obtaining of the proof of concept, which means the establishment of technical feasibility for production and the proof of a significant drug release from a pre-prototype. The optimization process and are not part of this work.

In Chapter 2 the straightforward high yield synthesis and purification of a model photolinker is described and shows an interesting potential for scale up. Chapter 3 details the process for the production of highly homogeneous ChipM. The assembling of a dedicated apparatus for the production of the porous material, the porous matrix producer (POMAP), improved considerably the maintaining of the material characteristics. A thermodynamic study based on finite element method (FEM) is proposed to describe the production process. The structure of the obtained material is finally investigated.

In Chapter 4 the surface modification of the porous matrices, first with the photolinker and then with the drug model, is presented. A procedure is suggested to obtain homogeneous surface attachment to the porous structure. On the same time, a quantitative study of the coupling capacity is made and the results are compared to the theoretical loading capacity of the matrix. In Chapter 5 the release of the model drug from the photosensitive drug loaded matrix is investigated *in-vitro* using human skin epidermis. The full system is subjected to UV light and a quantitative study is made to determine the drug release and diffusion through the epidermis. Furthermore, a mathematical model is suggested to describe the complex "release and diffusion" of the drug.

Finally, the Chapter 6 concerns the possibilities of use of the system, including the design and the programming of the system.

A nomenclature is also proposed in Appendix C to identify the surface modification and all the parameters involved for the obtaining of each drug loaded matrices.

1.6 Bibliography

[1] Prausnitz, M. R., Mitragotri, S. & Langer, R. Current status and future potential of transdermal drug delivery. *Nat. Rev. Drug. Discov.* **3**, 115-124 (2004).

[2] Kukull, W. A., Higdon, R., Bowen, J. D. & *et al.* Dementia and alzheimer disease incidence: A prospective cohort study. *Arch. Neurol.* **59**, 1737-1746 (2002).

[3] Patel, H. J., Patel, J. S. & Patel, K. D. Transdermal patch for Ketotifen fumarate (KTF) as asthmatic drug. *Int. J. PharmTech Res.* **1**, 1297-1304 (2009).

[4] Finnin, B. C. & Morgan, T. M. Transdermal Penetration Enhancers: Applications, Limitations, and Potential. *J. Pharm. Sci.* **88**, 955-958 (1999).

[5] Naik, A., Kalia, Y. N. & Guy, R. H. Transdermal drug delivery: overcoming the skin's barrier function. *Pharm. Sci. Technol. Today* **3**, 318-326 (2000).

[6] Arora, P. & Mukherjee, B. Design, development, physicochemical, and in vitro and in vivo evaluation of transdermal patches containing diclofenac diethylammonium salt. *J. Pharm. Sci.* **91**, 2076-2089 (2002).

[7] Langer, R. Transdermal drug delivery: past progress, current status, and future prospects. *Adv. Drug Deliv. Rev.* **56**, 557-558 (2004).

[8] Cleary, G. W. Transdermal & transdermal-like delivery system opportunities: today & the future. *Drug Delivery Technology* **3**, 34, 36-40 (2003).

[9] Thomas, B. J. & Finnin, B. C. The transdermal revolution. *Drug Discovery Today* **9**, 697-703 (2004).

[10] Luengo Contreras, J. E. (2007) *Human skin drug delivery using biodegradable PLGA-nanoparticles. Ph.D. Thesis.* Universität des Saarlandes: DE.

[11] Agrawal, S. S. & Munjal, P. Permeation studies of atenolol and metoprolol tartrate from three different polymer matrices for transdermal delivery. *Indian J. Pharm. Sci.* **69**, 535-539 (2007).

[12] Wentrup, A., Oertel, W. H. & Dodel, R. Once-daily transdermal rivastigmine in the treatment of Alzheimer's disease. *Drug Des., Dev. Ther.* **2**, 245-254 (2008).

[13] Cevc, G. Lipid vesicles and other colloids as drug carriers on the skin. *Adv. Drug Deliv. Rev.* **56**, 675-711 (2004).

[14] Sozio, P., Cerasa, L. S., Marinelli, L. & Di Stefano, A. Transdermal donepezil on the treatment of Alzheimer's disease. *Neuropsychiatr. Dis. Treat.* **8**, 361-368 (2012).

[15] De Jalon, E. G., Blanco-Prieto, M. J., Ygartua, P. & Santoyo, S. Topical application of acyclovir-loaded microparticles: quantification of the drug in porcine skin layers. *J. Control. Release* **75**, 191-197 (2001).

[16] Hadgraft, J. Skin, the final frontier. *Int. J. Pharm.* **224**, 1-18 (2001).

[17] Alexander, A. *et al.* Approaches for breaking the barriers of drug permeation through transdermal drug delivery. *J. Control. Release* **164**, 26-40 (2012).

[18] Barry, B. W. Novel mechanisms and devices to enable successful transdermal drug delivery. *Eur. J. Pharm. Sci.* **14**, 101-114 (2001).

[19] Alvarez-Roman, R., Naik, A., Kalia, Y. N., Guy, R. H. & Fessi, H. Enhancement of Topical Delivery from Biodegradable Nanoparticles. *Pharm. Res.* **21**, 1818-1825 (2004).

[20] Hadgraft, J. Skin deep. *Eur. J. Pharm. Biopharm.* **58**, 291-299 (2004).

[21] Mitragotri, S. Synergistic effect of enhancers for transdermal drug delivery. *Pharm. Res.* **17**, 1354-1359 (2000).

[22] Sinha, V. R. & Kaur, M. P. Permeation enhancers for transdermal drug delivery. *Drug Dev. Ind. Pharm.* **26**, 1131-1140 (2000).

[23] Benson, H. A. E. Transdermal drug delivery: Penetration enhancement techniques. *Curr. Drug Delivery* **2**, 23-33 (2005).

[24] Williams, A. C. & Barry, B. W. Penetration enhancers. *Adv. Drug Deliv. Rev.* **56**, 603-618 (2004).

[25] Abdul Rasool, B. K., Abu-Gharbieh, E. F., Fahmy, S. A., Saad, H. S. & Khan, S. A. Development and evaluation of ibuprofen transdermal gel formulations. *Trop. J. Pharm. Res.* **9**, 355-363 (2010).

[26] Pathan, I. B. & Setty, C. M. Chemical penetration enhancers for transdermal drug delivery systems. *Trop. J. Pharm. Res.* **8**, 173-179 (2009).

[27] Krishnaiah, Y. S. & Al-Saidan, S. M. Transdermal permeation of trimetazidine from nerodilol-based HPMC gel drug reservoir system across rat epidermis. *Med. Princ. Pract.* **17**, 37-42 (2008).

[28] Kavitha, K., Rajendra, M. M., Mangalbhai, P. D., Sandeep, D. S. & Ganesh, N. S. Chemical permeation enhancers for transdermal drug delivery: a brief review. *Der Pharmacia Lettre* **2**, 358-365 (2010).

[29] Challa, R., Ahuja, A., Ali, J. & Khar, R. K. Cyclodextrins in drug delivery: an updated review. *AAPS PharmSciTech* **6**, E329-357 (2005).

[30] Al-Saidan, S. M. Transdermal self-permeation enhancement of ibuprofen. *J. Control. Release* **100**, 199-209 (2004).

[31] Suhonen, T. M., Bouwstra, J. A. & Urtti, A. Chemical enhancement of percutaneous absorption in relation to stratum corneum structural alterations. *J. Control. Release* **59**, 149-161 (1999).

[32] Zhang, I., Shung, K. K. & Edwards, D. A. Hydrogels with Enhanced Mass Transfer for Transdermal Drug Delivery. *J. Pharm. Sci.* **85**, 1312-1316 (1996).

[33] Barry, B. W. Drug delivery routes in skin: a novel approach. *Adv. Drug Deliv. Rev.* **54**, S31-S40 (2002).

[34] Prausnitz, M. R., Bose, V. G., Langer, R. & Weaver, J. C. Electroporation of mammalian skin: A mechanism to enhance transdermal drug delivery. *Proc. Natl. Acad. Sci. U. S. A.* **90**, 10504-10508 (1993).

[35] Dvoretzky, I. & Kuleza, J. E. Enhanced delivery of combined drugs by heat treatment with exothermic pad. US20050208115A1 (2005).

[36] Tiwary, A. K., Sapra, B. & Jain, S. Innovations in transdermal drug delivery: formulations and techniques. *Recent Pat. Drug Deliv. Formul.* **1**, 23-36 (2007).

[37] Prausnitz, M. R. Microneedles for transdermal drug delivery. *Adv. Drug Deliv. Rev.* **56**, 581-587 (2004).

[38] Doukas, A. G. & Kollias, N. Transdermal drug delivery with a pressure wave. *Adv. Drug Deliv. Rev.* **56**, 559-579 (2004).

[39] Alvarez-Figueroa, M. J. & Blanco-Mendez, J. Transdermal delivery of methotrexate: iontophoretic delivery from hydrogels and passive delivery from microemulsions. *Int. J. Pharm.* **215**, 57-65 (2001).

[40] Kumari, A., Yadav, S. K. & Yadav, S. C. Biodegradable polymeric nanoparticles based drug delivery systems. *Colloids Surf.* B**75**, 1-18 (2010).

[41] Hamidi, M., Azadi, A. & Rafiei, P. Hydrogel nanoparticles in drug delivery. *Adv. Drug Deliv. Rev.* **60**, 1638-1649 (2008).

[42] Hans, M. L. & Lowman, A. M. Biodegradable nanoparticles for drug delivery and targeting. *Curr. Opin. Solid State Mater. Sci.* **6**, 319-327 (2002).

[43] Tartaj, P., Morales, M. d. P., Veintemillas-Verdaguer, S., Gonzalez-Carreno, T. & Serna, C. J. The preparation of magnetic nanoparticles for applications in biomedicine. *J. Phys. D: Appl. Phys.* **36**, R182-R197 (2003).

[44] Kohli, A. K. & Alpar, H. O. Potential use of nanoparticles for transcutaneous vaccine delivery: effect of particle size and charge. *Int. J. Pharm.* **275**, 13-17 (2004).

[45] Stevanovic, M., Savic, J., Jordovic, B. & Uskokovic, D. Fabrication, in vitro degradation and the release behaviours of poly(DL-lactide-co-glycolide) nanospheres containing ascorbic acid. *Colloids Surf.* B**59**, 215-223 (2007).

[46] Brannon-Peppas, L. Recent advances on the use of biodegradable microparticles and nanoparticles in controlled drug delivery. *Int. J. Pharm.* **116**, 1-9 (1995).

[47] Muller, R. H., Mader, K. & Gohla, S. Solid lipid nanoparticles (SLN) for controlled drug delivery - a review of the state of the art. *Eur. J. Pharm. Biopharm.* **50**, 161-177 (2000).

[48] Mei, Z., Chen, H., Weng, T., Yang, Y. & Yang, X. Solid lipid nanoparticle and microemulsion for topical delivery of triptolide. *Eur. J. Pharm. Biopharm.* **56**, 189-196 (2003).

[49] Anderson, J. M. & Shive, M. S. Biodegradation and biocompatibility of PLA and PLGA microspheres. *Adv. Drug Deliv. Rev.* **28**, 5-24 (1997).

[50] Catiker, E., Gumusderelioglu, M. & Guner, A. Degradation of PLA, PLGA homo- and copolymers in the presence of serum albumin: a spectroscopic investigation. *Polym. Int.* **49**, 728-734 (2000).

[51] Dunne, M., Corrigan, O. I. & Ramtoola, Z. Influence of particle size and dissolution conditions on the degradation properties of polylactide-co-glycolide particles. *Biomaterials* **21**, 1659-1668 (2000).

[52] Patterson, J., Stayton, P. S. & Li, X. In situ characterization of the degradation of PLGA microspheres in hyaluronic acid hydrogels by optical coherence tomography. *IEEE Trans. Med. Imaging* **28**, 74-81 (2009).

[53] Mandelbrot, B. How long is the coast of britain ? Statistical self-similarity and fractional dimension. *Science* **156**, 636-638 (1967).

[54] Kandavilli, S., Nair, V. & Panchagnula, R. Polymers in transdermal drug delivery systems. *Pharm. Technol. North Am.* **26**, 62-80 (2002).

[55] Mehdizadeh, A., Toliate, T., Rouini, M. R., Abashzadeh, S. & Dorkoosh, F. Design and in vitro evaluation of new drug-in-adhesive formulations of fentanyl transdermal patches. *Acta Pharm. (Zagreb)* **54**, 301-317 (2004).

[56] Escobar-Chaavez, J. J. *et al.* Transdermal nortriptyline hydrocloride patch formulated within a chitosan matrix intended to be used for smoking cessation. *Pharm. Dev. Technol.* **16**, 162-169 (2011).

[57] Sano, M. *et al.* Relationship between solubility of chitosan in alcoholic solution and its gelation. *Chem. Pharm. Bull.* **47**, 1044-1046 (1999).

[58] Ghosal, K., Rajan, R. & Nanda, A. Effects of chemical enhancers on the release of glipizide through matrix patch. *Int. J. ChemTech Res.* **1**, 1128-1130 (2009).

[59] Shaha, V., Jain, H., Krishna, J. & Patel, P. Microsponge drug delivery: a review. *Int. J. Res. Pharm. Sci.* **1**, 212-218 (2010).

[60] Eljarrat-Binstock, E., Bentolila, A., Kumar, N., Harel, H. & Domb, A. J. Preparation, characterization, and sterilization of hydrogel sponges for iontophoretic drug-delivery use. *Polymer. Adv. Tech.* **18**, 720-730 (2007).

[61] Lee, W.-F. & Lin, Y.-H. Effect of porosigen on the swelling behavior and drug release of porous N-isopropylacrylamide/poly(ethylene glycol) monomethylether acrylate copolymeric hydrogels. *J. Appl. Polym. Sci.* **102**, 5490-5499 (2006).

[62] Caykara, T., Bulut, M., Dilsiz, N. & Akyuez, Y. Macroporous Poly(Acrylamide) Hydrogels: Swelling and Shrinking Behaviors. *J. Macromol. Sci. Pure Appl. Chem.* **43**, 889-897 (2006).

[63] Park, H., Park, K. & Kim, D. Preparation and swelling behavior of chitosan-based superporous hydrogels for gastric retention application. *J. Biomed. Mater. Res., Part A* **76A**, 144-150 (2006).

[64] Madihally, S. V. & Matthew, H. W. T. Porous chitosan scaffolds for tissue engineering. *Biomaterials* **20**, 1133-1142 (1999).

[65] Li, L., Lin, Z. B., Yang, X., Wan, Z. Z. & Cui, S. X. A novel cellulose hydrogel prepared from its ionic liquid solution. *Chin. Sci. Bull.* **54**, 1622-1625 (2009).

[66] Saito, H., Sakurai, A., Sakakibara, M. & Saga, H. Preparation and properties of transparent cellulose hydrogels. *J. Appl. Polym. Sci.* **90**, 3020-3025 (2003).

[67] Khan, T. A., Peh, K. K. & Ch'ng, H. S. Mechanical, bioadhesive strength and biological evaluations of chitosan films for wound dressing. *J. Pharm. Pharmaceut. Sci.* **3**, 303-311 (2000).

[68] Noel, S. P., Courtney, H. S., Bumgardner, J. D. & Haggard, W. O. Chitosan sponges to locally deliver amikacin and vancomycin: a pilot in vitro evaluation. *Clin. Orthop. Relat. Res.* **468**, 2074-2080 (2010).

[69] Zheng, L.-Y. & Zhu, J.-F. Study on antimicrobial activity of chitosan with different molecular weights. *Carbohydr. Polym.* **54**, 527-530 (2003).

[70] Schmitt, K. & Hoffmann, C. Transdermal therapeutic system with waveguide-controlled drug release. WO2007131577A2 (2007).

Chapter 2

Design of a photolinker for UV controlled release

Abstract: Herein is presented a straightforward approach for the complete synthesis of a photolinker used in drug photorelease. This *o*-nitrobenzyl derivate, known as the 4-(4-(1-hydroxyethyl)-2-methoxy-5-nitrophenoxy)butanoic acid, was designed to allow at the same time an easy and stable coupling on a polymer support through an amide bound and a simple photosensitive covalent attachment of the drug to another part of the molecule. The full synthesis is described in depth and the possibility of gram scale-up using only high yield reactions and purification methods based on recrystallization is investigated.

2.1 General remarks

Photochemistry includes reactions induced by light absorption. Thus the radiant energy is converted to another form of energy such as heat that can imply a change of the electron state. In that case it is called photo-excitation and this light assisted electronic transition helps to reduce the activation energy of a reaction.

One of the most important photochemical reactions is the photosynthesis, occurring in plants, and using solar energy to convert carbon dioxide and water into glucose and oxygen. In the laboratory, photosensitive moieties are mainly used as protecting groups or to initiate coupling reactions. Common photochemical reactions include electrocyclic reactions, photoisomerizations and Norrish based reactions [1].

Photochemical reactions are very attractive processes and very good general reviews have been published in this field [1,2]. Many different photo-sensible moieties are already used depending on the activation wavelength, the mechanism or the solvent [1]. Photolytic cleavage of a chemical bond is, by essence, the consequence of photon absorption by a molecule.

The most popular photolabile group, either in liquid or solid phase, is the 6-nitroveratryloxycarbonyl group also called NVOC [3] and its derivatives (Figure 2.1). The original study was based on the NVOC-derived carbamates of amino acids. Two methoxy groups were then introduced to increase the absorbance at longer wavelengths.

Figure 2.1: General chemical structure of NVOC

The NVOC photocleavage relies on the photochemically-induced photoisomerisation of *o*-nitrobenzyl derivatives into *o*-nitrosobenzaldehyde [4]. Among all its possible photodegradation pathways, hydrogen subtraction in the γ-position is quite common and was identified very early by Norrish [5]. As a consequence, this process is now described, for carbonyl compounds, as a Norrish-type II reaction. This group of chemicals were also used for the protection of the hydroxy groups in carbohydrates, which was introduced in the 70's [3] with a first use in solid phase synthesis in 1973 [6].

Among NVOC derivatives, the α-methyl-6-nitroveratryl based [7] photolinker is the most studied even if β-substitutions are sometimes preferred [2,8]. Nevertheless, for this last one the cleavage mechanism is different [8,9].

The mechanism of photorelease from nitrobenzyl ether derivates has been already described in the literature [4,10,11] (Figure 2.2). While submitted to UV light ($\lambda = 365$ nm) a pale yellow solution of α-methyl-6-nitroveratryl in DMSO becomes brownish and water release is observed by NMR.

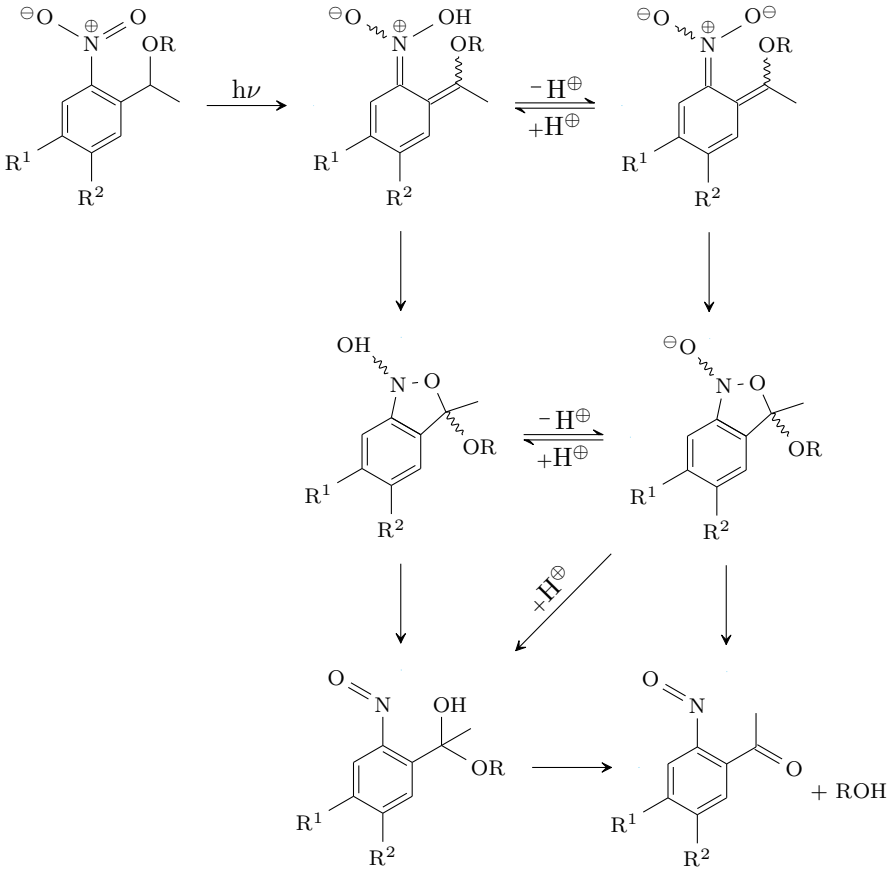

Figure 2.2: Mechanism of ether photorelease from an *o*-nitrobenzyl ether

O-nitrobenzyl derivates photocleavage kinetic in solution has been well reported in the literature [4,21,32] depending of the solvent [21], the pH [23], the power of the UV light and the wavelength [21]. As an example it is known that, in solution, α-methyl-6-nitroveratryl has superior and faster cleavage rate in aprotic than in protic solvents [17,22].

On the same time it is clearly established that the release capacities of that category of photolinker is influenced by substituents R^1 and R^2 [15] (Figure 2.2). However, when coupled to a solid support news factors appear compared to those in solution such as light scattering, shadowing effects of the support, stirring, etc. and important differences have already been observed between cleavage in solution or from solid support, $<$ 1 min to 1-1.5 h respectively [17], and a limit of 95% release is evoked without known explanation [17].

Many different groups have been studied for the release from *o*-nitrobenzyl derivatives and are listed in table 2.1.

Structure		Released molecule	Ref.
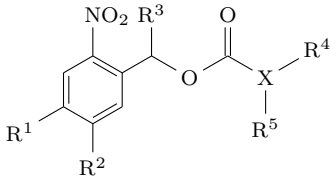	X = O (R^4 = ∅) X = N (R^4 = H) X = N (R^4 = alkyl chain)	Alcohol Primary amine Secondary amine	[13] [15] [17]
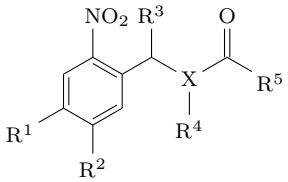	X = O (R^4 = ∅) X = N (R^4 = H) X = N (R^4 = alkyl chain)	Carboxylic acid Primary amine Secondary amine	[20] [22]
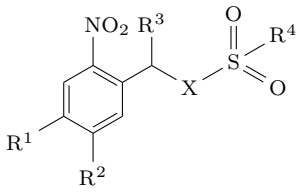	X = O (R^4 = ∅) X = NH (R^4 = alkyl chain)	Sulfonic acid Sulfonamide	[23] [24]
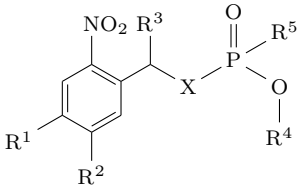	R^4 = H R^4 = alkyl chain	Phosphoester Phosphodiester	[2] [4] [10] [23]
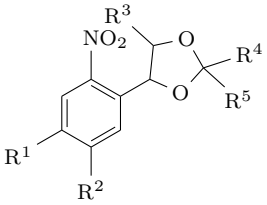	R^4 = H R^4 = alkyl chain	Aldehyde Ketone	[25]

Table 2.1: Potential release from NVOC group

2.2 Strategy

For drug controlled release, the strategy of this study is based on the photodegradation of a covalent bond between a polymer scaffold and a drug molecule preventing any modification of either the scaffold characteristics [26] or of the drug. The approach consists on a Norrish type II reaction [5] with the use of an *o*-nitrobenzyl derivate photolinker [1] to couple the drug to the polymer [27].

The photosensitive moiety of the photolinker is also of importance for the diversity of drug release to anticipate different bonds between drug and linker so a hydroxy group is an optimal candidate[15].

Moreover, the presence of a γ-methyl on the benzylic carbon limits the formation of reactive nitroso-aldehyde upon photolysis.

Among the existing *o*-nitrobenzyl derivatives, two molecules were selected as photolinker model for the production of the ATTS. Their full synthesis are well described in the literature using only accessible raw materials and high yield reactions. Moreover, the purification consists only in recrystallizations, allowing an easy scale-up.

The first photolinker model of this study, called PL1, is the 4-(4-(1-aminoethyl)-2-methoxy-5-nitrophenoxy) butanoic acid (CAS: 162827-97-6). However, in order to avoid self condensation during its attachment at the surface of the support, the terminal amino group is usually protected using a Fmoc group. The resulting protected photolinker, called PL1-Fmoc (Figure 2.3), is commercially available as 4-(4-(1-(9 fluorenylmethyloxy carbonylamino)ethyl)-2-methoxy-5-nitrophenoxy) butanoic acid (CAS: 162827-98-27). Its synthesis[28,29] is not presented here as this photolinker will be used only to prove the surface attachment by the removing of the Fmoc group which gives a easily quantifiable fluorescent adduct.

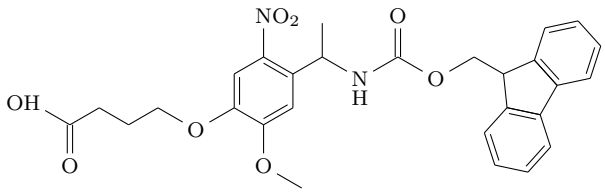

Figure 2.3: Photolinker PL1-Fmoc

The second photolinker model, called PL2, is the 4-(4-(1-hydroxyethyl)-2-methoxy-5-nitrophenoxy) butanoic acid (CAS: 175281-76-2). It consists on the hydroxy equivalent of PL1 (Figure 2.4). PL2 is also commercially available and makes the release of carboxylic acids, alcohols and amines possible. PL2 is known to have a short photocleavage time of 1 to 3 h[19] and also to be cleaved by photolysis in aqueous solvents.

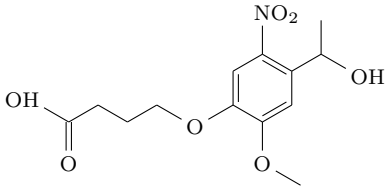

Figure 2.4: Photolinker PL2

Its synthesis is herein fully described[19,20,22,27,30,31]. A 4 steps synthesis was performed (Figure 2.5) consisting in a Williamson ether reaction between apocynin and ethyl-4-bromobutyrate followed by a nitration of the benzyl ring. The apocynin ketone moiety is then reduced and the ester bond is finally hydrolyzed.

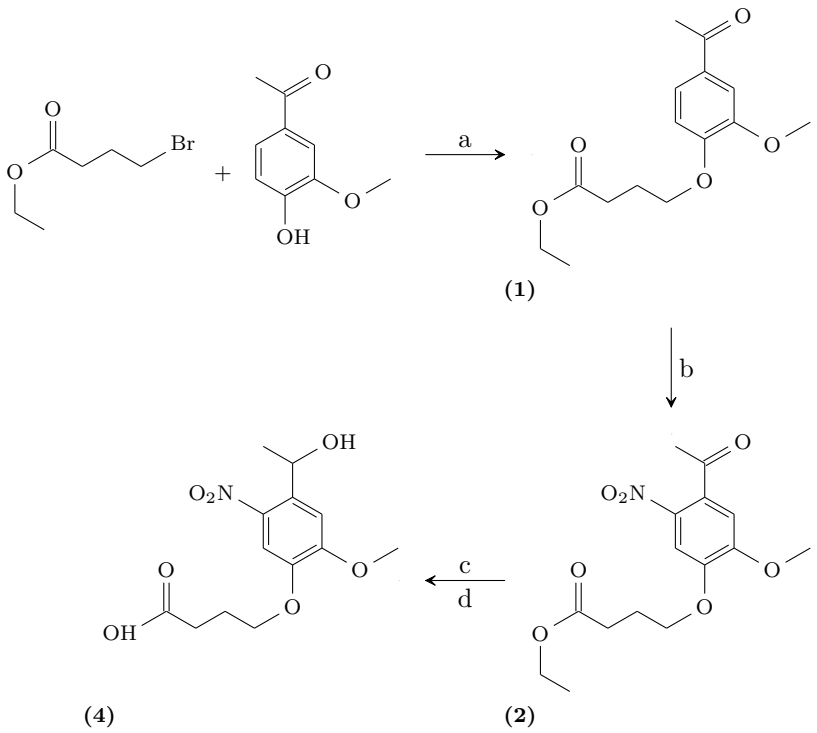

Figure 2.5: General scheme of the photolinker synthesis
Reagents are herein listed: (a) K_2CO_3, DMF ;
(b) 70% HNO_3/Ac_2O (20:7/v:v), 0 °C ;
(c) $NaBH_4$, THF/MeOH (2:1/v:v) ; (d) NaOH

2.3 Results and discussion

2.3.1 Characterization

The model photolinker PL2 was produced in gram scale with an overall yield for the four steps of 77.39%. Considering this success, a scale-up production can be envisaged and a significant improvement of the yield is expected using a better control of the reaction and recrystallization parameters.

2.3.2 Synthesis

2.3.2.1 Ethyl-4-(4-acetyl-2-methoxyphenoxy) butanoate

The first step of the synthesis, which consists in the coupling of apocynin and ethyl-4-bromobutyrate[18,19,27], is quantitative.

The Williamson ether synthesis, a SN_2 reaction, involves the reaction between an alkoxide ion and a primary alkyl halide. In this reaction, the alkoxide ion is produced *in-situ*.

2.3.2.2 Ethyl-4-(4-acetyl-2-methoxy-5-nitrophenoxy) butanoate

The second reaction is a nitration of the benzyl ring. In a first time nitric acid and acetic anhydride react together to give first dinitrogen pentoxide and acetic acid. In the absence of added acetic acid, this pentoxide reacts with acetic anhydride to give, in an exothermic reaction, almost quantitatively acetyl-nitrate[32].

It is well known that as solvent, acetic anhydride is particularly efficient in ring ortho-position nitration using relatively mild conditions. The mixture of nitric acid and acetic anhydride[19,32] was preferred to other methods using only nitric acid[22,31] or nitric acid in dichloromethane[27].

2.3.2.3 Ethyl-4-(4-(1-hydroxyethyl)-2-methoxy-5-nitrophenoxy) butanoate

The third step is the reduction of the keto group by $NaBH_4$. According to Pauling scale, boron has an electronegativity around 2.04 which is lower than that of hydrogen (2.20). As a consequence, the B-H bond is polarized with the boron positive and the hydrogen negative. For this reason, the electronic situation in this reaction can be compared to the electronic situation in a Grignard reagent and the B-H bond acts as a source of hydride ion.

2.3.2.4 4-(4-(1-Hydroxyethyl)-2-methoxy-5-nitrophenoxy) butanoic acid

The final step consists in the deprotection of the carboxylic acid moiety. This reaction is known as ester hydrolysis, or saponification. The carbonyl gives the corresponding sodium carboxylate which is then protonated by the HCl, giving PL2.

2.4 Experimental section

2.4.1 General materials and methods

2.4.1.1 Chemicals

Ethyl-4-bromobutyrate: 98% (Alfa Aesar GmbH & Co KG, Karlsruhe, D) ; DMSO-*d6*: cont. 0.03%(v:v) TMS, 99.8 atom% D (ARMAR AG, Döttingen, CH) ; HCl: ROTIPURAN® ≥ 32%, p.a., ISO ; NaCl: ≥ 99%, Ph.Eur., USP (Carl Roth GmbH & Co. KG, Karlsruhe, DE) ; DMF: Baker Analysed® A.C.S. Reagent; Hexane: (95% n-hexane), HPLC ; HNO_3: 69.0-70.0%, Baker Instra-Analysed® Reagent ; MeOH: Baker Analysed® LC-MS Reagent ; THF: Baker Analysed® A.C.S. Reagent (Mallinckrodt Baker B.V., Deventer, NL) ; NaOH: solution 1 $mol \cdot l^{-1}$ (1N), BASIC (Scharlab SL, Barcelona, ES) ; Apocynin: ≥ 98% ; Ac_2O: puriss. p.a., ACS reagent, ≥ 99.0% (NT) ;
EtOAc: puriss. p.a., ACS reagent, ≥ 99.5% (GC) ; K_2CO_3: purum p.a., anhydrous, ≥ 99.0% (T) ; $NaBH_4$: purum p.a., ≥ 96% (gas-volumetric) ; Na_2SO_4: ACS reagent, ≥ 99.0%, anhydrous, granular ; PL2 **(4)**: ≥ 98.0% (HPLC) (Sigma-Aldrich Chemie GmbH, Buchs, CH) were used as received. Milli-Q water with resistivity of more than 18.2 MΩ·cm was provided by a Millipore Milli-Q filtering system with filtration through a 0.22 µm Millipak filter.

2.4.1.2 Characterization

Synthesized products were characterized by ^{1}H and ^{13}C NMR spectra. (Appendix A for raw material NMR analysis). For the final product, a comparison was realized with the commercially available PL2. NMR spectra were measured with a Brucker AV-200 (200 MHz), and chemical shifts are reported in ppm downfield from internal TMS reference. Abbreviations used are s = singlet, d = doublet, dd = doublet of doublets, t = triplet, dt = doublet of triplet, q = quadruplet, m = multiplet.

2.4.2 Synthesis

2.4.2.1 Ethyl-4-(4-acetyl-2-methoxyphenoxy) butanoate

To a stirred solution of apocynin and K_2CO_3 in DMF, ethyl-4-bromobutyrate was added dropwise in a moderated exothermic reaction. After 20 hours of reaction at room temperature, water (400 ml) was poured in the solution until total dissolution of the observed solid. The obtained solution was then extracted with EtOAc (3 x 200 ml) and the organic phase evaporated.

The resulting yellow solution was partitioned between EtOAc (50 ml) and saturated NaCl solution (6 x 100 ml) to remove traces of DMF [19]. The organic phase was finally dried over Na_2SO_4 and evaporated until obtaining the keto-ester **(1)** (Figure 2.6) as yellowish oil which solidifies at room temperature (crude yield = 100%).

	Amount	Mw (g·mol^{-1})	CAS
Apocynin	30.0875 g	166.1739	498-02-2
DMF	140 ml	73.0937	68-12-2
Ethyl-4-bromobutyrate	38.7340 g	195.0543	2969-81-5
EtOAc	—	88.1051	141-78-6
K_2CO_3	38.4183 g	137.9121	584-08-7
NaCl	—	58.4427	7647-14-5
Na_2SO_4	—	142.0421	7757-82-6
(1)	51.0000 g	280.3163	174884-21-0

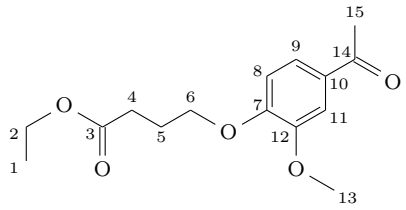

Figure 2.6: Ethyl-4-(4-acetyl-2-methoxyphenoxy) butanoate **(1)**

^{1}H-NMR (200 MHz, DMSO-*d6* δ) 1.19 (t, J = 7.1 Hz, 3H, H_1), 2.00 (dt, J = 7.3 Hz, J = 6.6 Hz, 2H, H_5), 2.47 (t, J = 7.3 Hz, 2H, H_4), 2.53 (s, 3H, H_{15}), 3.82 (s, 3H, H_{13}), 4.07 (q, J = 7.1 Hz, 2H, H_2), 4.08 (t, J = 6.6 Hz, 2H, H_6), 7.05 (d, J = 8.4 Hz, 1H, H_8), 7.45 (d, J = 2.1 Hz, 1H, H_{11}), 7.60 (dd, J = 8.4 Hz, J = 2.1 Hz, 1H, H_9).

^{13}C-NMR (200 MHz, DMSO-*d6* δ) 14.04 (C_1), 24.10 (C_5), 26.25 (C_{15}), 30.03 (C_4), 55.53 (C_{13}), 59.86 (C_2), 67.34 (C_6), 110.49 (C_{11}), 111.77 (C_8), 122.98 (C_9), 129.93 (C_{10}), 148.67 (C_{12}), 152.21 (C_7), 172.38 (C_3), 196.25 (C_{14}).

2.4.2.2 Ethyl-4-(4-acetyl-2-methoxy-5-nitrophenoxy) butanoate

The previously obtained ethyl-4-(4-acetyl-2-methoxyphenoxy) butanoate **(1)** was dissolved in 15 ml of Ac_2O and added dropwise to a stirred solution of 70% HNO_3 (100 ml) and Ac_2O (20 ml) at 0 °C. After 2.5 hours of reaction, the solution was poured into 300 ml of cold water, while a yellow precipitate was observed, and kept at 4 °C overnight.

The solid was filtered, washed with water and recrystallized in a MeOH/water mixture. Yellow needles of ethyl-4-(4-acetyl-2-methoxy-5-nitrophenoxy) butanoate **(2)** (Figure 2.7) were obtained and washed with water (yield = 79.96%) [19].

	Amount	M*w* (g·mol^{-1})	CAS
(1)	5.0000 g	280.3163	174884-21-0
Ac_2O	35 ml	102.0886	108-24-7
70% HNO_3	100 ml	63.0128	7697-37-2
MeOH	—	32.0418	67-56-1
(2)	4.6400 g	325.3138	1031702-80-3

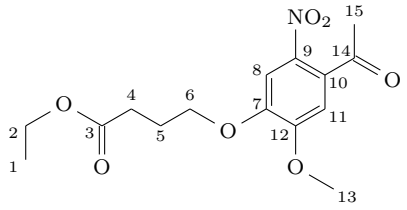

Figure 2.7: Ethyl-4-(4-acetyl-2-methoxy-5-nitrophenoxy) butanoate **(2)**

^{1}H-NMR (200 MHz, DMSO-*d6* δ) 1.19 (t, J = 7.1 Hz, 3H, H_1), 2.00 (dt, J = 7.3 Hz, J = 6.6 Hz, 2H, H_5), 2.47 (t, J = 7.3 Hz, 2H, H_4), 2.52 (s, 3H, H_{15}), 3.93 (s, 3H, H_{13}), 4.07 (q, J = 7.1 Hz, 2H, H_2), 4.14 (t, J = 6.6 Hz, 2H, H_6), 7.22 (s, 1H, H_{11}), 7.63 (s, 1H, H_8).

^{13}C-NMR (200 MHz, DMSO-*d6* δ) 14.03 (C_1), 23.90 (C_5), 23.93 (C_{15}), 29.98 (C_4), 56.63 (C_{13}), 59.90 (C_2), 68.13 (C_6), 108.05 (C_{11}), 109.83 (C_8), 131.17 (C_{10}), 138.33 (C_9), 148.45 (C_{12}), 153.30 (C_7), 172.35 (C_3), 199.21 (C_{14}).

2.4.2.3 Ethyl-4-(4-(1-hydroxyethyl)-2-methoxy-5-nitrophenoxy) butanoate

To a stirred solution of ethyl-4-(4-acetyl-2-methoxy-5-nitrophenoxy) butanoate **(2)** in THF (160 ml) and MeOH (80 ml) was added $NaBH_4$ (1.4256 g) at room temperature. After one hour of reaction, a second portion of $NaBH_4$ (0.4752 g) was added and the reaction mixture was stirred overnight giving **(3)** (Figure 2.8) [19].

	Amount	Mw (g·mol^{-1})	CAS
(2)	10.0000 g	325.3138	1031702-80-3
$NaBH_4$	1.9008 g	37.8325	16940-66-2
THF	160 ml	72.1057	109-99-9
MeOH	80 ml	32.0418	67-56-1
(3)	Not isolated	327.3297	1073426-06-8

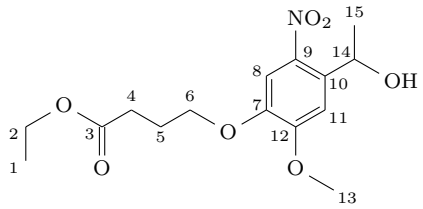

Figure 2.8: Ethyl-4-(4-(1-hydroxyethyl)-2-methoxy-5-nitrophenoxy) butanoate **(3)**

2.4.2.4 4-(4-(1-Hydroxyethyl)-2-methoxy-5-nitrophenoxy) butanoic acid

The previous reaction was followed by the addition of 1N NaOH (85 ml) and water (40 ml) to proceed to the saponification of the ester **(3)** during 8 hours. The mixture was concentrated under vacuum, acidified with 6N HCl ($\sim$ 17 ml) and extracted with EtOAc. The combined organic phases were dried over Na_2SO_4 and evaporated to give a yellow residue. Recrystallization from EtOAc/Hexane (300 ml/800 ml, respectively) afforded the photolinker PL2 **(4)** (Figure 2.9) (yield = 96.31%) [19].

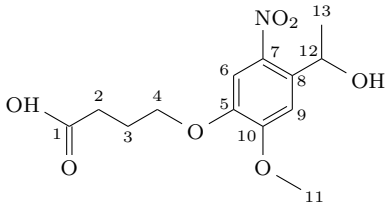

Figure 2.9: 4-(4-(1-hydroxyethyl)-2-methoxy-5-nitrophenoxy) butanoic acid **(4)**

	Amount	Mw (g·mol^{-1})	CAS
(3)	Not isolated	327.3297	1073426-06-8
EtOAc	—	88.1051	141-78-6
Hexane	—	86.1753	110-54-3
6N HCl	—	36.4609	7647-01-0
1N NaOH	85 ml	39.9971	1310-73-2
Na_2SO_4	—	142.0421	7757-82-6
(4)	8.8606 g	299.2765	175281-76-2

^{1}**H-NMR (200 MHz, DMSO-*d6* δ)** 1.37 (d, J = 6.3 Hz, 3H, H_{13}), 1.96 (dt, J = 7.3 Hz, J = 6.6 Hz, 2H, H_3), 2.40 (t, J = 7.3 Hz, 2H, H_2), 3.91 (s, 3H, H_{11}), 4.07 (t, J = 6.6 Hz, 2H, H_4), 5.27 (q, J = 6.3 Hz, 1H, H_{12}), 7.37 (s, 1H, H_9), 7.54 (s, 1H, H_6), 12.17 (COOH).

^{13}**C-NMR (200 MHz, DMSO-*d6* δ)** 24.04 (C_3), 25.11 (C_{13}), 29.94 (C_2), 56.05 (C_{11}), 63.89 (C_{12}), 67.95 (C_4), 108.52 (C_6), 109.17 (C_9), 137.99 (C_8), 138.92 (C_7), 146.21 (C_5), 153.45 (C_{10}), 173.95 (C_1).

2.5 Bibliography

[1] Bochet, C. G. Photolabile protecting groups and linkers. *J. Chem. Soc., Perkin Trans. 1* , 125-142 (2002).

[2] Pelliccioli, A. P. & Wirz, J. Photoremovable protecting groups: reaction mechanisms and applications. *Photochem. Photobiol. Sci.* **1**, 441-458 (2002).

[3] Patchornik, A., Amit, B. & Woodward, R. B. Photosensitive protecting groups. *J. Am. Chem. Soc.* **92**, 6333-6335 (1970).

[4] Il'ichev, Y. V., Schwoerer, M. A. & Wirz, J. Photochemical Reaction Mechanisms of 2-Nitrobenzyl Compounds: Methyl Ethers and Caged ATP. *J. Am. Chem. Soc.* **126**, 4581-4595 (2004).

[5] Bamford, C. H. & Norrish, R. G. W. Primary photochemical reactions. VII. Photochemical decomposition of isovaleraldehyde and dipropyl ketone. *J. Chem. Soc.* , 1504-1511 (1935).

[6] Rich, D. H. & Gurwara, S. K. Removal of protected peptides from an orthonitrobenzyl resin by photolysis. *J. Chem. Soc., Chem. Commun.* , 610-611 (1973).

[7] Rinnova, M., Novakova, M., Kasicka, V. & Jiracek, J. Side reactions during photochemical cleavage of an -methyl-6-nitroveratryl-based photolabile linker. *J. Pept. Sci.* **6**, 355-365 (2000).

[8] Smirnova, J., Woell, D., Pfleiderer, W. & Steiner, U. E. Synthesis of caged nucleosides with photoremovable protecting groups linked to intramolecular antennae. *Helv. Chim. Acta* **88**, 891-904 (2005).

[9] Woell, D., Smirnova, J., Pfleiderer, W. & Steiner, U. E. Highly efficient photolabile protecting groups with intramolecular energy transfer. *Angew. Chem., Int. Ed.* **45**, 2975-2978 (2006).

[10] Corrie, J. E. T., Barth, A., Munasinghe, V. R. N., Trentham, D. R. & Hutter, M. C. Photolytic cleavage of 1-(2-nitrophenyl)ethyl ethers involves two parallel pathways and product release is rate-limited by decomposition of a common hemiacetal intermediate. *J. Am. Chem. Soc.* **125**, 8546-8554 (2003).

[11] Aujard, I. *et al.* o-Nitrobenzyl photolabile protecting groups with red-shifted absorption: syntheses and uncaging cross-sections for one-and two-photon excitation. *Chem. Eur. J.* **12**, 6865-6879 (2006).

[12] Yamaguchi, S. *et al.* Photocontrollable Dynamic Micropatterning of Non-adherent Mammalian Cells Using a Photocleavable Poly(ethylene glycol) Lipid. *Angew. Chem., Int. Ed.* **51**, 128-131 (2012).

[13] Kim, I.-H. *et al.* Optimization of Amide-Based Inhibitors of Soluble Epoxide Hydrolase with Improved Water Solubility. *J. Med. Chem.* **48**, 3621-3629 (2005).

[14] Martin, E. H. & Brittain, W. J. A convenient laboratory preparation of aromatic polycarbonate. *Polym. Bull.* **47**, 517-520 (2002).

[15] Hasan, A. *et al.* Photolabile protecting groups for nucleosides: synthesis and photo-deprotection rates. *Tetrahedron* **53**, 4247-4264 (1997).

[16] McKeown, S. C., Watson, S. P., Carr, R. A. E. & Marshall, P. A photolabile carbamate based dual linker analytical construct for facile monitoring of solid phase chemistry: 'TLC' for solid phase ? *Tetrahedron Lett.* **40**, 2407-2410 (1999).

[17] Bochet, C. G. Wavelength-selective cleavage of photolabile protecting groups. *Tetrahedron Lett.* **41**, 6341-6346 (2000).

[18] Minkwitz, R. & Meldal, M. Application of a photolabile backbone amide linker for cleavage of internal amides in the synthesis towards melanocortin subtype-4 agonists. *QSAR Comb. Sci.* **24**, 343-353 (2005).

[19] Holmes, C. P. Model Studies for New o-Nitrobenzyl Photolabile Linkers: Substituent Effects on the Rates of Photochemical Cleavage. *J. Org. Chem.* **62**, 2370-2380 (1997).

[20] Holmes, C. P. & Jones, D. G. Reagents for Combinatorial Organic Synthesis: Development of a New o-Nitrobenzyl Photolabile Linker for Solid Phase Synthesis. *J. Org. Chem.* **60**, 2318-2319 (1995).

[21] Wenschuh, H. *et al.* Coherent membrane supports for parallel microsynthesis and screening of bioactive peptides. *Biopolymers* **55**, 188-206 (2000).

[22] Whitehouse, D. L., Savinov, S. N. & Austin, D. J. An improved synthesis and selective coupling of a hydroxy based photolabile linker for solid phase organic synthesis. *Tetrahedron Lett.* **38**, 7851-7852 (1997).

[23] Kim, M. S. & Diamond, S. L. Photocleavage of o-nitrobenzyl ether derivatives for rapid biomedical release applications. *Bioorg. Med. Chem. Lett.* **16**, 4007-4010 (2006).

[24] Akerblom, E. B. Six new photolabile linkers for solid phase synthesis. 2. Coupling of various building blocks and photolytic cleavage. *Molec. Divers.* **4**, 53-69 (1999).

[25] Gravel, D., Hebert, J. & Thoraval, D. o-Nitrophenylethylene glycol as photoremovable protective group for aldehydes and ketones: syntheses, scope, and limitations. *Can. J. Chem.* **61**, 400-410 (1983).

[26] Chen, G., Ushida, T. & Tateishi, T. Scaffold design for tissue engineering. *Macromol. Biosci.* **2**, 67-77 (2002).

[27] Teague, S. J. Facile synthesis of a o-nitrobenzyl photolabile linker for combinatorial chemistry. *Tetrahedron Lett.* **37**, 5751-5754 (1996).

[28] Frutos, A. G., Brockman, J. M. & Corn, R. M. Reversible Protection and Reactive Patterning of Amine- and Hydroxyl-Terminated Self-Assembled Monolayers on Gold Surfaces for the Fabrication of Biopolymer Arrays. *Langmuir* **16**, 2192-2197 (2000).

[29] Johnsson, R., Lackey, J. G., Bogojeski, J. J. & Damha, M. J. New light labile linker for solid phase synthesis of 2'-O-acetal-ester oligonucleotides and applications to siRNA prodrug development. *Bioorg. Med. Chem. Lett.* **21**, 3721-3725 (2011).

[30] Venkatesan, H. & Greenberg, M. M. Improved Utility of Photolabile Solid Phase Synthesis Supports for the Synthesis of Oligonucleotides Containing 3'-Hydroxyl Termini. *J. Org. Chem.* **61**, 525-529 (1996).

[31] Akerblom, E. B., Nygren, A. S. & Agback, K. H. Six new photolabile linkers for solid-phase synthesis. 1. Methods of preparation. *Mol. Diversity* **3**, 137-148 (1998).

[32] Hoggett, J. G., Moodie, R. B., Penton, J. R., Schofield, K. Nitration and aromatic reactivity, Cambridge University Press, Cambridge, pp. 76-105 (1971).

Chapter 3

Chitosan microporous structure production

Abstract: This study describes the development of a porous material for drug immobilization through a photolabile moiety. The material presents high porosity in order to achieve elevated drug loading in a reduced volume and diffusion pathway for the release. Herein, polymeric porous matrices were obtained using thermally induced phase separation of a polymer solution and subsequent sublimation of the solvent. The chitosan is a natural and biocompatible polymer presenting interesting properties. Chitosan porous matrices obtained can be considered as a material with immense possibilities. To improve the results, as reproducibility and matrices homogeneity, a special cryo-unit, the POMAP, has been designed. To complete this process, a mathematical model is suggested to predict heat exchanges occurring during the freezing and influencing the scaffold properties.

3.1 General remarks

Polymer materials are well described in TTS as their tunable properties allow to easily influence the release. In particular, porous scaffolds made of natural polymers gained attention considering their immense potential for innovative applications. In the case of drug release engineering, ideal scaffolds present the following characteristics:

- Three dimensional and highly interconnected porous structure ;
- Excellent biocompatibility ;
- Good mechanical properties ;
- Easy production process to form a variety of shapes and sizes ;
- Suitable surface chemistries for surface modification.

Chitosan, a natural linear polysaccharide similar in structure to cellulose [1], is composed of randomly distributed β-(1-4)-linked *D*-glucosamine, or glucosamine (GlcNH), and *N*-acetyl-*D*-glucosamine, or *N*-acetylglucosamine (GlcNAc) (Figure 3.1). It is obtained by deacetylation of chitin which is a structural component of crab and shrimp shells, insects exoskeletons or fungi cell walls [2,3,4,5].

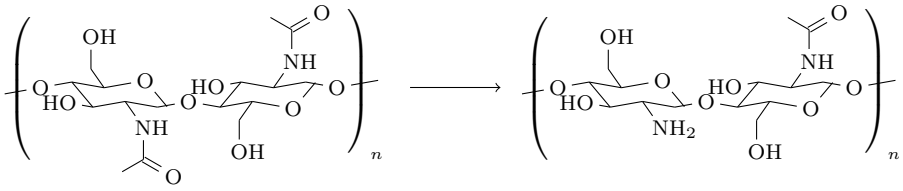

Figure 3.1: Chitosan obtained by chitin through a deacetylation reaction

Usually considered as the second most abundant polysaccharide in nature [6] with a annual production, only for the marine resources, estimated to 2.3 million tons per year [7] and around 10 billion tons considering the full worldwide production [2,8], chitin and its derivates are used in a wide variety of fields such as food science [3,9], water treatment [2,10] or paper industry [2].

Due to remarkable properties such as low toxicity, biocompatibility [11], hemostatics [12] and antibacterial effect [13], chitosan is an attractive material for biomedical applications [14].

The production of chitosan porous structures has several applications such as support material for surgical reconstruction [6,15], drug therapy systems, synthetic prosthesis, medical devices [4,5,16] or cell culture scaffolds [17,18].

Moreover, it is approved by the FDA for drug delivery and various sterilization methods such as ionizing radiation, X-ray, heat or chemical methods are adapted for sterilization of chitosan scaffolds in clinical applications [1].

Finally, chitosan reactivity allows typical reactions of amines thus a lot of chemical modifications are easily obtained under mild conditions [5,19]. It is also more reactive than chitin regarding the free primary amino groups regularly distributed in its molecular chain [4,20,21]. For this reason, chitosan is easily soluble in aqueous solutions of inorganic and organic acids [20].

3.2 Strategy

Different techniques exist to create chitosan porous structures such as fiber extrusion, 3D printing[22], electrospinning[23], gas foaming[24] of phase separation. In particular, the phase separation can be obtained from a chitosan solution using a pH change to precipitate the chitosan[25] or via thermally induced phase separation (TIPS)[6,15,16].

The TIPS method is based on a thermodynamic demixing of an aqueous polymer solution into a polymer rich phase and a polymer poor phase by cooling the solution below its freezing temperature[16]. During the process, polymer aggregates are formed between growing ice crystals giving a continuous interpenetrating network of ice and precipitates. After sublimation of ice, a highly porous polymer structure is obtained[15]. Due to the ease of chitosan dissolution in acidic aqueous solutions, TIPS is an interesting way to produce ChipM[26].

Many different parameters influence the final morphology of a matrix obtained by TIPS. As an example, the pore structure of the scaffold can be manipulated by acting on solvent volume fraction, size of the ice crystals, polymer concentration, etc. However, the fine control of the porous structure remains difficult.

3.3 Results and discussion

3.3.1 Chitosan characterization

Chitosan physico-chemical properties such as solubility, reactivity or biodegradability highly depend on its degree of deacetylation (DDA) and degree of polymerization (DP).

3.3.1.1 Determination of chitosan DDA

Analytical techniques such as UV or IR spectroscopy[27], chromatography, titration[10] or NMR[10,11,28] are used to determine chitosan DDA. Among these methods ^{1}H-NMR is recognized as a particularly potent tool. Reasons include no need of calibration, no need to know precisely the amount and no purification step[11]. ^{1}H-NMR using DCl solution at 70 ℃ is widely accepted for chitosan NMR[11]. However, this method suffers from long experiment duration due to significant relaxation time at this temperature. Moreover, although the high temperature of analysis reduces sample viscosity, the sensitivity decreases dramatically.

In this study, the acquisition time is reduced by performing the experiment at 27 ℃ in DCl[11]. Data are treated by measuring proton signal area after Fourier transformation of the free induction decay (FID) signal. Finally DDA is calculated (Equation 3.1) using the signal from protons 2 to 6 of both monomers and the peak of acetyl groups (Figure 3.14)[10].

$$DDA = 100 \left[1 - \frac{H_{AC}/3}{H_{2-6}/6}\right] \tag{3.1}$$

For the chitosan used in this study, the obtained DDA is 81.80%, meaning a large preponderance of GlcNH units which is in accordance with data provided by the supplier.

3.3.1.2 Determination of chitosan DP

According to the supplier, the material used for this study has a molecular weight comprised between 190,000 and 310,000 g·mol^{-1}. By knowing these minimal and maximal values, corresponding DP values were calculated using the relation (Equation 3.2) between monomer molecular weights, DDA and the amount of water loss as product of the virtual condensation reaction of polymerization.

Chitosan DP comes from the relation:

$$DP = \frac{Mw_{chitosan} - Mw_{H_2O}}{DDA\ Mw_{GlcNH} + (1 - DDA)\ Mw_{GlcNAc} - Mw_{H_2O}} \tag{3.2}$$

Using the values:

$Mw_{chitosan}$	190,000 - 310,000 g·mol^{-1}
Mw_{GlcNAc}	221.20780 g·mol^{-1}
Mw_{GlcNH}	179.17112 g·mol^{-1}
Mw_{H_2O}	18.01528 g·mol^{-1}

The estimated average of the chitosan sample is comprised between 1126 and 1836. It reveals short length polymer chains that will potentially impact on the properties of the ChipM. This value is also of interest for the determination of the free amine concentration in chitosan solutions. Indeed, it is generally accepted that the acid concentration needed to dissolve chitosan is at least equal to the amine concentration [8].

3.3.2 ChipM production by TIPS method

3.3.2.1 Fixed parameters

Chitosan dissolution is function of parameters that also influence the biocompatibility and the microstructure of the material obtained by the TIPS process. However, this study is mainly focused on the influence of freezing conditions on the TIPS method rather than on other parameters variations. For this reason, the following parameters were kept constant.

3.3.2.1.a The acid

Type of the acid

Appropriated solvent systems for chitosan dissolution include hydrochloric acid [26], oxalic acid [29], acetic acid [18,25,30] and lactic acid [31,32] aqueous solutions. Nevertheless comparisons between scaffolds obtained using lactic and acetic acid to dissolve the polymer showed that acetic acid based scaffolds are more skin irritant than lactic acid equivalents [31]. On the same time, scaffolds obtained from lactic acid solution (LA) are known to be softer, more flexible, pliable and bioadhesive than the acetic acid equivalent [31]. As a consequence, only LA is used in this study for the production of ChipM.

Acid concentration

For polyelectrolytes such as chitosan, the pH of dissolution is not constant [8] and is highly influenced by the electrolytic dissociation behavior of the polymer. The relation is well described by Katchalsky's equation (Equation 3.3) [33,34]:

$$pH = pK_0 - log\left(\frac{1-\alpha}{\alpha}\right) + 0.4343\ \frac{\varepsilon\ \Psi_0}{K_B} \tag{3.3}$$

With pK_0 the intrinsic dissociation constant of the monomeric unit, α the degree of ionization of the polymer, Ψ_0 the electrostatic surface potential of the polyion, K_B the Boltzmann constant and ε the electron charge. In the case of $\alpha = 1$, the polymer becomes uncharged so $\varepsilon = 0$ and $pH = pK_0$. For chitosan, $pK_0 \approx 6.5$ [35] and is independent of the DDA [8]. Considering parameters introduced by Katchalsky's equation, all solutions were prepared using a LA concentration of 2%(v:v).

3.3.2.1.b Chitosan concentration

Besides its influence on the pH of the solution, the polymer concentration also plays a critical role on scaffold properties as the volume fraction of the polymer may change porosity, pore sizes and surface area of the material. Therefore, the pore structure can be manipulated by varying the polymer concentration [16]. In this study, the chitosan concentration is kept at 20 g of chitosan per liter of 2%(v:v) LA.

3.3.2.1.c Freeze drying conditions

Once the TIPS occurred, the frozen material is freeze dried to sublimate the ice. Since the freeze drying process has never been reported as having any influence on the final structure of the scaffold, the conditions were kept constant for all the experiments using a normal low pressure sublimation during at least 12 hours.

3.3.2.1.d Washing conditions

After the freeze drying, freshly obtained ChipM appear opaque and inelastic. In order to be used as drug delivery system, they are hydrated. However, when immersed in a neutral aqueous medium, they rapidly dissolve, revealing a structure composed of soluble chitosan lactate [36]. For this reason, dry ChipM are rehydrated in particular conditions.

Several solutions can be used for that purpose among sodium hydroxide solution [26,32], series of EtOH solutions with a regular increase of water content (0%, 30%, 50% and 100%) [26,36] or ammonia solution (AS) [12,37]. In this study, the rehydrating solutions consist on EtOH solutions with a regular increase of ammonia concentration.

3.3.2.2 Influence on freezing conditions on TIPS process

During the freezing of a chitosan solution, a phase separation occurs and leads to the demixing of the solution into a non frozen liquid microphase of concentrated chitosan solution and growing ice crystals.

The porous structure of the ChipM is determined at that stage as the space occupied by the ice later becomes pores. However the freezing conditions showed a significant effect on the size of the pores [19,26,38] which consequently influence tensile properties of the scaffolds [26] and drug release kinetic.

Moreover, pore size, pore shape and porosity are also important as they define the surface area and, in that case, the amount of amine moieties available for drug loading. Ice crystals are smaller when they have a short time to grow [39] resulting in small pores [26]. It has been demonstrated that the final freezing temperature has a negligible effect compared to the freezing rate which seems to be the key factor to control the scaffold structure [38,40]. Indeed, the lower the freezing temperature is, the quicker is the freezing rate. In term of thermodynamic, the freezing rate reflects the heat transfer rate.

In most of the cases, freezing is an exothermic process. By changing from liquid to solid state, a solution release heat which is known as latent heat or enthalpy of solidification. During the TIPS, this released energy creates a local temperature increase and directly impacts the ice nucleation, ice crystals growing and finally the structure of the ChipM [39,40,41]. For this reason, heat has to be removed from the freezing liquid otherwise the freezing process stops. Using the same polymer solution, consisting in 2 g of chitosan dissolved in 100 ml of a 2%(v:v) LA, three TIPS experiments were conducted with variations in freezing conditions. In experiments A and B, the chitosan solutions were frozen respectively by simple cooling at constant temperature T = -12 °C in a freezer and using an uncontrolled cooling rate (R_c) from T_0 = -5 °C to T_1 = -15 °C. Experiment C was conducted on a dedicated freezing apparatus, the POMAP.

Using Peltier effect, the POMAP makes it possible to precisely control the R_c of a solution from T_0 = -5 °C to T_1 = -15 °C. In experiment C, the cooling rate is R_c = 1.0 °C·min^{-1}. For all the samples, a porous top surface, consisting in open and interconnected pores was observed with important variations in pore size and shape. On the contrary, for all the samples the bottom surface shows a skin layer, which can be explained by interaction between mold and polymer chains.

3.3.2.2.a Experiment A and B

Top surface

Analyzing the optical pictures, ChipM obtained by experiment A (Figure 3.2A_0) are much more heterogeneous than matrices produced by experiment B (Figure 3.2B_0). This result confirms that the ChipM structure is highly dependent of the freezing conditions.

The partial destroying of ChipM in experiment A (Figure 3.2A_0) can be explained by a low and ineffective heat extraction, leading to an increased size of ice crystals. Since the larger ice crystals push chitosan chains to a greater extent, they may have destroyed the structure. On the contrary for experiment B (Figure 3.2B_0), the EtOH bath used to cool down the chitosan solution induced a better heat dissipation and consequently the formation of many nuclei of ice, resulting in the formation of smaller pores [19].

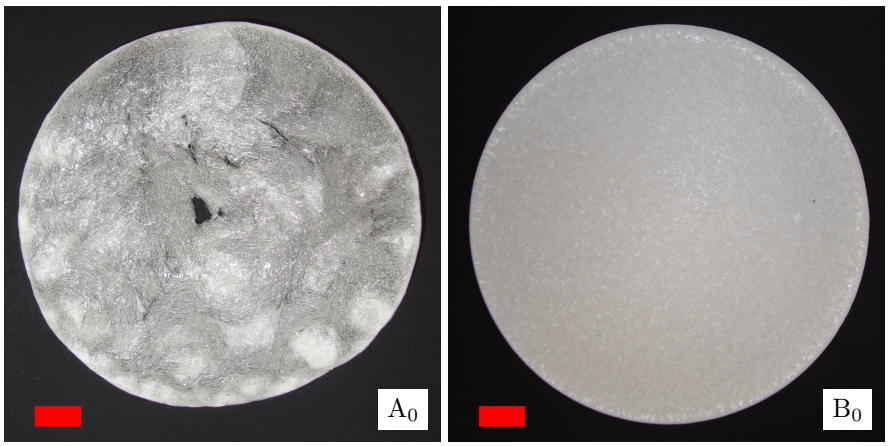

Figure 3.2: Optical picture of ChipM (scale bar 10 mm)
A_0: Experiment A ; B_0: Experiment B

For experiment A, the analysis of the SEM pictures (Figure 3.3A_T) corroborates the presence of large and irregular pores. An explanation would be the existence of poor contact regions between the mold and the freezer surface resulting in a temperature distribution. This induced a space and time variable heat transfer through the suspension, leading to heterogeneous nucleation, ice crystals growing and ultimately pore size distribution.

On the poor contact regions, the heat exchange is ineffective and gives time to the crystals to grow and reach large size. In experiment B (Figure 3.3B_T), the previous hypothesis of homogeneous heat removing using EtOH as heat transfer fluid is confirmed by the presence of regular and small pores. In other words, the difference in pore size between experiment A and B reflects the different rates of heat transfer. It follows that a sufficiently rapid rate of cooling better extracts the latent heat of solidification, preventing the formation of long ice crystals.

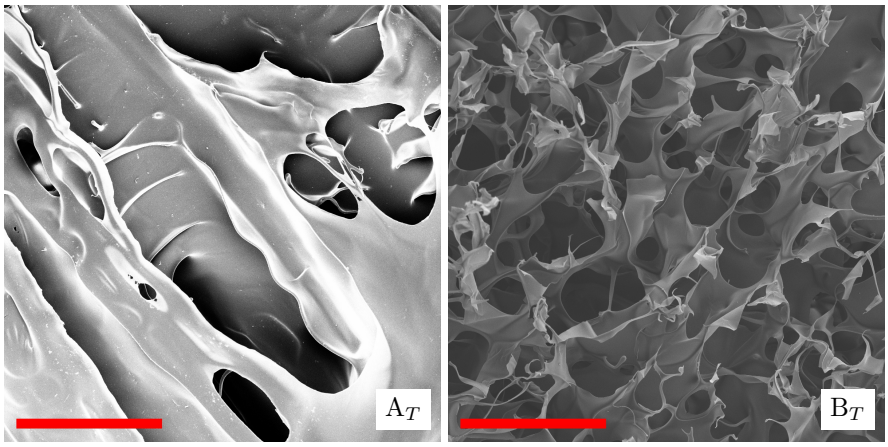

Figure 3.3: SEM pictures of ChipM (scale bar 200 µm)
A_T: Experiment A, top surface ; B_T: Experiment B, top surface

Bottom surface

As it appears in SEM pictures of the bottom surface (Figure 3.4), both experiments A and B present a similar skin like layer on the side in contact with the mold during the TIPS process. The reason of the formation of this skin is not clear but may result from a local increase of chitosan concentration due to electrostatic affinity between the mold and polymer molecules.

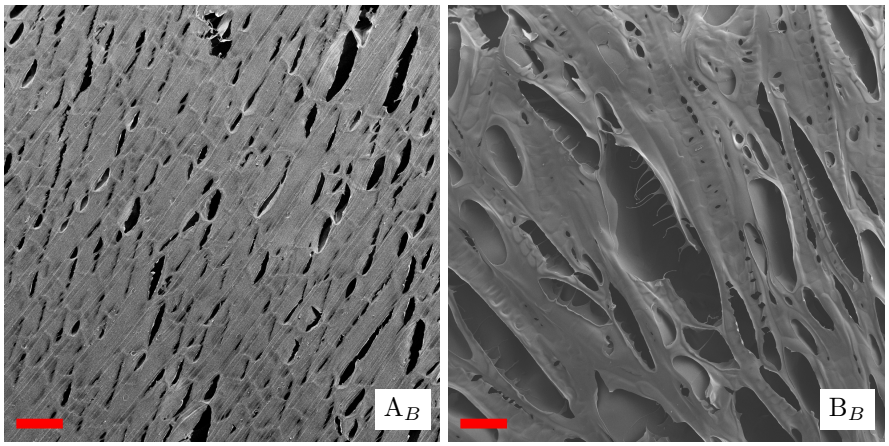

Figure 3.4: SEM pictures of ChipM (scale bar 200 µm)
A_B: Experiment A, bottom surface ; B_B: Experiment B, bottom surface

Differences between experiment A and B bottom surfaces can derive from the cooling rate as in both cases the bottom of the mold is the first part subjected to the cooling. In experiment A (Figure 3.4A_B), the freezing time, few hours, leaves the time to polymer chains to diffuse and cover completely the mold. In the case of experiment B (Figure 3.4B_B), a faster freezing implies a short time for polymer chains rearrangement. For this project the presence of that skin is not a problem as the drug delivery can be made from the top side of the ChipM. However, it can be avoided by using specials procedures [38].

Cross section

In order to fully describe the influence of the freezing conditions on the structure of the ChipM, cross section SEM pictures of experiments A and B ChipM were taken. In experiment A (Figure 3.5A_S), a multi layer structure is visible. However, ChipM obtained in experiment B (Figure 3.5B_S) shows a highly interconnected and fine porous structure.

This difference is directly attributable to the freezing conditions and in particular to a more efficient heat removing in experiment B. This comparison confirms the hypothesis of heat exchange influence in the final ChipM structure. Indeed, it is clearly perceptible that a non efficient heat transfer in experiment A gave time to ice crystals to reach a millimeter size while crystals obtained in experiment B only grew until dozens of micrometers.

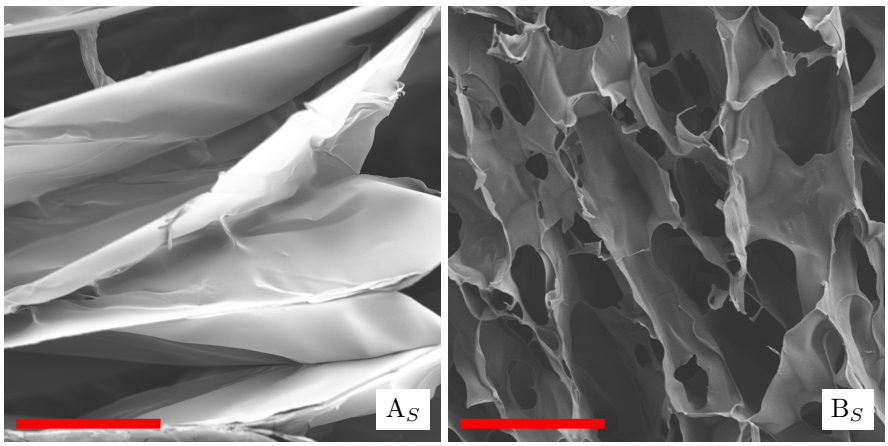

Figure 3.5: SEM pictures of ChipM (scale bar 200 µm)
A_S: Experiment A, section ; B_S: Experiment B, section

Experiments A and B demonstrate that the difference in structures produced by the TIPS method is mainly influenced by the way of evacuating the heat released. In experiment B, EtOH is a better heat transfer fluid than air used for experiment A. As a consequence, homogeneous ChipM can be produced by controlling heat exchange parameters.

3.3.2.2.b Experiment C: ChipM on POMAP

Previous experiments show limitation of using air or EtOH as heat transfer fluids. For this reason, a dedicated apparatus, the POMAP, using thermoelectric effect of peltier modules (PM) as cooling system, has been designed. In particular, this device makes it possible to control the mold temperature and remove easily the heat released during solution freezing. The equipment consists in an insulated chamber in which the temperature is automatically controlled and continuously adjusted by the feedback of a thermocouple.

The temperature of the chamber can be monitored from T_0 = -5 °C to T_1 = -15 °C with a precise cooling rate that can go from R_c = 0.1 °C·min^{-1} to R_c = 1.0 °C·min^{-1}. In experiment C, the mold, containing the chitosan solution, was placed into the chamber and after temperature equilibrium, submitted to a linear temperature decrease at R_c = 1.0 °C·min^{-1}. The ChipM produced using the POMAP (Figure 3.6C_0) appears significantly much more homogeneous throughout the entire scaffold than ChipM produced using other techniques.

Looking at the SEM pictures (Figure 3.7), a highly open porous structure presenting an important interconnectivity can be observed. Images analysis reveal a pore aperture around 10 µm which is almost 10 times smaller than the average pore size obtained in experiment B.

With the POMAP it is possible to achieve high reproducibility as the insulating chamber limits interactions with external conditions such as temperature or humidity. Moreover, the possibility to control the cooling rate gives interesting possibilities to produce ChipM having different porous structures.

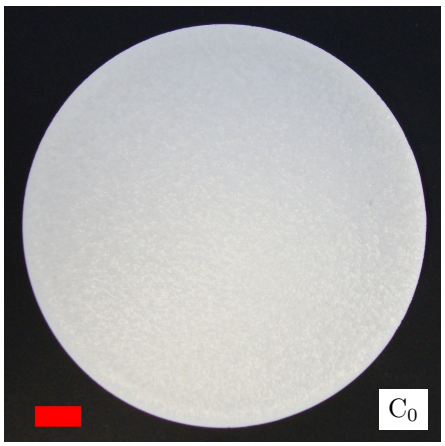

Figure 3.6: Optical picture of ChipM (scale bar 10 mm)
Experiment C

By varying only three parameters during the TIPS process among acid (type and concentration), chitosan (DDA, DP, and concentration) and cooling rate, many different ChipM can be produced. For this reasons, a nomenclature describing 550 potential ChipM is proposed (Appendix C).

According to this nomenclature, the matrix $\left({}^{2}_{LA}|40\right)\cdot$ChipM was considered as a good candidate to pursue this study.

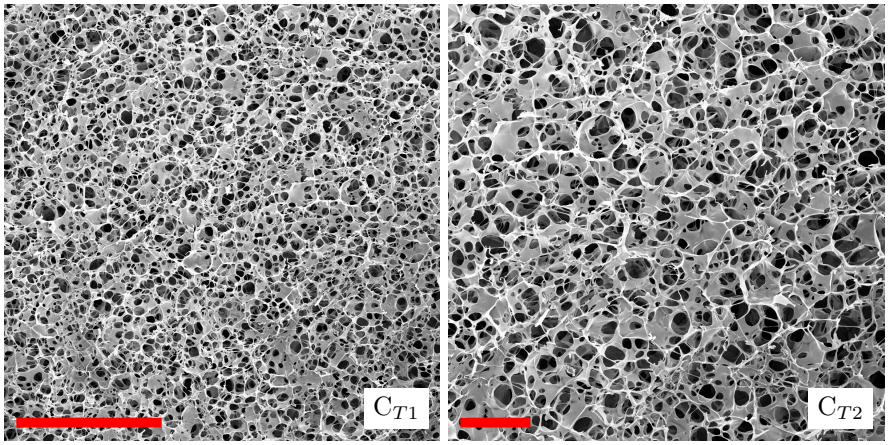

Figure 3.7: SEM pictures of ChipM (scale bar C_{T1} = 200 µm, C_{T2} = 50 µm)
Experiment C, top surface

3.3.2.3 Washing procedure

Once submitted to the freeze drying, the ChipM were thoroughly washed using a series of EtOH solutions with regular increase of amount of ammonia. During the last washing step, the pure ammonia solution containing the ChipM is subjected to vacuum in order to remove trapped air from the matrix.

This washing procedure is the same for all the samples and does not modify the porous structure of the obtained matrices as it has been proved by comparison of ChipM SEM pictures before and after it. However, it should be noticed that the initial ChipM aspect, characterized by an important rigidity and a low transparency (Figure 3.8a), evolves little by little with the increase of the ammonia concentration to become highly flexible and transparent in 0.1%(v:v) AS (Figure 3.8b). Another interesting aspect concerns the role of the vacuum step as it is clearly obvious that it removes all traces of air (Figure 3.8c).

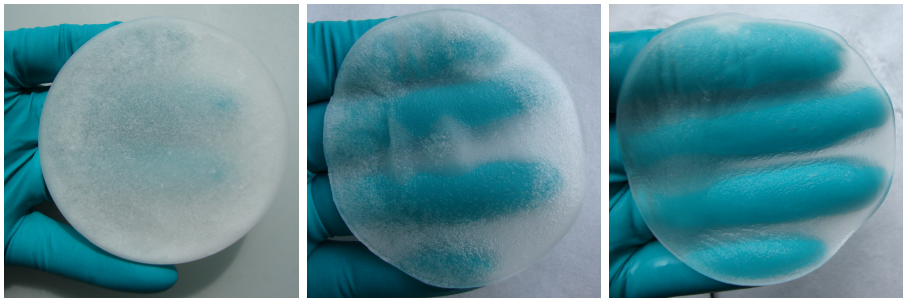

(a) 100% EtOH **(b)** 100% AS **(c)** 100% AS + vacuum

Figure 3.8: Optical pictures of ChipM, evolution during washing procedure

3.3.2.4 Cutting

The use of a mold to prepare ChipM necessarily induced the presence of a border effect. This border effect implies a local increase of the ChipM thickness as a consequence of the surface tension of the chitosan solution at the periphery of the mold.

This thickness discontinuity and the need to work with small pieces of ChipM for characterization, or for future surface modification, justified the cutting of the ChipM into small disks. Considering the fine porous structure of the ChipM, two methods were tested to find the less destructive.

The first method consists in a direct cutting after the freeze drying (Dry state cutting) while in the second method the ChipM is cut after the washing (Wet state cutting). SEM pictures of ChipM cross sections made by these two methods establish the second method as the best alternative. Indeed, on the ChipM cut in dry state (Figure 3.9B$_{s/d}$) pores appears collapsed and did not recover their initial shape. On the same time, pores of the ChipM cut in wet state (Figure 3.9B$_{s/w}$) conserved their shape.

Considering these results, the $\binom{2}{LA}|40)\cdot$ChipM used in this study were cut in disks after the washing procedure using a hollow punch. They were then conserved in hermetically closed glass containers with ammonia solution at 4 °C and protected from light.

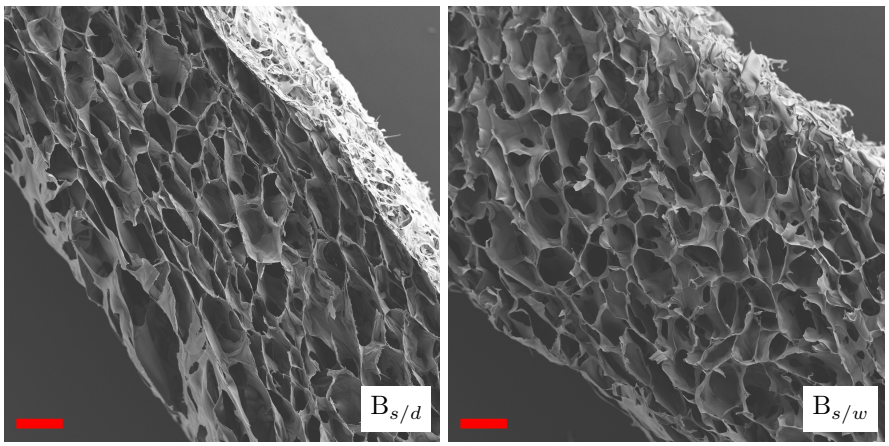

Figure 3.9: SEM pictures of ChipM from experiment B (scale bar 200 µm)
$B_{s/d}$: Section, dry state cut ; $B_{s/w}$: Section, wet state cut

3.3.3 Role of latent heat during freezing

As it has been proved by previous experiments, the differences in the pore size and inner structure of ChipM is influenced by the heat transfer rate during the TIPS process. A rapid rate of cooling better extracts the latent heat released during the freezing. For this reason the study of the heat exchange in the POMAP remains of great importance and a model of heat exchanges should help to control precisely the structure of the ChipM. Furthermore, in order to scale-up the POMAP cryo-unit a better understanding of the phase change and a good estimation of the temperature profile during the process is crucial.

In order to describe the role of the cooling rate on the structure of ChipM produced, a mathematical model based on FEM was developed. The introduction of latent heat in the heat transfer equation over a small temperature range is a key problem during modeling of a phase change. Moreover, during the freezing, sudden changes occur in properties of the material such as specific heat or thermal conductivity.

In this model, the influence of the latent heat on the TIPS process is investigated and more generally the effect of a phase change on the heat transfer is studied. Predictions are in accordance with experimental data and a better description of parameters and geometry should improve the quality of the results. Herein, the problem was solved using two hypothesis:

- Freezing of pure water instead of acidic polymer solution ;
- Simplified geometry (2 mm of aluminum, 2 mm of water and 1 mm of air).

3.3.3.1 Prediction results

This model uses FEM to solve heat equation in a one dimensional geometry for which thermodynamic characteristics are function of the position and of the time. Computation results (Figure 3.10) show interesting heat transfer through the simplified geometry.

Following the initial state, where the entire system is at the same temperature T_0 = -5 ℃, the temperature imposed at the bottom of the aluminum plate (x = 0 mm) regularly decreases with a cooling rate R_c = 1 ℃·min^{-1}. Under these conditions, the bottom part of the plate reaches the final temperature T_1 = -15 ℃ after τ = 600 s.

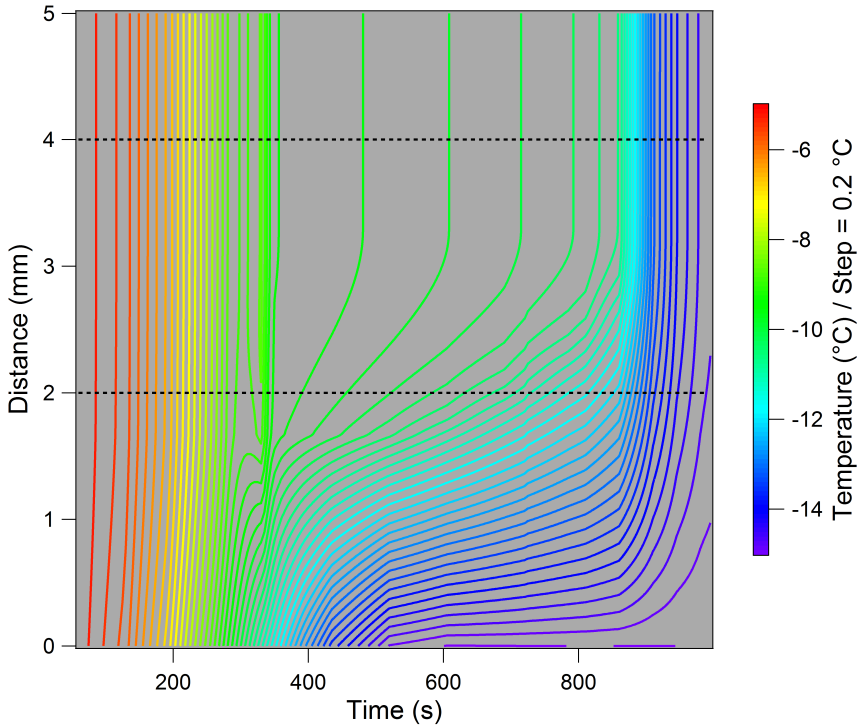

Figure 3.10: Temperature profile estimates using FEM model
[0 mm ; 2 mm] → Aluminum, [2 mm ; 4 mm] → Water, [4 mm ; 5 mm] → Air

Between t = 280 s and t = 360 s, a visible temperature change appears in the aluminum plate (x = 1.5 mm) and the temperature decreases slowly after that point. This corresponds to the time at which the water begins to freeze and releases latent heat. In the first seconds of the freezing, the temperature of the water (x = 3.0 mm) suddenly increases from T = -8.82 ℃ at t = 300 s to T = -8.55 ℃ at t = 330 s (Figure 3.11), before going down to T = -9.14 ℃ in less than 10 seconds at t = 340 s. This change is explained by the heat released during the phase change.

However, the freezing continues as the temperature of the water/ice stays around T = -10.00 ℃ during 300 seconds. This period is visualized as a steady state and the heat released by water is absorbed by surrounding ice crystals which melt and freeze again in a cyclic way until the cooling dissipates all the energy from the system as it can be observed after 850 seconds when the entire systems reaches T = -15.00 ℃. This is also confirmed by the cooling delay in the aluminium plate (x = 1.5 mm).

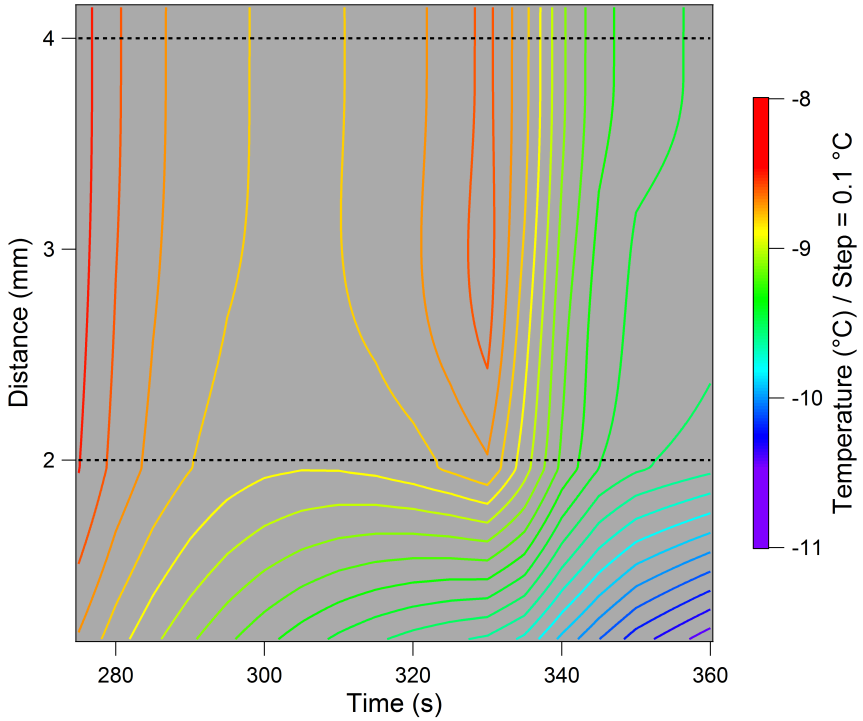

Figure 3.11: Detail of temperature profile estimates using FEM model (from figure 3.10)

3.3.3.2 Comparison with experimental results

By plotting the curves in a different way (Figure 3.12), the effect of the phase change in the temperature profile is more visible. While subjected to the temperature decrease in x = 0 mm, the system follows the decrease until the temperature of the solution reaches T = -9.00 ℃ (The transition interval was fixed to dT = 2 K and centered in T_{trans} = -10.00 ℃ for this model). At that point, the solution begins to freeze and the latent heat is released, increasing the temperature of the solution and of the mold. In the model, the linear dissipation of the energy (x = 0 mm) explains the steady state observed while the phase separation occurs. A final temperature drop brings the entire system to the final temperature when the TIPS is finished at t = 850 s.

The model predictions are validated by experimental data (Figure 3.13). Indeed, the temperature measured by the thermocouple in the POMAP is also characterized by a temperature increase around t = 350 s and a cooling delay until t = 850 s. It is important to notice that the experimental data were measured in the 6 mm aluminum plate of the POMAP. Moreover, the chitosan solution is not in direct contact with it but placed in a mold that adds 2 mm of steel between the thermocouple and the solution. This difference shows that the heat released experimentally is more important than in the model. However, this difference can be explained by the approximations of the model.

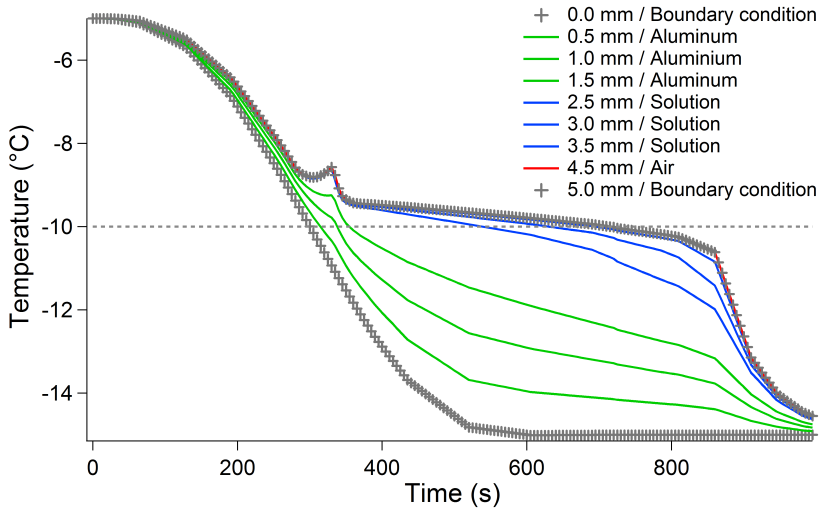

Figure 3.12: Temperatures estimates using FEM model (from figure 3.10 cross section)

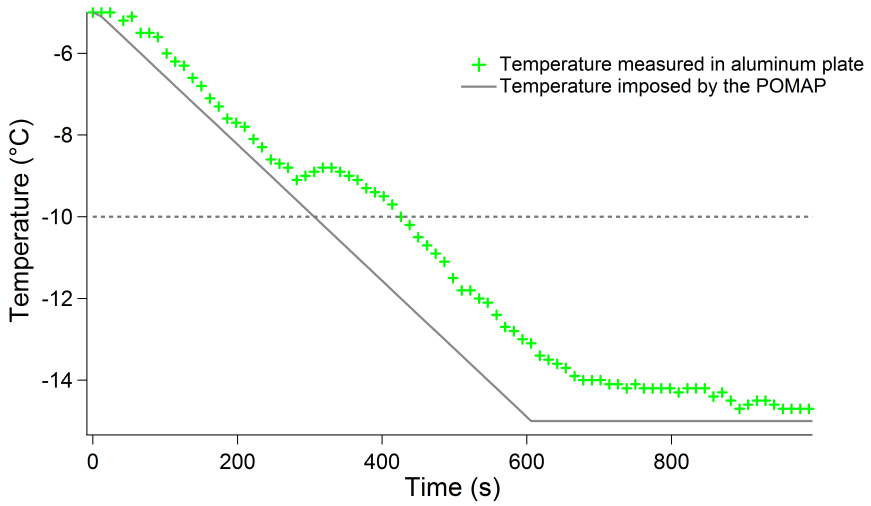

Figure 3.13: Experimental temperatures in POMAP

Further studies would make it possible to introduce the latent heat of demixing for the chitosan[42] and for the lactic acid.

Finally, the porous structure of the scaffold produced using the TIPS method can be modified by controlling the area of the latent heat peak. A fine control of this peak area, for example by increasing the PM capacity during the phase change, should allow a perfect control of the pore structure of the scaffold. Significant improvements of the POMAP prototype are in progress to further optimize the system.

3.4 Experimental section

3.4.1 General materials and methods

3.4.1.1 Chemicals

DCl: 20%(w:v), in deuterium oxide, 100 atom% D ; D_2O: 99.8 atom% D ; TSP-*d4*: 99 atom% D (ARMAR AG, Dottingen, CH) ; Ammonium hydroxide solution: ACS reagent, 28.0-30.0% NH_3 basis ; Chitosan: medium molecular weight (190,000 - 310,000 g·mol^{-1}) with a DDA between 75% and 85% ; *DL*-lactic acid: $\sim$ 90% (T) (Sigma-Aldrich Chemie GmbH, Buchs, CH) were used as received. Milli-Q water with resistivity of more than 18.2 MΩ·cm was provided by a Millipore Milli-Q filtering system with filtration through a 0.22 µm Millipak filter.

3.4.1.2 Characterization

^{1}H-NMR spectra were recorded at 27 °C on a Bruker AVIII-600 (600 MHz). Acquisition time (AQ) and relaxation delay (D1) were set to 1 s and 12 s respectively. Using 90° pulses, 128 scans were acquired (experiment time = 28 min so $\sim$ 13 seconds per pulse). The spectral width and data points were set to 8,000 Hz and 32,000 points respectively. Chemical shifts are expressed in ppm downfield from internal TSP-*d4* (0.00 ppm) reference. SEM micrographs were obtained using a Supra 40 (Carl Zeiss AG, Germany). Samples were coated using a gold sputter (45 s, 20 mV) prior to observation at 10 kV.

3.4.2 Chitosan characterization

5 mg of chitosan were dissolved in a NMR tube containing a 2%(v:v) DCl solution in D_2O and heated at 70 °C for one hour to speed up the dissolution. By working at 27 °C, the solvent residual peak (5.04 ppm) moves away from the integration area. As the data treatment is realized between 1.7 ppm and 4.4 ppm this method allows measurement with higher precision even with chitosan having high water content. The DDA value was determined from the relative integrals of combined H_2-H_6 protons (Figure 3.14) and acetyl groups, including *N*-acetyl and AcOH. Indeed, the acidic conditions lead to the hydrolysis of some of the *N*-acetyl groups and finally to the production of free AcOH. Therefore, both the *N*-acetyl and the AcOH signals were considered for the signal integration.

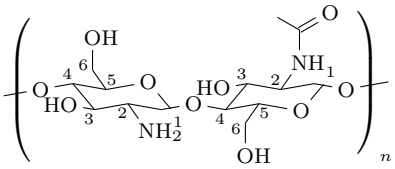

Figure 3.14: Labelled chitosan structure

^{1}H-NMR (600 MHz, D_2O/DCl δ**)** 2.08 (CH_3, NAc), 2.22 (AcOH), 3.20 (H_2, GlcNH), 3.77 (H_3-H_6), 3.93 (H_2, GlcNAc), 4.58 (H_1, GlcNAc), 4.90 (H_1, GlcNH).

3.4.3 ChipM preparation

3.4.3.1 Solution preparation

3.4.3.1.a Lactic acid solution (LA)

The 2%(w:v) LA was prepared by diluting 2 g of acid with water for a total volume of 100 ml. The use of a (w:v) concentration is justified by the viscosity of the lactic acid which makes the volume measurement difficult. Once prepared, the pH of the solution was compared to the predicted pH value which is about 2.28 ± 0.050 (Appendix B).

3.4.3.1.b Ammonia solution (AS)

The 0.1%(v:v) ammonium hydroxide solution was prepared by diluting 100 µl of ammonia with water for a total volume of 100 ml. Once prepared, the pH of the solution was compared with the predicted pH value which is about 10.70 ± 0.0007 (Appendix B).

3.4.3.1.c Chitosan solution

Dissolution

Chitosan solutions were prepared by dissolving 2 g of the polymer in 100 ml of LA. The final volume is not of 100 ml so the solution is not called X%(w:v).

Clarification and degassing

After dissolution, chitosan solutions contained impurities and air bubbles. For the removal of trapped air, sonication appeared as a good alternative [30]. However, it does not remove solid impurities. Thus chitosan solutions were cleared and degassed by centrifugation at 3,000 rpm for 15 minutes [26].

3.4.3.2 ChipM production by TIPS

Three experiments were conducted to study the influence of freezing conditions on the ChipM structure. The volume and composition of the solutions are identical and the mold used to freeze them is the same. The freezing conditions are presented below:

Experiment	Freezing conditions
1	Constant temperature T = -12 °C in a freezer
2	Uncontrolled cooling rate from T_0 = -5 °C to T_1 = -15 °C
3	POMAP, controlled cooling rate from T_0 = -5 °C to T_1 = -15 °C

After the freezing steps, the frozen chitosan solutions were submitted to freeze drying during at least 12 hours using the same conditions.

3.4.3.2.a Molding

The mold used for this study consists of a stainless steel cylindrical flat bottom container (external ∅ = 112.25 mm, internal ∅ = 91.25 mm, bottom thickness = 2mm). For all experiments, the mold was carefully filled with 13 ml of chitosan solution, giving ∼ 2 mm thick solution film. Because of the high viscosity of the chitosan solution, a volumetric pump was necessary to obtain a precise volume determination. Once the mold was filled, the solution was gently distributed on the recipient by tilting it.

3.4.3.2.b TIPS process

Experiment A and B

For the experiment A, the mold was kept in the freezer at T = -12 ℃. The complete freezing of the chitosan solution was observed after three hours. In experiment B, the mold was initially exposed to an EtOH bath at T_0 = -5 ℃ using an external cooling device that controlled the temperature of the EtOH bath through a jacketed reactor vessels. After the equilibrium of temperatures, the EtOH bath was cooled down from T_0 = -5 ℃ to T_1 = -15 ℃. However, using this method the cooling rate could not be controlled by the cooling device as its capacity depends of the ambient temperature. Basically a minimum of 40 minutes was necessary to reach the final temperature.

Experiment C

The POMAP cryo-unit (Figure 3.15) consists of a thermally insulated chamber in which a cooling unit using PM is incorporated. The bottom part of the PM is maintained at T = -15 ℃ using an external cooling device. The advantages of the PM are their great sensitivity to any temperature change and the possibility to impose a controlled cooling rate, here from T_0 = -5 ℃ to T_1 = -15 ℃.

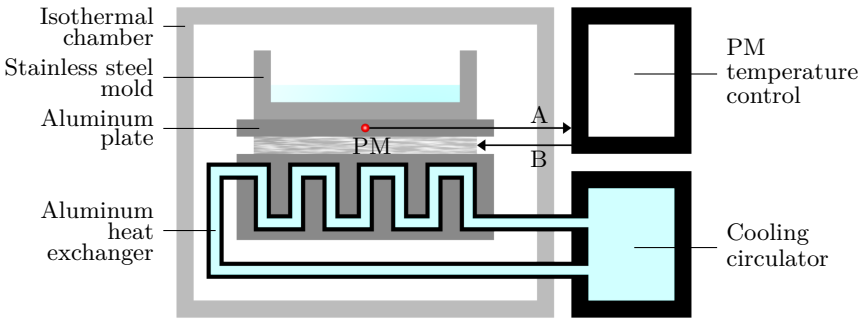

Figure 3.15: Schematic view of the POMAP for production of ChipM
PM: Peltier modules ; A: feed back from temperature sensor ;
B: continuous adjustment of PM temperature

For the experiment C, the chitosan solution was frozen using the POMAP. In that case, the mold was placed in the chamber at T_0 = -5 ℃ until the equilibrium. A linear decrease of the temperature was finally applied to the bottom of the mold with a pre-determined cooling rate R_c = 1 ℃·min^{-1} until T_1 = -15 ℃ were reached.

The temperature sensor allows at the same time the temperature determination in the aluminum plate and helps to adjust continuously the temperature of the chamber. According to the nomenclature (Appendix C), the resulting material for experiment C is called $\binom{2}{LA}|40)\cdot$ChipM.

The number *2* corresponds to the concentration of acid solution used to dissolve chitosan, here 2%(w:v), *LA* is the lactic acid solution. The number *40* describes on the same time the cooling rate and the mass of chitosan dissolved in 100 ml of LA as the 40th column on the nomenclature table.

3.4.3.2.c Washing

Once the freeze drying was realized, the obtained ChipM were immediately immersed in dry EtOH to avoid contact with humidity of the air. They were then submitted to a series of washing baths under gentle shaking during 20 minutes according to the procedure:

Wahsing step	Bath composition	Volume
1	100% EtOH	65 ml (5 x chitosan solution volume)
2	100% EtOH	
3	EtOH/AS (7:3/v:v)	
4	EtOH/AS (1:1/v:v)	
5	100% AS + vacuum	

The final vacuum step helps to remove air bubbles[36]. The final ChipM were kept in fresh ammonia solution, at 4 °C[37] and were protected from light.

Cutting

ChipM were cut in small disks using a hollow punch or a scalpel.

3.4.3.3 Characterization by electron microscopy

In all cases, ChipM were freeze dried a second time, directly after the washing step or after cutting, before being imaged by SEM.

3.4.4 Mathematical modelling of the TIPS

In order to describe the ChipM formation by TIPS and the release of heat during, a mathematical model based on FEM using COMSOL software is proposed.

3.4.4.1 Geometry and parameters definition

3.4.4.1.a Geometry

In order to model the freezing of a water film, a one dimensional geometry was created. This geometry consists in three layers which represent, in order, an aluminum plate (L_{Al} = 2 mm), a water film (L_{H_2O} = 2 mm) and finally a thin layer of air (L_{Air} = 1 mm) giving to the system a full size of L_{tot} = 5 mm.

3.4.4.1.b Thermodynamic parameters

The parameters introduced in the model are ρ the density in kg·m^{-3}, Cp the specific heat capacity in J·kg^{-1}·K^{-1}, T the temperature in K, and k the thermal conductivity in W·m^{-1}·K^{-1}. The values are given later as constants or functions of temperature and pressure, for air and aluminum. In the case of the water, the phase change induces its simultaneous presence in liquid and solid state with corresponding values:

Water in liquid state (liq)	Water in solid state (sol)
ρ_{liq} = 997 kg·m^{-3}	ρ_{sol} = 918 kg·m^{-3}
Cp$_{liq}$ = 4179 J·kg^{-1}·K^{-1}	Cp$_{sol}$ = 2052 J·kg^{-1}·K^{-1}
k$_{liq}$ = 0.613 W·m^{-1}·K^{-1}	k$_{sol}$ = 2.31 W·m^{-1}·K^{-1}

As a consequence, Cp$_{H_2O}$, k$_{H_2O}$ and ρ_{H_2O} are volume average of the form:

$$Cp_{H_2O} = \theta_{liq}\ Cp_{liq} + \theta_{sol}\ Cp_{sol} \tag{3.4}$$

$$k_{H_2O} = \theta_{liq}\ k_{liq} + \theta_{sol}\ k_{sol} \tag{3.5}$$

$$\rho_{H_2O} = \frac{\theta_{liq}\ \rho_{liq}\ Cp_{liq} + \theta_{sol}\ \rho_{sol}\ Cp_{sol}}{\theta_{liq}\ Cp_{liq} + \theta_{sol}\ Cp_{sol}} \tag{3.6}$$

where θ is the volumetric content of liquid or solid water in function of the temperature (Figure 3.16). Here the temperature of the transition is set as observed experimentally so T$_{trans}$ = -10 °C.

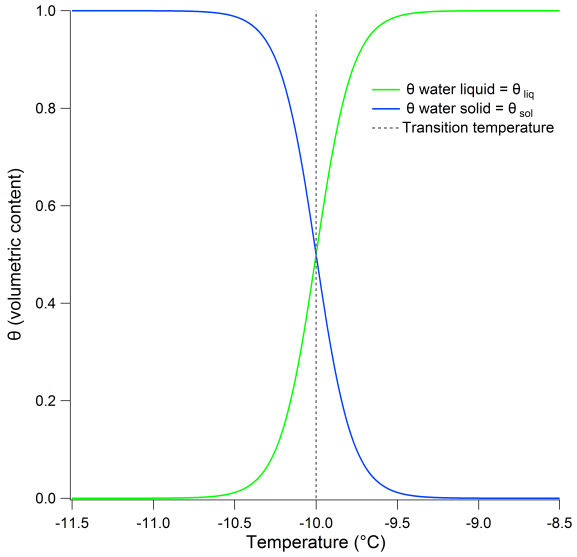

Figure 3.16: Volumetric content in liquid and solid water in function of the temperature

3.4.4.2 Meshing and mathematical modelling

3.4.4.2.a Boundary conditions

During the liquid to ice phase change, the density is modified, resulting in a volume expansion. To solve the heat equation, the Lagrangian coordinates are more appropriated since the deformation do not need to be taken into account.

After an equilibrium time of t_0, the initial temperature of the system is stable and fixed at T_0 = -5 °C. In the POMAP, the temperature in x = 0 mm decreases with a rate $R_c = 1.0$ °C·min^{-1} until the final temperature T_1 = -15 °C (Figure 3.17, in blue) is reached. On the other side, the top part of the system is considered as perfectly insulated. As a consequence, the boundary conditions for this model are:

$$\begin{cases} \mathbf{n} \cdot (-k\nabla T) = 0 & x = 5\ mm \\ \\ \begin{cases} T_0 & t < t_0 \\ T_0 - R_c\ t & t_0 \leq t \leq t_0 + \tau \\ T_1 & t > t_0 + \tau \end{cases} & x = 0\ mm \end{cases} \qquad \tau = \left| \frac{T_1 - T_0}{R_c} \right| \tag{3.7}$$

However, the FEM model is not able to work with the discontinuities of this piecewise function. To avoid this, the temperature decrease was modeled by a smoothed sigmoidal function $T_{imp}(t)$ (Figure 3.17, in green) that also brings the temperature from T_0 = -5 °C to T_1 = -15 °C in τ = 600 s but without discontinuity.

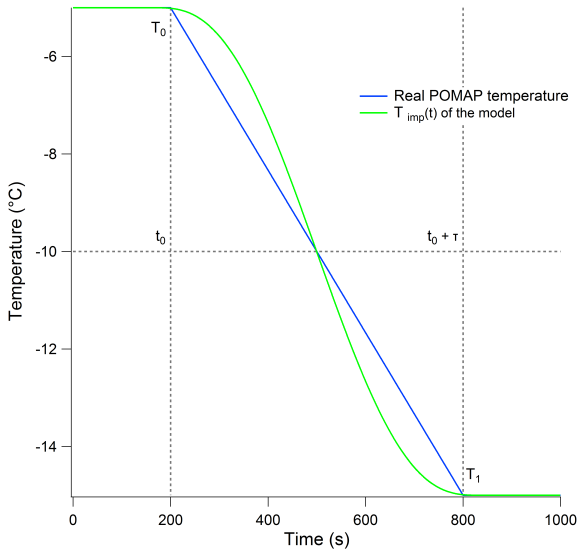

Figure 3.17: POMAP temperature piecewise function and model smoothed function $T_{imp}(t)$

As a consequence, the boundary conditions become:

$$\begin{cases} \mathbf{n} \cdot (-k\nabla T) = 0 & & x = 5\ mm & \\ & & & \tau = \left| \dfrac{T_1 - T_0}{R_c} \right| \\ \begin{cases} T_0 & t < t_0 & & \\ T_{imp}(t) & t_0 \leq t \leq t_0 + \tau & x = 0\ mm & \\ T_1 & t > t_0 + \tau & & \end{cases} & & & \end{cases} \tag{3.8}$$

3.4.4.2.b Phase change

During a phase change, energy is released. This energy is called latent heat of fusion and in the case of water $\lambda = 333.5$ kJ·kg^1. In the model the latent heat of fusion λ is incorporated in Cp_{H_2O} which becomes:

$$Cp_{H_2O} = \theta_{liq}\ Cp_{liq} + \theta_{sol}\ Cp_{sol} + \lambda\ D(T) \tag{3.9}$$

By adding the function D(T) in K^{-1}, this expression of the specific heat capacity describes the release of the latent heat as a normalized pulse around the temperature transition dT = 2K where liquid and solid coexist.

However, the integral of the function D(T) must equal unity to satisfy the following:

$$\int_{T_0}^{T_1} \rho_{H_2O}\ D(T)\ \lambda\ \ \mathrm{d}T = \rho_{H_2O}\ \lambda \tag{3.10}$$

3.4.4.3 Generalized description on COMSOL

A one dimensional geometry of the system was created as shown in the table 3.1. The mesh size was optimized for solution with 150 elements (maximum size 0.335 mm, minimum size 0.0015 mm) using the functions and the parameters describes previously.

3.4.4.4 Data treatment

A series of curves giving the temperature as function of the distance every 5 seconds during t_{tot} = 1,000 s were collected. This corresponds to t_0 = 200 s, τ = 600 s and another waiting time of t = 400 s to reach the equilibrium.

Data were converted on the IGOR-pro software to obtain a 3D surface giving the temperature as function of time and distance T = f(x,t).

Using this scatter plot, the isothermal contour plot was extracted as RGB values to describe the temperature, from $T_0 = (1,0,0)_{RGB}$ to $T_1 = (0,0,1)_{RGB}$ (Figure 3.10).

Finally, the curves giving T = f(t) for x = [0.5;1;1.5;2.5;3;3.5;4.5] were isolated (Figure 3.12).

Boundary $\mathbf{n} \cdot (-k\nabla T) = 0$	—
L_{air}: 1 mm $\rho_{air}\ Cp_{air}\ \frac{\partial T}{\partial t} = \nabla \cdot (-k_{air}\ \nabla T) + Q$	$R_{air} = 1.4$ Cp_{air} = f(T) by default ρ_{air} = f(P,T) by default k_{air} = f(T) by default
L_{H_2O}: 2 mm $\rho_{H_2O}\ Cp_{H_2O}\ \frac{\partial T}{\partial t} = \nabla \cdot (-k_{H_2O}\ \nabla T) + Q$	$R_{H_2O} = 1$ Cp_{H_2O} = f(θ_{liq},θ_{sol}) ρ_{H_2O} = f(θ_{liq},θ_{sol}) k_{H_2O} = f(θ_{liq},θ_{sol})
L_{Al}: 2 mm $\rho_{Al}\ Cp_{Al}\ \frac{\partial T}{\partial t} = \nabla \cdot (-k_{Al}\ \nabla T) + Q$	$R_{Al} = 1$ Cp_{Al} = 900 J·kg^{-1}·K^{-1} ρ_{Al} = 2700 kg·m^{-3} k_{Al} = 160 W·m^{-1}·K^{-1}
Boundary $T(t) = T_{imp}(t)$	—

Table 3.1: Mathematical description of the model

3.5 Bibliography

[1] Agnihotri, S. A., Mallikarjuna, N. N. & Aminabhavi, T. M. Recent advances on chitosan-based micro- and nanoparticles in drug delivery. *J. Control. Release* **100**, 5-28 (2004).

[2] Krajewska, B. Application of chitin- and chitosan-based materials for enzyme immobilizations: a review. *Enzyme Microb. Technol.* **35**, 126-139 (2004).

[3] Ogawa, K., Yui, T. & Okuyama, K. Three D structures of chitosan. *Int. J. Biol. Macromolec.* **34**, 1-8 (2004).

[4] Dutta, P. K., Dutta, J. & Tripathi, V. S. Chitin and chitosan: chemistry, properties and applications. *J. Sci. Ind. Res.* **63**, 20-31 (2004).

[5] Ravi Kumar, M. N. V. Chitin and chitosan fibers: a review. *Bull. Mater. Sci.* **22**, 905-915 (1999).

[6] Fernandes, L. L. *et al.* Cytocompatibility of chitosan and collagen-chitosan scaffolds for tissue engineering. *Polim.: Cienc. Tecnol.* **21**, 1-6 (2011).

[7] Jeuniaux, C. & Voss-Foucart, M. F. Chitin biomass and production in the marine environment. *Biochem. Syst. Ecol.* **19**, 347-356 (1991).

[8] Pillai, C. K. S., Paul, W. & Sharma, C. P. Chitin and chitosan polymers: Chemistry, solubility and fiber formation. *Prog. Polym. Sci.* **34**, 641-678 (2009).

[9] Batista, M. K. S., Pinto, L. F., Gomes, C. A. R. & Gomes, P. Novel highly-soluble peptide-chitosan polymers: Chemical synthesis and spectral characterization. *Carbohydr. Polym.* **64**, 299-305 (2006).

[10] Lavertu, M. *et al.* A validated 1H NMR method for the determination of the degree of deacetylation of chitosan. *J. Pharm. Biomed. Anal.* **32**, 1149-1158 (2003).

[11] Fernandez-Megia, E., Novoa-Carballal, R., Quinoa, E. & Riguera, R. Optimal routine conditions for the determination of the degree of acetylation of chitosan by 1H-NMR. *Carbohydr. Polym.* **61**, 155-161 (2005).

[12] Wang, X., Yan, Y. & Zhang, R. A comparison of chitosan and collagen sponges as hemostatic dressings. *J. Bioact. Compat. Polym.* **21**, 39-54 (2006).

[13] Zheng, L.-Y. & Zhu, J.-F. Study on antimicrobial activity of chitosan with different molecular weights. *Carbohydr. Polym.* **54**, 527-530 (2003).

[14] Hamidi, M., Azadi, A. & Rafiei, P. Hydrogel nanoparticles in drug delivery. *Adv. Drug Deliv. Rev.* **60**, 1638-1649 (2008).

[15] Chun, H. J., Kim, G.-W. & Kim, C.-H. Fabrication of porous chitosan scaffold in order to improve biocompatibility. *J. Phys. Chem. Solids* **69**, 1573-1576 (2007).

[16] Chen, G., Ushida, T. & Tateishi, T. Scaffold design for tissue engineering. *Macromol. Biosci.* **2**, 67-77 (2002).

[17] Heinemann, C. *et al.* In vitro osteoclastogenesis on textile chitosan scaffolds. *Eur. Cells Mater.* **19**, 96-106 (2010).

[18] Ho, M.-H. *et al.* Preparation of porous scaffolds by using freeze-extraction and freeze-gelation methods. *Biomaterials* **25**, 129-138 (2004).

[19] Ko, Y.-G., Kawazoe, N., Tateishi, T. & Chen, G. Preparation of chitosan scaffolds with a hierarchical porous structure. *J. Biomed. Mater. Res., Part B Appl. Biomater* **93B**, 341-350 (2010).

[20] Brugnerotto, J. *et al.* An infrared investigation in relation with chitin and chitosan characterization. *Polymer* **42**, 3569-3580 (2001).

[21] Hojo, K. *et al.* Facile synthesis of a chitosan hybrid of a laminin-related peptide and its antimetastatic effect in mice. *J. Pharm. Pharmacol.* **52**, 67-73 (2000).

[22] Ang, T. H. *et al.* Fabrication of 3D chitosanhydroxyapatite scaffolds using a robotic dispensing system. *Materials Science and Engineering: C* **20**, 35-42 (2002).

[23] Chen, L. *et al.* A human-like collagen/chitosan electrospun nanofibrous scaffold from aqueous solution: Electrospun mechanism and biocompatibility. *J. Biomed. Mater. Res., Part A* **99A**, 395-409 (2011).

[24] Ji, C., Annabi, N., Khademhosseini, A. & Dehghani, F. Fabrication of porous chitosan scaffolds for soft tissue engineering using dense gas CO2. *Acta Biomater.* **7**, 1653-1664 (2011).

[25] Ko, H.-F., Sfeir, C. & Kumta, P. N. Novel synthesis strategies for natural polymer and composite biomaterials as potential scaffolds for tissue engineering. *Phil. Trans. R. Soc. A* **368**, 1981-1997 (2010).

[26] Hsieh, C.-Y. *et al.* Analysis of freeze-gelation and cross-linking processes for preparing porous chitosan scaffolds. *Carbohydr. Polym.* **67**, 124-132 (2007).

[27] Huang, R. Y. M., Moon, G. Y. & Pal, R. N-acetylated chitosan membranes for the pervaporation separation of alcohol/toluene mixtures. *J. Membr. Sci.* **176**, 223-231 (2000).

[28] Kasaai, M. R. Determination of the degree of N-acetylation for chitin and chitosan by various NMR spectroscopy techniques: A review. *Carbohydr. Polym.* **79**, 801-810 (2010).

[29] Sano, M. *et al.* Relationship between solubility of chitosan in alcoholic solution and its gelation. *Chem. Pharm. Bull.* **47**, 1044-1046 (1999).

[30] Escobar-Chaavez, J. J. *et al.* Transdermal nortriptyline hydrocloride patch formulated within a chitosan matrix intended to be used for smoking cessation. *Pharm. Dev. Technol.* **16**, 162-169 (2011).

[31] Khan, T. A., Peh, K. K. & Ch'ng, H. S. Mechanical, bioadhesive strength and biological evaluations of chitosan films for wound dressing. *J. Pharm. Pharmaceut. Sci.* **3**, 303-311 (2000).

[32] Noel, S. P., Courtney, H. S., Bumgardner, J. D. & Haggard, W. O. Chitosan sponges to locally deliver amikacin and vancomycin: a pilot in vitro evaluation. *Clin. Orthop. Relat. Res.* **468**, 2074-2080 (2010).

[33] Katchalsky, A., Shavit, N. & Eisenberg, H. Dissociation of weak polymeric acids and bases. *J. of Polym. Sci.* **13**, 69-84 (1954).

[34] Furukawa, M., Farinato, R. S. & Kokufuta, E. Potentiometric titration behavior of poly(acrylic acid) within a cross-linked polymer network having amide groups. *Colloid Polym. Sci.* **286**, 1452-1453 (2008).

[35] Roberts, G. A. F. *Chitin Chemistry*, Macmillan Press, London (1992).

[36] Madihally, S. V. & Matthew, H. W. T. Porous chitosan scaffolds for tissue engineering. *Biomaterials* **20**, 1133-1142 (1999).

[37] Viyoch, J., Patcharaworakulchai, P., Songmek, R., Pimsan, V. & Wittaya-Areekul, S. Formulation and development of a patch containing tamarind fruit extract by using the blended chitosan-starch as a rate-controlling matrix. *Int. J. Cosmet. Sci.* **25**, 113-125 (2003).

[38] Van, V. S. *et al.* Porous Gelatin Hydrogels: 1. Cryogenic Formation and Structure Analysis. *Biomacromolecules* **8**, 331-337 (2007).

[39] O'Brien, F. J., Harley, B. A., Yannas, I. V. & Gibson, L. Influence of freezing rate on pore structure in freeze-dried collagen-GAG scaffolds. *Biomaterials* **25**, 1077-1086 (2003).

[40] Kang, H.-W., Tabata, Y. & Ikada, Y. Fabrication of porous gelatin scaffolds for tissue engineering. *Biomaterials* **20**, 1339-1344 (1999).

[41] Russell, A. B., Cheney, P. E. & Wantling, S. D. Influence of freezing conditions on ice crystallisation in ice cream. *J. Food Eng.* **39**, 179-191 (1999).

[42] Van, E. P. T. & Smolders, C. A. Phase separation of polymer solutions. Calculation of the cloudpoint curve with a concentration and temperature-dependent free energy correction parameter. *Eur. Polym. J.* **9**, 157-167 (1973).

Chapter 4

Photosensitive ibuprofen loaded porous structure

Abstract: This chapter presents the surface modifications of chitosan porous matrices. The modifications described are of two types. One concerns a primary coupling of photolinkers PL1 and PL2 or the acetylation of the matrices. At the same time, the use of PL1-Fmoc and its deprotection makes the quantification of the surface loading possible. The second type of the surface modification is the attachment of ibuprofen at the very end of the photolinker PL2. Ibuprofen loaded matrices will then be used to demonstrate the drug release upon illumination of the matrices. The suggested chemistry, based on peptide synthesis, is very flexible and one-pot coupling conditions have been developed using simple and highly efficient conditions to obtain drug loaded matrices.

4.1 General remarks

Solid phase surface modification is known since the 60's[1,2,3]. This method allows an easy production of the final product with high purity as a simple washing of the support is sufficient to remove excess reagents.

The first use of solid phase synthesis for peptide synthesis was quickly followed by the introduction of photolinkers[4]. Reaction between an amine and a carboxylic acid is thermodynamically not favorable as an acid-base reaction normally occurs to form a stable salt. For this reason, amide bond formation usually requires activation of a carboxylic acid moiety in the presence of coupling reagents. Activation consists of the replacement of the hydroxyl group of the carboxylic acid with a leaving group. The *in-situ* activation have been described using carbodiimides, phosphonium or phosphinic salts such as the Castro's reagent (BOP). However, since the BOP is known to produce the highly toxic HMPA as by-product[5,6], other related salts that produce less toxic wastes have been developed[7].

This is the case for aminium/uronium salts such as HATU, HBTU or TBTU. Indeed in the presence of tertiary amine bases such as NMM, DIPEA or TEA[7], these salts have proved to be more effective than those carried out with phosphonium reagents or carbodiimides. One of the most reactive, HATU, is expensive and an alternative is the HBTU (Figure 4.1a). However, since these salts are known to be guanidylation agents, it has become popular to introduce auxiliary nucleophiles as for the carbodiimides, to avoid side reactions[7]. The most commonly used additive remaining the HOBt (Figure 4.1b).

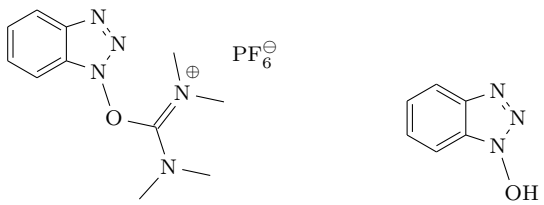

(a) HBTU **(b)** HOBt

Figure 4.1: Chemical structures of coupling reagents

4.2 Strategy

Surface immobilization represents a key step to obtain the proof of concept for the ATTS. Since the photolinker synthesis has been established (Chapter 2) and the polymer support production proposed (Chapter 3), this part consists to gather them in order to produce photosensitive drug loaded matrices able to release ibuprofen when exposed to UV light. Considering the wide-spread use of photolinkers in solid phase peptide synthesis[8,9,10,11] this work is based on peptide synthesis chemistry. The synthesis method proposed is divided into primary and secondary coupling reactions.

The primary coupling, meaning a permanent attachment is realized, with photolinkers PL1-Fmoc and PL2 on ChipM, using the peptide synthesis method with HBTU, HOBt and DIPEA [5,6]. Another primary coupling, the acetylation of the chitosan is described to obtain chitin porous matrices.

The secondary coupling reactions are temporal attachment. The only secondary coupling presented is the immobilization of the drug model, the ibuprofen, to the photolabile moiety of the photolinker. This reaction is realized on PL2 using similar method than for primary coupling. However, in that case the reaction consists in a Steglich esterification [12].

4.2.1 Solvent system

The choice of the solvent is an important parameter considering the material and the structure of the support. Indeed, the chitosan is stable in common organic solvents used for the surface attachment of the photolinker [13,14,15,16], but its porous structure implies the choice of a solvent in which all compounds (reagents, reactants and residues) are soluble to avoid any deposition inside of the structure. DMF is often used in peptide synthesis, but since it is recognized as possible carcinogen, it tends to be baned from industrial process.

A good alternative, the NMP presents the same characteristics than DMF as water miscibility and high polarity but with lower toxicity. Finally, the solvent was the same for all the reactions in order to avoid the time consuming phase of solvent exchange in the porous structure.

4.2.2 Photolinker coupling on support

The photolinker attachment on the chitosan structure is realized using the well known solid phase peptide synthesis technique [7,15,16,17,18,19,20]. The coupling procedure is the same for PL1-Fmoc and PL2. However, in the case of PL1-Fmoc, the Fmoc group has to be removed after coupling. This deprotection is usually realized using a base, mainly secondary amines [21].

4.2.3 Drug coupling on photolinker

4.2.3.1 Ibuprofen as drug model

The proof of concept is established by the release of a carboxylic acid bearing molecule from PL2. Ibuprofen, known as 2-(4-(2-methylpropyl)phenyl) propanoic acid (Figure 4.2), is a non steroidal anti-inflammatory drug used in the treatment of acute and chronic arthritic conditions and was chosen as drug model for this study. It is a weak acid ($pK_a = 4.41$), soluble in organic solvents with variable water solubility at 25 °C from 0.19 mg·ml^{-1} at pH = 1 up to 1000 mg·ml^{-1} at pH = 10. Transdermal delivery of ibuprofen using various formulations has been described in the literature [22,23].

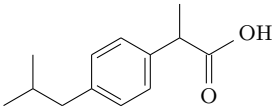

Figure 4.2: Chemical structure of ibuprofen

4.2.3.2 Ibuprofen attachment on photolinker

The attachment of ibuprofen to the photolinker PL2 is achieved using the Steglich esterification [12]. In this reaction the same reagents as for the amide bond formation are used but a pyridine derivative, the DMAP is introduced as a catalyst [24,25].

4.3 Results and discussion

4.3.1 Solvent exchange

After their production by TIPS, ChipM were stored in 0.1%(v:v) AS (Chapter 3). However, before any surface modification, a solvent exchange is necessary as the chemical reactions are conducted in NMP. Moreover, water traces are susceptible to disturb coupling reactions. For solvent exchange, ChipM were soaked in 5%(v:v) DIPEA in NMP [14,15]. As a consequence, the initial transparent and flexible ChipM became hard and non deformable anymore.

4.3.2 Primary coupling on ChipM with PL1

Quantification in solid phase is a problematic topic. PL1-Fmoc is not considered as a good candidate for the release of drug. However, its reactivity can be considered as close enough to the PL2 reactivity because of their similar structure. Its capacity to release the DBF can be used to quantify the surface loading and to optimize coupling conditions of PL2. The coupling of PL1-Fmoc was realized on ChipM produced using experiment B conditions (Chapter 3).

4.3.2.1 Coupling and deprotection of PL1-Fmoc

The use of chitosan for solid phase peptide synthesis is well reported [14,15,16,26]. For this reason, the coupling reaction of the PL1-Fmoc on ChipM was performed using classical solid phase peptide coupling conditions (Figure 4.3).

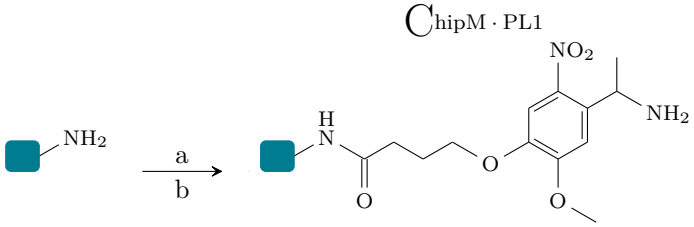

Figure 4.3: ChipM·PL1 synthesis
Reagents are herein listed:
(a) PL1-Fmoc, HBTU, HOBt, DIPEA in NMP ;
(b) 2%(v:v) DBU in NMP

The coupling agent used was HBTU which is considered as one of the most efficient coupling agent [20]. At the same time, HOBt was introduced to improve the yields and DIPEA to activate the PL1-Fmoc. After the reaction, the initial became yellow which is the characteristic of the sensitive photolinker.

Qualitatively, a ChipM treated under the same conditions but without coupling agent stayed completely white, proving that the photolinker is not trapped by the ChipM walls but coupled to the surface.

The second chemical reaction conducted on the modified ChipM is the removal of the Fmoc group from the PL1-Fmoc. Usually 20%(v:v) piperidine in DMF [15,26,27,28] or NMP [29] is used. However, the use of highly concentrated piperidine solution implies a difficult washing of the porous support. For this reason, the less volatile and less toxic DBU (Figure 4.4) was preferred [8].

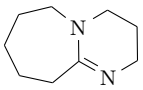

Figure 4.4: Chemical structure of DBU

Indeed, it was demonstrated that submitting Fmoc protected amino acid to a 2%(v:v) DBU solution during 5 minutes [28] induced a fast, efficient and quantitative Fmoc cleavage [30,31], proving its better efficiency compared to piperidine cleavage [8,19,32]. Moreover, the resulting DBF product (Figure 4.5) can be precisely quantified [28,31,32,33,34].

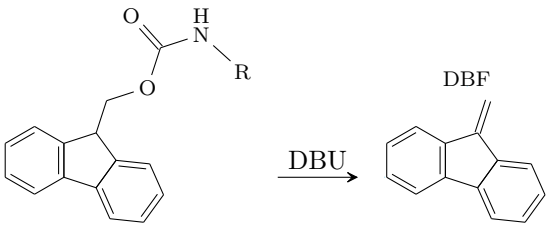

Figure 4.5: DBU cleavage of the Fmoc group

4.3.2.2 Quantification of PL1 loading

Several methods are reported for the determination of amine loading on solid phase using the ninhydrin test [26,35,36] or the bromophenol blue test [37]. Another method consists of indirected quantification by the determination of DBF released after the Fmoc deprotection. However, attempts to DBF isolation results in an insoluble polymeric species [33].

As a consequence, calibrations were carried out by its *in-situ* production [28], submitting Fmoc protected glycine (Gly-Fmoc) solutions to DBU [33] before analyzing DBF concentration by HPLC. As internal standard, a known concentration of anthracene was incorporated. The advantage of the anthracene is that its peak is close enough to the DBF peak, allowing a complete analysis in 10 minutes.

4.3.2.2.a Calibration

Considering the need of the loading determination with high precision, a calibration method is suggested. The calculations reveal a Pearson correlation coefficient $\rho^2 = 0.999839$ proving a good correlation between the DBF concentration in calibration solutions and absorbance signal.

However, the homoscedasticity test gives $\chi^2_{OBS} = 21.7 > \chi^2_5 = 11.1$, which means that at least one non considered parameter intervenes in the calibration. This can be explained by the method used to prepared the calibration solutions as the uncertainties on volume increases with the working volume.

Nevertheless, 4 calibration regressions consisting into two linear models and two quadratic models were established. For the linear model without constant (1.WOC), the test of validity gives $F_{OBS}(1.WOC) = 78.6 > F_{5,24}(0.95) = 2.6$. This value is too high to confirm the rightness of the regression and proves that the calibration did not reach the quality required.

However, since this 1.WOC model does not modify the proof of concept results, it is used without correction. Finally, the method proposed reveals that a correlation coefficient ρ^2 close to one is not representative for a good calibration. The problem met in this study clearly demonstrate the very high sensibility of this calibration method.

4.3.2.2.b Theoretical loading determination

The theoretical loading is the amount of amino groups per mass unit of chitosan. This value can be calculated using DDA, DP and $Mw_{chitosan}$ determined in Chapter 3 and the relation:

$$n_{NH_2} = \frac{DDA\ DP}{Mw_{chitosan}} \tag{4.1}$$

Since the chitosan molecular weight $Mw_{chitosan} \in [190{,}000;310{,}000]$ g·mol^{-1}, the result is $n_{NH_2} \in [4.8453;4.8455]$ mmol·g^{-1}. It is interesting to notice that the n_{NH_2} value is almost independent of $Mw_{chitosan}$. This means that if the DP influences the physical characteristics of the ChipM, its impact on the surface chemistry is low.

By comparing with reported values giving $n_{NH_2} \in [0.08;0.35]$ mmol·g^{-1} [15], it is clear that all amine moieties are not accessible for chemical reactions. A way to increase there accessibility is to increase the specific surface of the material.

4.3.2.2.c Quantification

Estimation of ChipM mass

The quantification study was carried on ChipM produced using conditions of experiment B (Chapter 3). Briefly, a chitosan solution (V = 13.0 cm^3) obtained by dissolving 2 g of polymer in 100 ml of LA was frozen in a stainless steel mold (internal diameter $Ø_1 = 9.125$ cm), before freeze drying and washing.

In order to simplify calculations a 2%(w:v) chitosan solution without surface tension is considered. As a consequence, the thickness of the ChipM is uniform and equal to $H_{ChipM} = 0.199$ cm. The matrix was finally cut into disks having a radius $Ø_2 = 2.8$ cm. The corresponding mass of chitosan in these portions can be estimated to $m_{chitosan}(Ø = 2.8) = 24.481$ mg.

Loading results

By working with 5 ChipM in 10 ml of NMP, the quantification of DBF concentration gives a loading of 168.99 µmol·g^{-1}.

This value is comparable with the expected loading found in literature and stays far from the theoretical loading as it represents ∼ 3.48% of theoretical amine amount. However, by comparing modification conditions with those used to obtain a loading close to 350 µmol·g^{-1} [15], it can be noticed by working with a 10 times smaller concentration, a good loading value is reached (Table 4.1). This can be explained by the procedure used to produce the porous matrix as the specific surface is certainly much higher in this case.

—	Experimental conditions	Conditions from literature [15]
Base	∼ 30 mM (3 eq.)	400 mM (6 eq.)
Coupling agent	∼ 20 mM (2 eq.)	300 mM (4.5 eq.)
HOBt	∼ 20 mM (2 eq.)	300 mM (4.5 eq.)
Linker	∼ 10 mM (1 eq.)	66.6 mM (1 eq.)
Chitosan	122.40 mg (5 ChipM)	150 mg
Loading	168.99 µmol·g^{-1}	80 to 350 µmol·g^{-1}

Table 4.1: Comparisons of experimental conditions with literature

An obvious way to increase the coupling would be to increase the molarity of the reagents, change the temperature of the reaction [8,15] or use microwave irradiations [27]. An other option consists to work with a fully deacetylated chitosan. Moreover, by optimizing the pore size of the support material, an important increase of the specific surface is expected. This is confirmed by the pore size observed on ChipM produced on the POMAP (Experiment C, Chapter 3).

4.3.3 Primary coupling on ChipM with PL2

In this part of the study, the temperature of the reaction was set at 50 °C, photolinker concentration was multiplied by 5 and other reactant concentrations by 7 (Figure 4.6). The coupling of PL2 was realized on ChipM produced on the POMAP (Experiment C, Chapter 3).

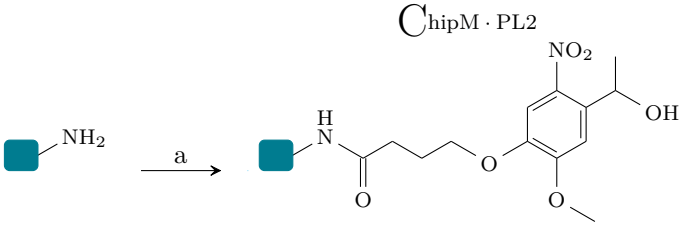

Figure 4.6: ChipM·PL2 synthesis
Reagents are herein listed :
(a) PL2, HBTU, HOBt, DIPEA in NMP

A qualitative observation of the obtained material compared to the material produced previously with PL1 shows a really much more efficient loading. Indeed, the $\left({}^{2}_{LA}|40\right)\cdot$ChipM·PL2 is strongly colored in yellow while the ChipM·PL1 appears light yellow (Figure 4.7). Difference can come from the really important excess of reagents, from the temperature at which was conducted the reaction or from the surface area that should be higher with $\left({}^{2}_{LA}|40\right)\cdot$ChipM.

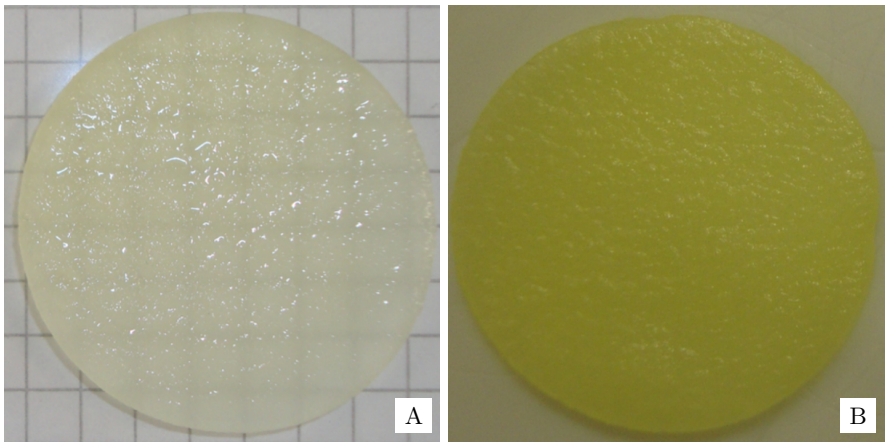

Figure 4.7: Coupling comparison for PL1 and PL2 on ChipM
A: ChipM·PL1 ; B: $\left({}^{2}_{LA}|40\right)\cdot$ChipM·PL2

4.3.4 Primary coupling on ChipM with acetylation

Among many reactions involved in chitosan modification, the acylation of chitosan has gained special interest [17] since the capping of remaining amine moieties by acetylation gives the possibility to produce water stable chitin porous matrices. Indeed, free amino groups are responsible for the good solubilization properties of chitosan in acidic solutions. In the frame of this project, chitin porous matrices could serve as support for passive TTS by simple loading with a drug loaded dM.

Many different methods exist for the acetylation of chitosan using mixtures of Ac_2O with DIPEA in DMF [8,9,27,29,38], Ac_2O with pyridine [15] or derivates [39] and also AcOH with coupling agents as for peptide synthesis [40]. Here, a mixture of Ac_2O/DIPEA in NMP [19] was used to convert $\left({}^{2}_{LA}|40\right)\cdot$ChipM into chitin porous matrices or $\left({}^{2}_{LA}|40\right)\cdot$ChipM·OAc (Figure 4.8).

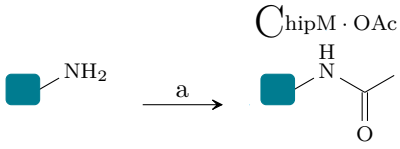

Figure 4.8: ChipM·OAc synthesis
Reagents are herein listed:
(a) Ac_2O, DIPEA in NMP

4.3.5 Secondary coupling on ChipM PL2 with ibuprofen

Using the $\left(^{2}_{LA}|40\right)\cdot$ChipM·PL2 previously prepared, ibuprofen loaded matrices were produced. The chemical reaction involved is an esterification, also known as Steglich esterification [12]. This reaction is similar to the peptide synthesis as it consists to activate the carboxylic acid to facilitate the reaction with the hydroxyl group of the PL2.

Compared to the Fischer esterification, this reaction presents the advantage to be quantitative, which is particularly interesting for the coupling of expensive drugs. The reaction (Figure 4.9) was conducted using DIC as coupling agent in the presence of HOBt [39].

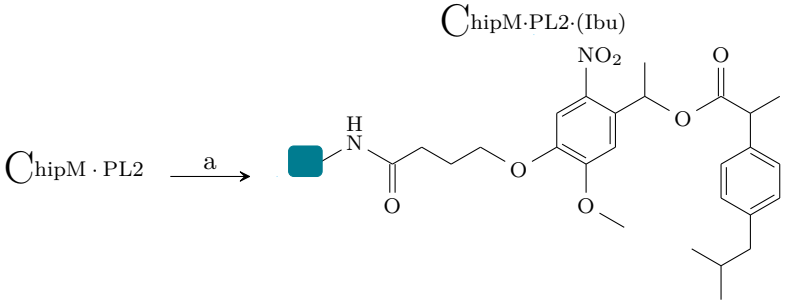

Figure 4.9: ChipM·PL2·(Ibu) synthesis
Reagents are herein listed :
(a) Ibuprofen, DIC, HOBt, DMAP in NMP

The quantification of ibuprofen surface loading has not been realized for reasons evoked before. However, indirect methods based on saponification and quantification of the released acid in solid phase exist [40]. According to the nomenclature for secondary couplings (Appendix C), the matrices are called ChipM·PL2·(Ibu) .

4.4 Experimental section

ChipM used for surface modification were produced using the TIPS method described in Chapter 3. They were cut in small disks of Ø = 2.8 cm in diameter using a hollow punch. Differences between ChipM used for surface modifications come from the freezing procedure.

For PL1 coupling and acetylation reaction, ChipM were obtained using the experiment B procedure (Chapter 3) while for PL2 and ibuprofen coupling, ChipM were obtained using the POMAP cryo-unit (Chapter 3).

4.4.1 General materials and methods

4.4.1.1 Chemicals

PL1-Fmoc: (abcr GmbH & Co. KG, Karlsruhe, D) ; TFA: gradient tested for HPLC peptide and protein analysis, UV cutoff $\lambda = 210$ nm (Mallinckrodt Baker B.V., Deventer, NL) ;

ACN: CHROMASOLV® gradient grade, for HPLC, ≥ 99.9% ; Ac_2O: puriss. p.a., ACS reagent, ≥ 99.0% (NT) ; Anthracene: analytical standard, for environmental analysis ; DBU: puriss., ≥ 99.0% (GC) ; DIC: purum, ≥ 98.0% (GC) ; DIPEA: 99.5% , biotech. Grade ; DMAP: ReagentPlus®, ≥ 99.9% ; Gly-Fmoc: ≥ 98.0% (T) ; HBTU: ≥ 98.0% (T) ; HOBt: wetted with not less than 14 wt.% water, 97% ; Ibuprofen: ≥ 98.0% (GC) ; NMP: anhydrous, 99.5% (Sigma-Aldrich Chemie GmbH, Buchs, CH) ; PL2: Obtained by synthesis (Chapter 2) were used as received. Milli-Q water with resistivity of more than 18.2 MΩ·cm was provided by a Millipore Milli-Q filtering system with filtration through a 0.22 µm Millipak filter.

4.4.1.2 Characterization

Chromatography were carried using an Agilent 1100 series HPLC instrument equipped with a high pressure gradient pump, an auto-injector set at 10 µl and a UV-Visible detector set at $\lambda = 254$ nm. The separations were carried out on a 5 µm Sphereclone ODS (2) column (Phenomex, 150 mm x 4.60 mm i.d.) at 25 °C and eluted at 1.0 ml·min^{-1} (pressure ∼ 52 bars) using an isocratic mixture of 30% H_2O cont. 0.1%(v:v) and 70% ACN cont. 0.1%(v:v). The column was coupled to a security guard cartridge system.

The signal measurements were obtained by rationing the areas of the DBF absorbance signal to the anthracene absorbance signal after baseline correction on the IGOR-Pro software. The limit integration intervals, determined by differentiation of the signal curve, were [6.54;7.34] min for the DBF and [7.34;8.48] min for the anthracene.

Using this method, the blank retention time is $t_0 = 1.51$ min and the retention times are $t_{DBF} = 5.42$ min and $t_{anth} = 6.24$ min for the DBF and the anthracene respectively. The resolution is R = 1.59, which is high enough to be used.

4.4.2 Solvent exchange

Before surface modifications, the ChipM were submitted to a solvent exchange which consists in soaking the ChipM disks in 5%(v:v) DIPEA in NMP during 20 minutes, using 2 ml per ChipM. This procedure was repeated three times with clean DIPEA/NMP mixture each time.

4.4.3 PL1 coupling on ChipM

4.4.3.1 PL1-Fmoc on ChipM

To a solution of DIPEA and PL1-Fmoc in 8 ml of NMP, were added 5 ChipM (experiment B, Chapter 3). The solution was gently shaken at room temperature during 15 minutes before adding HBTU and HOBt dissolved in 2 ml of NMP. After one hour of reaction, the ChipM·PL1-Fmoc were submitted to three washes with a 5%(v:v) DIPEA/NMP mixture.

	Amount	Mw (g·mol^{-1})	Concentration	CAS
DIPEA	38.7 mg	129.2432	29.94 mM	7087-68-5
HBTU	75.5 mg	379.2518	19.90 mM	94790-37-1
HOBt	27.0 mg	135.1234	19.98 mM	123333-53-9
NMP	10 ml	—	—	872-50-4
PL1-Fmoc	52.0 mg	520.5305	9.98 mM	162827-98-7

4.4.3.2 Fmoc removing

To a 10 ml solution of 2%(v:v) DBU in NMP, were added 5 ChipM·PL1-Fmoc (experiment B, Chapter 3). The solution was gently shaken at room temperature. After one hour of reaction, aliquots of the solution were taken out and immediately analyzed by HPLC to quantify the DBF. The obtained ChipM·PL1 were submitted to three washes with a 5%(v:v) DIPEA/NMP mixture.

	Amount	Mw (g·mol^{-1})	Concentration	CAS
DBU	0.2 ml	152.2367	133.73 mM	6674-22-2
NMP	9.8 ml	—	—	872-50-4

4.4.4 Quantification

4.4.4.1 Calibration procedure

4.4.4.1.a Standard solution

Stock solutions

To reduce uncertainties due to the measurement of low mass, concentrated anthracene and Gly-Fmoc stock solutions, S_{A0} and S_{G0} respectively, were prepared before being diluted to give S_{A1} and S_{G1}.

S_{A0}	35.6 mg of anthracene in 10 ml of NMP	$[\text{Anth}]_{S_{A0}} \approx 20$ mM
S_{A1}	100 µl of S_{A0} diluted to 10 ml with NMP	$[\text{Anth}]_{S_{A1}} \approx 200$ µM
S_{G0}	30.0 mg of Gly-Fmoc in 10 ml of NMP	$[\text{Gly-Fmoc}]_{S_{G0}} \approx 10$ mM
S_{G1}	200 µl of S_{G0} diluted to 10 ml with NMP	$[\text{Gly-Fmoc}]_{S_{G1}} \approx 200$ µM

Calibration solutions

A series of N = 6 calibration solutions S_Ci were prepared using increasing volumes $V_{S_{G1}}$i of S_{G1}, constant volumes of DBU (V_{DBU} = 200 µl) and S_{A1} ($V_{S_{A1}}$ = 1.0 ml) and diluted to 10 ml with NMP.

—	$V_{S_{G1}} \rightarrow S_C$i	[Gly-Fmoc]$_{S_Ci}$
S_C1	0.00 ml	[Gly-Fmoc]$_{S_C1}$ = 0.00000 µM
S_C2	0.25 ml	[Gly-Fmoc]$_{S_C2}$ = 5.04530 µM
S_C3	0.50 ml	[Gly-Fmoc]$_{S_C3}$ = 10.0906 µM
S_C4	1.00 ml	[Gly-Fmoc]$_{S_C4}$ = 20.1812 µM
S_C5	1.50 ml	[Gly-Fmoc]$_{S_C5}$ = 30.2719 µM
S_C6	2.00 ml	[Gly-Fmoc]$_{S_C6}$ = 40.3625 µM

Once prepared, calibration solutions were stored at room temperature in the dark prior to analysis. The analysis were conducted 5 times (p = 5) for each of the N standard solutions. The obtained signals were called $y_{N,p}$.

4.4.4.1.b Calculations

The traditional method for regression calculation considers the statistic value R^2, called coefficient of determination, as a good parameter to describe the validity of a model. However, this value is really difficult to interpret as there is no limit value. In this study, the quality of the calibration is characterized using another method which is presented here.

Pearson product-moment correlation coefficient

By defining:

$$\overline{X} = \frac{1}{N}\sum_{i=1}^{N} X_i \qquad Y_i = \frac{1}{p}\sum_{j=1}^{p} y_{i,j} \qquad \text{and} \qquad \overline{Y} = \frac{1}{N}\sum_{i=1}^{N} Y_i \tag{4.2}$$

with $\overline{X}$ the average on the N concentrations X_i, Y_i the average on p repetitions for one concentration X_i, $\overline{Y}$ the average of the Y_i for N concentrations the variances and covariances are:

$$\mathrm{Var}(X) = \frac{1}{N}\sum_{i=1}^{N}(X_i - \overline{X})^2 \qquad \mathrm{Var}(Y) = \frac{1}{N}\sum_{i=1}^{N}(Y_i - \overline{Y})^2 \tag{4.3}$$

$$\text{and} \quad \mathrm{Cov}(X|Y) = \sum_{i=1}^{N} \frac{(X_i - \overline{X})(Y_i - \overline{Y})}{N} \tag{4.4}$$

The Pearson product-moment correlation coefficient is defined as:

$$\rho^2 = \left(\frac{\mathrm{Cov}(X|Y)}{\sqrt{\mathrm{Var}(X)\mathrm{Var}(Y)}} \right)^2 \tag{4.5}$$

Homoscedasticity

When p responses $y_{i,j}$ are determined for the concentration X_i, the standard deviation can be calculated for this concentration using the relation:

$$S_i = \sqrt{\sum_{j=1}^{p} \frac{(y_{i,j} - Y_i)^2}{\nu_i}} \quad \text{with } \nu_i = \text{ p – 1 the degree of freedom of } S_i \tag{4.6}$$

The main idea of the homoscedasticity study is to compare the N standard deviations. Two different possibilities exist for the study of variance homogeneity. The first one is the Bartlett's test which allows to work with different values of p. The second one is the Cochran's test in which all samples must have the same size p. However, the Bartlett's test gives the possibility to calculate the merged standard deviation S_*, determined with the relation:

$$S_* = \sqrt{\sum_{i=1}^{N} \frac{\nu_i (S_i)^2}{\nu_*}} \quad \text{with } \nu_* = \sum_{i=1}^{N} \nu_i \text{ the degree of freedom of } S_* \tag{4.7}$$

$$\text{Finally} \quad \chi^2_{OBS} = \frac{1}{D} \left(\nu_* ln(S_*^2) - \sum_{i=1}^{N} \nu_i ln(S_i^2) \right) \tag{4.8}$$

$$\text{with} \quad D = 1 + \frac{\sum_{i=1}^{N} \left(\frac{1}{\nu_i} - \frac{1}{\nu_*} \right)}{3(N-1)} \tag{4.9}$$

To determine if the calibration is homoscedastic or not, the χ^2_{OBS} is compared to the $\chi^2_{N-1}(0.95)$ in table of critical values for Pearson correlation. If $\chi^2_{OBS} > \chi^2_{N-1}$, the N standard deviations are not on the same order of magnitude and the calibration has to be repeated. In particular, the reasons of variation in Y_i are different between samples. In that case, this reason must be identified before continuing.

When $\chi^2_{OBS} < \chi^2_{N-1}$, the N standard deviations are on the same order of magnitude and the calibration can be made. In that case the S_i are considered as equal to:

$$S_0 = \frac{S_*}{\sqrt{p}} \quad \text{and the degree of freedom becomes } \nu_0 = \nu_* \tag{4.10}$$

The advantage is that the standard deviation is known more precisely. Here $\rho^2 = 0.999839$, $S_0 = 0.0005371924628$, $\nu_0 = 24$ and $\chi^2_{OBS} = 21.7 > \chi^2_5 = 11.1$. As a consequence, this calibration can not be considered as homoscedastic.

Regression parameters

The regression model proposed makes it possible to calculate any polynomial regression. For that study, only 4 different regressions were considered:

Model	Type of model	Model
1.WIC	Linear with constant effect	$Y = B_{1.WIC} \cdot X + A_{1.WIC}$
1.WOC	Linear without constant effect	$Y = B_{1.WOC} \cdot X$
2.WIC	Quadratic with constant effect	$Y = C_{2.WIC} \cdot X^2 + B_{2.WIC} \cdot X + A_{2.WIC}$
2.WOC	Quadratic without constant effect	$Y = C_{2.WOC} \cdot X^2 + B_{2.WOC} \cdot X$

The regression parameters are calculated using a matrix least squares method. The matrix of coefficients Co is given by solving the matrix equation:

$$Co = ({}^tSS)^{-1}\ {}^tS\ Y \tag{4.11}$$

With S the matrix of effects and Y the matrix of responses. Detailed calculations are not presented here. The results are:

For 1.WIC:

$Y = 0.02192498762 \cdot X + 0.00292215366$

For 1.WOC:

$Y = 0.02202550669 \cdot X$

For 2.WIC:

$Y = -0.00002240679177 \cdot X^2 + 0.02282343312 \cdot X - 0.001440693984$

For 2.WOC:

$Y = -0.00001959400292 \cdot X^2 + 0.02267993034 \cdot X$

When coefficients are determined, the residual values for each X_i are calculated:

For 1.WIC:

$\mathrm{e}_i = \mathrm{Y}_i - \hat{Y}_i$ with $\hat{Y}_i = \mathrm{B}_{1.WIC} \cdot \mathrm{X}_i + \mathrm{A}_{1.WIC}$

For 1.WOC:

$\mathrm{e}_i = \mathrm{Y}_i - \hat{Y}_i$ with $\hat{Y}_i = \mathrm{B}_{1.WOC} \cdot \mathrm{X}_i$

For 2.WIC:

$\mathrm{e}_i = \mathrm{Y}_i - \hat{Y}_i$ with $\hat{Y}_i = \mathrm{C}_{2.WIC} \cdot \mathrm{X}_i^2 + \mathrm{B}_{2.WIC} \cdot \mathrm{X}_i + \mathrm{A}_{2.WIC}$

For 2.WOC:

$\mathrm{e}_i = \mathrm{Y}_i - \hat{Y}_i$ with $\hat{Y}_i = \mathrm{C}_{2.WOC} \cdot \mathrm{X}_i^2 + \mathrm{B}_{2.WOC} \cdot \mathrm{X}_i$

The residual standard deviation S_r of each model are calculated with:

$$S_r = \sqrt{\frac{\sum_{i=1}^{N} e_i^2}{N-k-1}} \quad \text{with} \quad \begin{array}{ll} \mathrm{k}_{1.WIC} = 1 & \mathrm{k}_{1.WOC} = 0 \\ \mathrm{k}_{2.WIC} = 2 & \mathrm{k}_{2.WOC} = 1 \end{array} \tag{4.12}$$

Significance of coefficients

The individual significance of each coefficient is then calculated with a Student's test. This one is done by calculating the standard deviations of each coefficients by solving the matrix equation:

$$\mathrm{Var}(Co) = S_r^2 \ ({}^tSS)^{-1} \tag{4.13}$$

Var(Co) represents the matrix of variance/covariance for the coefficients. Here again the calculations details are not presented. When the variance of coefficients are known, the standard deviation is deduced by:

$$S_{Co} = \sqrt{\mathrm{Var}(Co)} \tag{4.14}$$

To determine if a coefficient is significant or not, the $\mathrm{t}_{OBS}(\mathrm{Co})$ is calculated for each coefficient using the generalized relation:

$$t_{OBS}(Co) = \frac{|Co|}{S_{Co}} \tag{4.15}$$

$\mathrm{t}_{OBS}(\mathrm{Co})$ is finally compared to the $\mathrm{t}_{N-k-1}(0.95)$ in the table of the Student's distribution. If $\mathrm{t}_{OBS}(\mathrm{Co}) > \mathrm{t}_{N-k-1}(0.95)$, the coefficient is considered as significant. Otherwise, the coefficient can be removed from the model.

For this calibration the results are:

Model	$t_{N-k-1}(0.95)$	$t_{OBS}(0.95)$	Result
1.WIC	$t_4(0.95) = 2.776$	$t_{OBS}(B_{1.WIC}) = 157.76$ $t_{OBS}(A_{1.WIC}) = 0.92$	significant not significant
1.WOC	$t_5(0.95) = 2.571$	$t_{OBS}(B_{1.WOC}) = 256.53$	significant
2.WIC	$t_3(0.95) = 3.182$	$t_{OBS}(C_{2.WIC}) = 3.28$ $t_{OBS}(B_{2.WIC}) = 80.51$ $t_{OBS}(A_{2.WIC}) = 0.66$	significant significant not significant
2.WOC	$t_4(0.95) = 2.776$	$t_{OBS}(C_{2.WOC}) = 3.93$ $t_{OBS}(B_{2.WOC}) = 131.80$	significant significant

Models validity

A model must always be validated before being used. This is done by controlling if the residual values are on the same order of magnitude than uncertainties of the measurement. The validation of a model can be demonstrated by a Fisher's test, in this case the comparison between S_r and S_0. To know if a model is valid or not, the F_{OBS} is calculated with:

$$F_{OBS} = \left(\frac{S_r}{S_0}\right)^2 \tag{4.16}$$

The F_{OBS} is then compared to the $F_{\nu_1,\nu_2}(0.95)$ in F-tables of Fisher-Snedecor using ν_1 = N-k-1 and $\nu_2 = \nu_0$.

If $F_{OBS} < F_{\nu_1,\nu_2}(0.95)$ the model is valid and explains totally the responses to experimental data. As a consequence, it can be used for quantitative analysis and uncertainty determination. Otherwise the model is not valid, i.e. parameters act on the response with higher complexity than those introduced in the matrix effect. For this calibration, the validity test gives:

Model	F_{OBS}	$F_{\nu_1,\nu_2}(0.95)$	Result
1.WIC	$F_{OBS}(1.WIC) = 80.9$	$F_{4,24}(0.95) = 2.78$	not valid
1.WOC	$F_{OBS}(1.WOC) = 78.6$	$F_{5,24}(0.95) = 2.62$	not valid
2.WIC	$F_{OBS}(2.WIC) = 23.4$	$F_{3,24}(0.95) = 3.01$	not valid
2.WOC	$F_{OBS}(2.WOC) = 20.2$	$F_{4,24}(0.95) = 2.78$	not valid

4.4.4.2 Quantification procedure

For the quantification, the response of an aliquot was measured n = 6 times by HPLC giving an average ratio Y. According to 1.WOC model, the corresponding DBF concentration [DBF] was calculated with the corresponding uncertainties using the relations:

$$[DBF] = \frac{Y}{B_{1.WOC}} \tag{4.17}$$

And

$$\delta[DBF] = \frac{S_r(1.WOC) \cdot t_5(0.95)}{B_{1.WOC}} \cdot \sqrt{\frac{1}{N} + \frac{1}{n} + \frac{(Y - \overline{Y_{S_C i}})^2}{N \cdot B_{1.WOC}^2 \cdot \mathrm{Var}([Gly - Fmoc]_{S_C i})}} \tag{4.18}$$

4.4.4.2.a DBF quantification

For the quantification, 1 ml of solution S_{A1} and 100 µl of the collected aliquots from the reaction solution were mixed, diluted to 10 ml with NMP and analyzed by HPLC. Using the signal from the 6 samples, a relative ratio Y = 0.45563 was found.

The calibration curve gives [DBF] = 20.6864 ± 0.320463 µM which corresponds to the amount of DBF released by Fmoc degradation. As a consequence, the estimated amount of PL1 coupled to 5 ChipM in 10 ml of NMP is 20.6864 µmol.

4.4.5 PL2 coupling on ChipM

To a solution of DIPEA and PL2 in 8 ml of NMP, were added 5 $\left(^2_{LA}|40\right)$·ChipM (experiment C, Chapter 3). The solution was gently shaken at 50 °C during 15 minutes before adding HBTU and HOBt dissolved in 2 ml of NMP.

After one hour of reaction, the $\left(^2_{LA}|40\right)$·ChipM·PL2 were submitted to three washes with a 5%(v:v) DIPEA/NMP mixture.

	Amount	Mw (g·mol^{-1})	Concentration	CAS
DIPEA	259.7 mg	129.2432	200.93 mM	7087-68-5
HBTU	568.8 mg	379.2418	149.98 mM	94790-37-1
HOBt	203.0 mg	135.1234	150.23 mM	123333-53-9
NMP	10.0 ml	—	—	872-50-4
PL2	149.6 mg	299.2765	49.98 mM	175281-76-2

4.4.6 Acetylation of ChipM

To a solution of Ac_2O and DIPEA in NMP, were added 5 ChipM (experiment B, Chapter 3). The solution was gently shaken at room temperature. After 30 minutes of reaction, the ChipM·AcO were submitted to three washes with a 5%(v:v) DIPEA/NMP mixture.

	Amount	Mw (g·mol^{-1})	Concentration	CAS
Ac_2O	2.0 ml	102.0886	2119.72 mM	108-24-7
DIPEA	0.5 ml	129.2432	287.05 mM	7087-68-5
NMP	7.5 ml	—	—	872-50-4

4.4.7 Ibuprofen coupling on ChipM PL2

4 $\binom{2}{LA}|40)$·ChipM·PL2 were added to a solution of DMAP and ibuprofene in 6 ml of NMP. The solution was gently shaken at 50 °C during 15 minutes before adding DIC and HOBt dissolved in 2 ml of NMP. After 24 hours of reaction, the $\binom{2}{LA}|40)$·ChipM·PL2·(Ibu) were submitted to three washes with a 5%(v:v) DIPEA/NMP mixture.

	Amount	Mw (g·mol^{-1})	Concentration	CAS
DIC	189.4 mg	126.1995	150.07 mM	693-13-0
DMAP	6.2 mg	122.1677	5.07 mM	1122-58-3
HOBt	203.0 mg	135.1234	150.23 mM	123333-53-9
Ibu	102.6 mg	206.2808	49.73 mM	15687-27-1
NMP	8.0 ml	—	—	872-50-4

4.5 Bibliography

[1] Merrifield, R. B. Solid phase peptide synthesis. I. The synthesis of a tetrapeptide. *J. Am. Chem. Soc.* **85**, 2149-2154 (1963).

[2] Meienhofer, J. *et al.* Solid phase synthesis without repetitive acidolysis. Preparation of leucyl-alanyl-glycyl-valine using 9-fluorenylmethyloxycarbonylamino acids. *Int. J. Pept. Protein Res.* **13**, 35-42 (1979).

[3] Frank, R., Heikens, W., Heisterberg-Moutsis, G. & Bloecker, H. A new general approach for the simultaneous chemical synthesis of large numbers of oligonucleotides: segmental solid supports. *Nucleic Acids Res.* **11**, 4365-4377 (1983).

[4] Rich, D. H. & Gurwara, S. K. Removal of protected peptides from an ortho-nitrobenzyl resin by photolysis. *J. Chem. Soc., Chem. Commun.* , 610-611 (1973).

[5] Dubey, L. V. & Dubey, I. Y. Onium salts as coupling reagents in the preparation of silica polymer supports for oligonucleotide synthesis. *Ukr. Bioorg. Acta* **1**, 23-28 (2004).

[6] Dubey, L. V. & Dubey, I. Y. Side reactions of onium coupling reagents BOP and HBTU in the synthesis of silica polymer supports. *Ukr. Bioorg. Acta* **2**, 13-19 (2005).

[7] Joullie, M. M. & Lassen, K. M. Evolution of amide bond formation. *ARKIVOC (Gainesville, FL, U. S.)* , 189-250 (2010).

[8] Ast, T., Heine, N., Germeroth, L., Schneider-Mergener, J. & Wenschuh, H. Efficient assembly of peptomers on continuous surfaces. *Tetrahedron Lett.* **40**, 4317-4318 (1999).

[9] Lin, Q., O'Neill, J. C. & Blackwell, H. E. Small Molecule Macroarray Construction via Ugi Four-Component Reactions. *Org. Lett.* **7**, 4455-4458 (2005).

[10] Scharn, D., Germeroth, L., Schneider-Mergener, J. & Wenschuh, H. Sequential Nucleophilic Substitution on Halogenated Triazines, Pyrimidines, and Purines: A Novel Approach to Cyclic Peptidomimetics. *J. Org. Chem.* **66**, 507-513 (2001).

[11] Whitehouse, D. L., Savinov, S. N. & Austin, D. J. An improved synthesis and selective coupling of a hydroxy based photolabile linker for solid phase organic synthesis. *Tetrahedron Lett.* **38**, 7851-7852 (1997).

[12] Neises, B. & Steglich, W. 4-Dialkylaminopyridines as acylation catalysts. 5. Simple method for the esterification of carboxylic acids. *Angew. Chem.* **90**, 556-557 (1978).

[13] Batista, M. K. S., Pinto, L. F., Gomes, C. A. R. & Gomes, P. Novel highly-soluble peptide-chitosan polymers: Chemical synthesis and spectral characterization. *Carbohydr. Polym.* **64**, 299-305 (2006).

[14] Hojo, K. *et al.* Preparation of a chitosan hybrid of an antimetastatic laminin-related peptide. *Pharm. Pharmacol. Commun.* **5**, 277-280 (1999).

[15] Neugebauer, W., Williams, R. E., Barbier, J.-R., Brzezinski, R. & Willick, G. Peptide synthesis on chitin. *Int. J. Pept. Protein Res.* **47**, 269-275 (1996).

[16] Neugebauer, W. A., D'Orleans-Juste, P. & Bkaily, G. Peptide synthesis on chitosan/chitin. *Adv. Chitin Sci.* **4**, 411-416 (2000).

[17] Huang, R. Y. M., Moon, G. Y. & Pal, R. N-acetylated chitosan membranes for the pervaporation separation of alcohol/toluene mixtures. *J. Membr. Sci.* **176**, 223-231 (2000).

[18] Agnihotri, S. A., Mallikarjuna, N. N. & Aminabhavi, T. M. Recent advances on chitosan-based micro- and nanoparticles in drug delivery. *J. Control. Release* **100**, 5-28 (2004).

[19] Moccia, M., Roviello, G. N., Bucci, E. M., Pedone, C. & Saviano, M. Synthesis of a L-lysine-based alternate alpha,epsilon-peptide: A novel linear polycation with nucleic acids-binding ability. *Int. J. Pharm.* **397**, 179-183 (2010).

[20] Montalbetti, C. A. G. N. & Falque, V. Amide bond formation and peptide coupling. *Tetrahedron* **61**, 10827-10852 (2005).

[21] Isidro-Llobet, A., Alvarez, M. & Albericio, F. Amino Acid-Protecting Groups. *Chem. Rev.* **109**, 2455-2504 (2009).

[22] Al-Saidan, S. M. Transdermal self-permeation enhancement of ibuprofen. *J. Control. Release* **100**, 199-209 (2004).

[23] Akhter, S. A. & Barry, B. W. Absorption through human skin of ibuprofen and flurbiprofen; effect of dose variation, deposited drug films, occlusion and the penetration enhancer N-methyl-2-pyrrolidone. *J. Pharm. Pharmacol.* **37**, 27-37 (1985).

[24] Haslam, E. Recent developments in methods for the esterification and protection of the carboxyl group. *Tetrahedron* **36**, 2409-2433 (1980).

[25] Pon, R. T., Yu, S. & Sanghvi, Y. S. Rapid Esterification of Nucleosides to Solid-Phase Supports for Oligonucleotide Synthesis Using Uronium and Phosphonium Coupling Reagents. *Bioconjugate Chem.* **10**, 1051-1057 (1999).

[26] Ha, B.-J., Lee, O.-S. & Lee, Y.-S. A new synthetic method of peptide-chitosan conjugates: solid-phase synthesis of GHK coupled to chitosan. *J. Ind. Eng. Chem.* **1**, 57-63 (1995).

[27] Lin, Q. & Blackwell, H. E. Rapid synthesis of diketopiperazine macroarrays via Ugi four-component reactions on planar solid supports. *Chem. Commun.* 2884-2886 (2006).

[28] Varady, L., Rajur, S. B., Nicewonger, R. B., Guo, M. & Ditto, L. Fast and quantitative high-performance liquid chromatography method for the determination of 9-fluorenylmethoxycarbonyl release from solid-phase synthesis resins. *J. Chromatogr., A* **869**, 171-179 (2000).

[29] Heine, N. *et al.* Synthesis and screening of peptoid arrays on cellulose membranes. *Tetrahedron* **59**, 9919-9930 (2003).

[30] Talbo, G., Wade, J. D., Dawson, N., Manoussios, M. & Tregear, G. W. Rapid semi-online monitoring of Fmoc solid-phase peptide synthesis by matrix-assisted laser desorption/ionization mass spectrometry. *Lett. Pept. Sci.* **4**, 121-127 (1997).

[31] Gude, M., Ryf, J. & White, P. D. An accurate method for the quantitation of Fmoc-derivatized solid phase supports. *Lett. Pept. Sci.* **9**, 203-206 (2003).

[32] Wade, J. D., Bedford, J., Sheppard, R. C. & Tregear, G. W. DBU as an N α-deprotecting reagent for the fluorenylmethoxycarbonyl group in continuous flow solid-phase peptide synthesis. *Pept. Res.* **4**, 194-199 (1991).

[33] Freeman, C. E. & Howard, A. G. Measurement of the FMOC loading of protected amine-functionalised polymer beads. *Talanta* **65**, 574-577 (2005).

[34] Lehmann, C., Xu, Y. Z., Christodoulou, C., Tan, Z. K. & Gait, M. J. Solid-phase synthesis of oligoribonucleotides using 9-fluorenylmethoxycarbonyl (Fmoc) for 5'-hydroxyl protection. *Nucleic Acids Res.* **17**, 2379-2390 (1989).

[35] Sarin, V. K., Kent, S. B. H., Tam, J. P. & Merrifield, R. B. Quantitative monitoring of solid-phase peptide synthesis by the ninhydrin reaction. *Anal. Biochem.* **117**, 147-157 (1981).

[36] Sun, S.-W., Lin, Y.-C., Weng, Y.-M. & Chen, M.-J. Efficiency improvements on ninhydrin method for amino acid quantification. *J. Food Compos. Anal.* **19**, 112-117 (2005).

[37] Krchnak, V., Vagner, J., Safar, P. & Lebl, M. Amino acids and peptides. Part CCVI. Noninvasive continuous monitoring of solid-phase peptide synthesis by acid-base indicator. *Collect. Czech. Chem. Commun.* **53**, 2542-2548 (1988).

[38] Kamradt, T. & Volkmer-Engert, R. Cross-reactivity of T lymphocytes in infection and autoimmunity. *Molec. Divers.* **8**, 271-280 (2004).

[39] McKeown, S. C., Watson, S. P., Carr, R. A. E. & Marshall, P. A photolabile carbamate based dual linker analytical construct for facile monitoring of solid phase chemistry: 'TLC' for solid phase? *Tetrahedron Lett.* **40**, 2407-2410 (1999).

[40] Shimizu, Y. & Hayashi, J. Acylation of cellulose with carboxylic acids. *Cellul. Chem. Technol.* **23**, 661-670 (1989).

Chapter 5

Transdermal release

Abstract: The aim of this chapter is to demonstrate the proof of concept for the ATTS. The proof of concept consists in the significant release of ibuprofen and its diffusion through human skin epidermis while the drug loaded photosensitive matrix is exposed to UV light. This study demonstrates that is is possible to produce a support able to reach the requirement for transdermal delivery to human skin. Photo-induced release opens the way to several applications as it makes a precise and tuned control of drug release possible to individual patient treatment by a simple programming of the UV emission.

5.1 General remarks

The *in-vitro* studies of drug permeation through the skin are the most used techniques for skin formulations such as TTS. Several techniques are available to test the efficiency of a transdermal formulation. However, the choice of the method depends of the substance studied and the formulation applied to the skin. Among different equipments, the most widespread remain the Franz diffusion cell (FD-C) and the Saarbrücken penetration model (SB-M) [1].

The FD-C (Figure 5.1) study involves the diffusion measurements of substances through the skin, or skin like membrane, to a receiving solution (RS) assembled in a diffusion cell in function of time. In that case, the formulation is placed in a donor chamber and separated from a receptor compartment by a membrane which can be natural or synthetic.

The receptor usually contains a buffer solution that mimics physiological conditions [2,3] and the system is maintained at constant temperature to simulate the skin temperature [1,4,5]. Constant stirring of the receptor compartment ensures the diffusion of the drug by homogenization of the RS. Finally, a sampling is performed either in a continuous form or at pre-determined times intervals [6] for quantification.

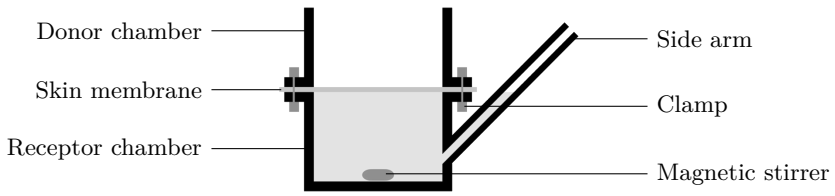

Figure 5.1: Schematic representation of a static FD-C system

5.2 Strategy

According to the recommendations of the Organization for Organisation for Economic Co-operation and Development (OECD) concerning the transdermal studies, the use of real skin instead of reconstructed skin is preferred as they do not exhibit the same barrier properties (OECD test guideline 428). As a consequence, this study was conducted using real human skin sample. However, considering the important thickness of the dermis layer, the proof of concept was established using only the epidermis [4].

In this study, the ibuprofen modified support is placed into the donor chamber and the full system is irradiated at $\lambda = 365$ nm. Once the matrix is activated by the light the photocleavable linker releases the ibuprofen which is quantified by HPLC. For the proof of concept, $\left(^{2}_{LA}|40\right)\cdot$ChipM·PL2·(Ibu), used as mS, were exposed to UV light and the ibuprofen released through human epidermis or in RS was quantified.

5.3 Results and discussion

5.3.1 Human epidermis preparation

Several methods exist for the separation of the dermal layers among the enzymatic separation with dispase[7,8,9], mechanical methods using a dermatome able to cut thin layers of skin, thermal separation by heating of the skin at 60 °C during 90 secondes[4].

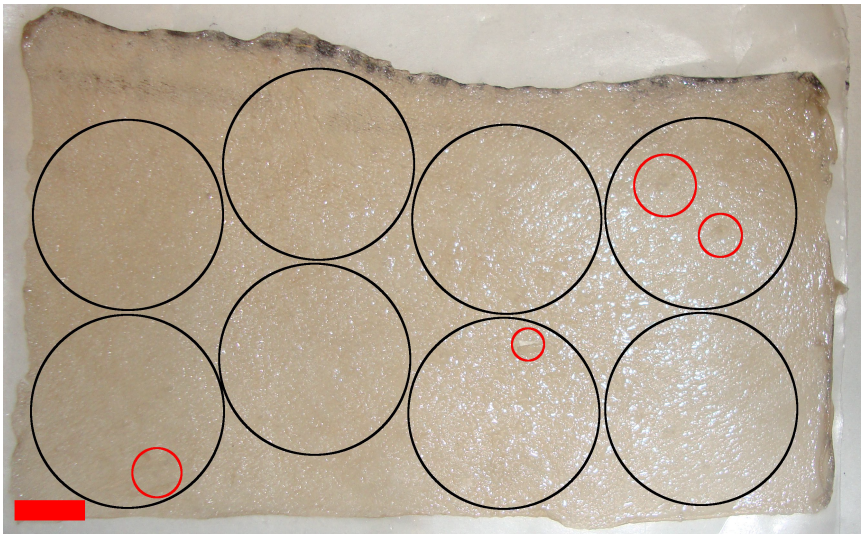

Figure 5.2: Human epidermis sample (scale bar 10 mm)
Red circle: non usable parts ; Black circle: used parts

For this study, the separation protocol was given by the skin supplier and is based on lysis to denature cells at the dermis/epidermis interface. This method is very efficient and allows to isolate the epidermis from large surface skin samples (Figure 5.2).

It should be noticed that the obtained epidermis surface represents 130% of the initial sample surface due to important skin invaginations. This means that the real skin surface exposed to a ChipM during drug release is certainly higher that what is observed in this transdermal study since the surface of exchange is larger than the surface of a ChipM.

5.3.2 In-vitro permeation study

The ibuprofen release study from $\binom{2}{LA}|40)\cdot$ChipM·PL2·(Ibu) is divided into two parts. In a first time, the release was realized in solution to characterize quantitatively the release under UV light.

In a second time, the release was triggered under the same conditions but the quantification was investigated after diffusion of ibuprofen through an epidermis sample using a FD-C.

5.3.2.1 ChipM preparation

While released from the , the pores represent the only pathway for the ibuprofen to leave the structure. As a consequence, the liquid filling the pores is of major importance in the release. Moreover, its characteristics directly influence the drug solubility, skin acceptability or kinetic of the release.

The dM is the continuous liquid phase that allows the drug diffusion in the ChipM. In this study, a 10 mM Sørensen's buffer is used as dM model and its implementation into the pores was obtained by repeated soakings in buffer. According to the nomenclature (Appendix C), the obtained ChipM are called $\binom{2}{LA}|40)\cdot$ChipM$\cdot$PL2$\cdot$(Ibu)$\cdot\{$Sø$\}$.

5.3.2.2 Release

The FD-C experiment was carried out using epidermis positioned between the donor and acceptor chamber while the free release experiment was conducted by immersing directly the ChipM in RS.

In both cases a negative control was performed by keeping one drug loaded ChipM protected from light. The RS was made of $V_{RS} = 8.0$ ml of a 10 mM Sørensen's buffer, at pH = 7.4, and was stirred with a magnetic bar at 500 rpm.

At pre-determined time intervals, aliquots of $V_a = 500$ µl were collected from RS and replaced immediately with the same volume of buffer. Samples were collected during 24 hours and analyzed by HPLC.

After only 10 minutes, a clear color change appears on ChipM submitted to UV light, while the negative controls remained unchanged. After 24 hours of illumination, the difference is even more noticeable (Figure 5.3).

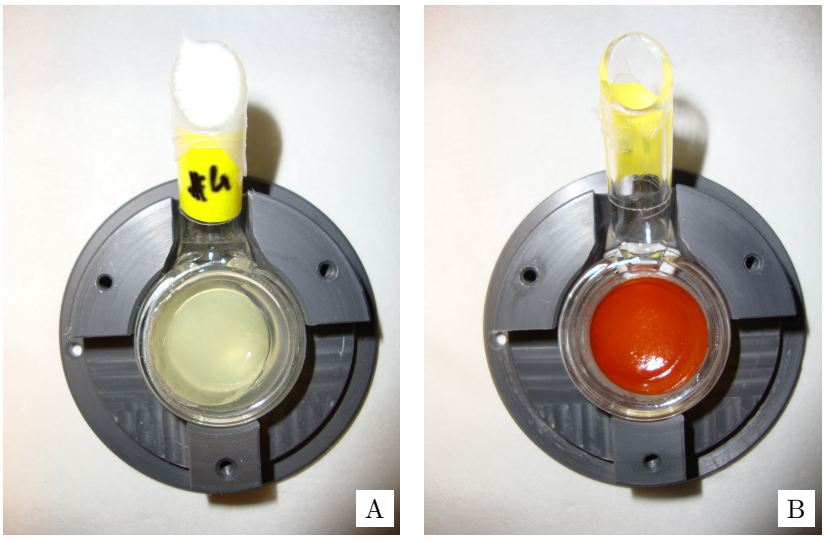

Figure 5.3: ChipM after 24 hours of experiment
A: Negative control ; B: Exposed to UV light

This color change can be explained by the conversion of the aromatic center of the photolinker from an *o*-nitrobenzyl ether to an *o*-nitrosobenzaldehyde [10,11].

5.3.2.2.a Calibration

A special attention was carried in the treatment of the data as the ChipM production (Chapter 3) is not optimized. Moreover, as the volume $V_{RS} = 8$ ml is important, a highly precise method was essential for ibuprofen quantification.

Since the proof of concept is considered as established by the obtaining of significant ibuprofen release under UV light, the calibration was realized using the method developed in Chapter 4. By applying this method to the calibration of ibuprofen, the calculations reveal that a linear model (1.WOC) reached the quality required for a precise quantification.

5.3.2.2.b Ibuprofen quantification

The release experiment shows a significant release of ibuprofen for the ChipM exposed to UV while the negative control, without activation of the photolinker, confirms the absence of release (Figure 5.4).

By comparing the evolution of the ibuprofen concentration in RS for the two experiments, a very clear difference is observed. Indeed, for the free release in solution (Figure 5.4, Left), the time necessary to observe a significant release is short (about 30 minutes for ~ 9.7 µg) but is close to 300 minutes for the release of ~ 7.6 µg through the epidermis (Figure 5.4, Right).

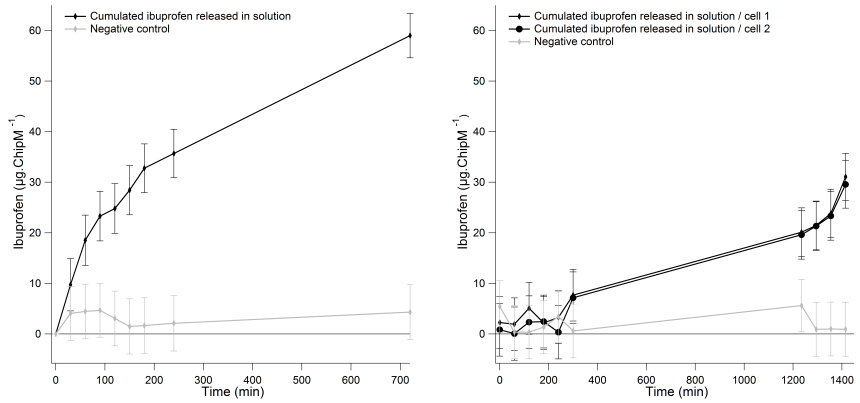

Figure 5.4: Cumulated ibuprofen released from loaded ChipM
Left: Free release in solution ; Right: Release through human epidermis

Moreover, it can be noticed that in both cases the released amount does not exceed 100 µg·ChipM^{-1}. An optimization of the production process should considerably improve this result as the theoretical coupling is approximately of 0.35 mmol·g^{-1} of chitosan [12,13], giving ~ 1.7 mg for a 28 mm in diameter ChipM.

5.3.3 Mathematical model of ibuprofen release

In order to describe the release of ibuprofen from ChipM a mathematical model based on kinetic equations instead of Fick's law was developed. Results for the free release and release through the epidermis (Figure 5.5) show interesting correlations with the experimental data.

Indeed, the obtained values gave $ibu_0 = 60$ µg·ChipM^{-1}, as the amount of ibuprofen immobilized, and kinetics constants $k_1 = 0.01066$ for photocleavage, $k_2 = 0.00711$ for diffusion in dM and $k_3 = 0.00063$ for diffusion into epidermis.

It clearly appears that the release is affected by the diffusion into the epidermis which is in accordance with the observations for drug diffusion into the skin[4].

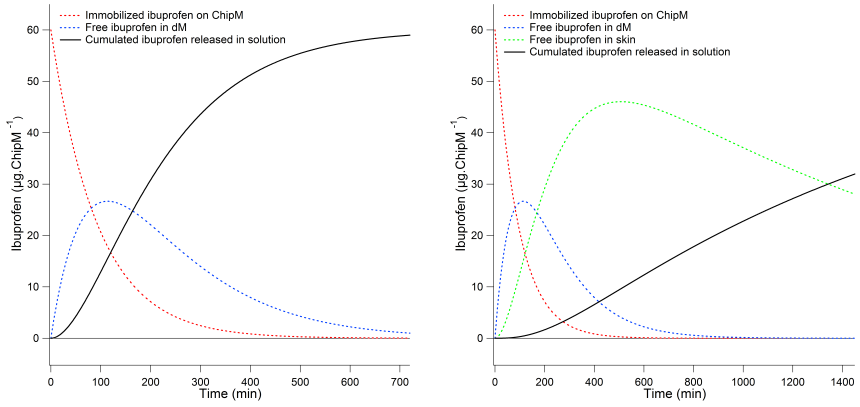

Figure 5.5: Estimated cumulated ibuprofen released from loaded ChipM using model
Left: Free release in solution ; Right: Release though human epidermis

In terms of production, this model shows that the release can be controlled not only by modifying the time of illumination of the photosensitive ChipM but also by adapting parameters to play on each kinetics. As an example, below are listed some of the parameters able to influence the release kinetics of a drug.

$[ibu]_t^{ChipM}$ influenced by:

- Photolinker: cleavage wavelength, sensitivity ;
- ChipM: loading, light diffraction, diffusion, evanescence and reflection (possibility to add doping agents to the ChipM) ;
- dM: interactions with the photocleavage reaction rate, pH, light diffraction, etc. (same than ChipM).

$[ibu]_t^{dM}$ influenced by:

- ChipM: porosity, pore size, mechanical properties ;
- dM: viscosity, pH, physico-chemical interactions with drug molecules.

$[\mathbf{ibu}]_t^{epi}$ influenced by:

- dM: pH, physico-chemical interactions with the skin (possibility to add permeation enhancers) ;
- Drug: physico-chemical interactions with the skin (possibility to use drug carriers).

5.4 Experimental section

5.4.1 General materials and methods

Three buffers were used to conduct this study. Two of them (Sørensen's buffers) were used for the establishment of the ibuprofen calibration curve, as dM in drug loaded matrices and as RS. The third one (McIlvaine's buffer) was used in the HPLC procedure.

5.4.1.1 Chemicals

ACN: CHROMASOLV® gradient grade, for HPLC, $\geq$ 99% ; Citric acid: ACS reagent, $\geq$ 99.5% ; EDTA: BioUltra, anhydrous, $\geq$ 99% (titration) ; Ibu: $\geq$ 98% (GC) ; Isopropanol: BioReagent, for molecular biology, $\geq$ 99.5% ; NaH_2PO_4: BioReagent, for molecular biology, anhydrous, $\geq$ 98% ; $NaH_2PO_4 \cdot 2H_2O$: BioUltra, for molecular biology, $\geq$ 99.0% (T) ; PMSF: $\geq$ 99.9% (T) (Sigma-Aldrich Chemie GmbH, Buchs, CH) were used as received. Milli-Q water with resistivity of more than 18.2 MΩ·cm was provided by a Millipore Milli-Q filtering system with filtration through a 0.22 µm Millipak filter.

5.4.1.2 Skin sample

Excised human skin from Caucasian patient (Genoskin, Toulouse, FR) who had undergone abdominal surgery was received frozen after being decontaminated and tested for HIV/AIDS 1/2, B and C hepatitis.

5.4.1.3 Franz diffusion cells

The diffusion experiments were performed in FD-C (diffusion area 1.77 cm^2, acceptor volume 10 ml) and in glass containers for the free release. In order to compare results from free release and release on FD-C, the experiments were both conducted at 39 °C using 10 mM Sørensen's buffer as RS. In both cases aliquots having a volume of V_a = 500 µl were taken out regularly from the RS and replaced with buffer to keep the volume constant [14].

5.4.1.4 Characterization

Chromatography was carried using an Agilent 1100 series HPLC instrument equipped with a high pressure gradient pump, an auto-injector set at 100 µl and a UV-Visible detector set at λ = 238 nm. The separations were carried out on a 5 µm Sphereclone ODS (2) column (Phenomex, 150 mm x 4.60 mm i.d.) at 40 °C and eluted at 1.5 ml·min^{-1} (pressure $\sim$ 73 bars) using an isocratic mixture of 55% ACN and 45% McIllvaine's buffer [14]. The column was coupled to a security guard cartridge system.

The signal measurements were obtained by integrating the peak area of the ibuprofen absorbance signal after baseline correction on the IGOR-Pro software. The limit integration interval [3.60;4.22] min was determined by differentiation of the signal curve. Using this method, the blank retention time is $t_0 = 0.85$ min and the retention time for ibuprofen is $t_{ibu} = 3.05$ min.

5.4.2 Buffers preparation

5.4.2.1 25 mM Sørensen's buffer pH 7.4

The 25 mM Sørensen's buffer was prepared by dissolving 3.0 g of NaH_2PO_4 in 900 ml of water. The pH of the solution was adjusted to pH = 7.42 before being diluted to one liter, giving a final buffer with pH = 7.4.

	Amount	Mw ($g{\cdot}mol^{-1}$)	Concentration	CAS
NaH_2PO_4	3.0 $g{\cdot}l^{-1}$	119.9770	25 mM	7558-80-7

5.4.2.2 10 mM Sørensen's buffer pH 7.4

The 10 mM Sørensen's buffer was prepared by dissolving 1.2 g of NaH_2PO_4in 900 ml of water. The pH of the solution was adjusted to pH = 7.42 before being diluted to one liter, giving a final buffer with pH = 7.4.

	Amount	Mw ($g{\cdot}mol^{-1}$)	Concentration	CAS
NaH_2PO_4	1.2 $g{\cdot}l^{-1}$	119.9770	10 mM	7558-80-7

5.4.2.3 100 mM McIlvaine's buffer pH 2.2

The 100 mM McIlvaine's buffer pH = 2.2 is usually obtained by mixing 980 ml of a 100 mM citric acid solution and 20 ml of 200 mM $NaH_2PO_4{\cdot}2H_2O$ solution[15]. Instead of this, the buffer was prepared by dissolving the corresponding amount of $NaH_2PO_4{\cdot}2H_2O$ and citric acid in 1 l of water and the pH adjusted to pH = 2.2.

	Amount	Mw ($g{\cdot}mol^{-1}$)	Concentration	CAS
Citric acid	18.8281 $g{\cdot}l^{-1}$	192.1235	$\sim$ 98 mM	77-92-9
$Na_2HPO_4{\cdot}2H_2O$	0.7119 $g{\cdot}l^{-1}$	117.9894	$\sim$ 4 mM	10028-24-7

5.4.3 Skin preparation

The separation of the dermis from the epidermis was realized by immersing the thawed skin in a dedicated solution according to a procedure given by the skin supplier.

This solution was obtained by mixing 10 ml of a 50 mM EDTA solution (in 10 mM Sørensen's buffer, pH adjusted to pH = 8 with NaOH), 500 µl of a 100 mM PMSF (in isopropanol) and 90 ml of a 10 mM Sørensen's buffer at 56 °C during 15 minutes. The skin was then washed in 100 ml of 10 mM Sørensen's buffer at 4 °C during 5 minutes. The epidermis layer was peeled carefully from the dermis using a flat tweezer and washed several times with buffer. Finally, epidermis disks ($Ø_{epi}$ = 28 mm) were punched out from epidermis and pre-hydrated in buffer at 4 °C during one hour prior to use.

	Amount	Mw (g·mol^{-1})	Concentration	CAS
EDTA	730.6 mg in 50 ml	292.2426	50 mM	60-00-4
PMSF	174.2 mg in 10 ml	174.1927	100 mM	329-98-6

5.4.4 Permeation experiment

5 $\left(^{2}_{LA}|40\right)$·ChipM·PL2·(Ibu) with $Ø_{ChipM}$ = 28 mm, were used (Chapter 3, experiment C for $\left(^{2}_{LA}|40\right)$·ChipM production, Chapter 4 for surface immobilization conditions).

5.4.4.1 ChipM preparation

The implementation of the dM in the ChipM was realized by soaking the drug loaded porous structures during 20 minutes in the 10 mM Sørensen's buffer. This exchange was repeated three times with 5 ml of buffer per ChipM.

5.4.4.2 Release procedure

5.4.4.2.a Release on Franz diffusion cells

3 $\left(^{2}_{LA}|40\right)$·ChipM·PL2·(Ibu)·{Sø} were used for this experiment. The assembly of the FD-C was made by placing the epidermis onto the FD-C with the SC side facing the ChipM porous side and the dermal side in contact with the RS[16].

The system was maintained by a plastic support and screwed to assure tight junction. The donor compartment was finally sealed with a transparent plastic foil while the receptor chamber was filled with V_{RS} = 8 ml of 10 mM Sørensen's buffer using the side arm of the FD-C.

Two equipped FD-C were placed in a UV box (CL-1000 Ultraviolet crosslinker UVP, 1 mJ·cm^{-1}). The third one was kept protected from light and used as a negative control.

5.4.4.2.b Free release in solution

2 $\left(^{2}_{LA}|40\right)$·ChipM·PL2·(Ibu)·{Sø} were used for the free release experiment. They were immersed in V_{RS} = 8 ml of 10 mM Sørensen's buffer and the container sealed with a plastic foil. One was placed in the UV box while the second one was kept protected from light and used as a negative control.

5.4.5 Quantification

5.4.5.1 Calibration procedure

5.4.5.1.a Standard solutions

Stock solutions

To reduce uncertainties due to the measurement of low mass and speed-up the dissolution of ibuprofen, a concentrated ibuprofen stock solutions S_0 was prepared using the 25 mM Sørensen's buffer before being diluted to give S_1. For the preparation of S_0, ibuprofen was let to dissolve 24 hours protected from light at room temperature under stirring.

S_0	50.0 mg of ibuprofen in 200 ml of 25 mM Sørensen's buffer	$[ibu]_{S_0} = 0.25$ mg·ml^{-1} in 25 mM Sørensen's buffer
S_1	10.0 ml of S_0 diluted to 25 ml with pure water	$[ibu]_{S_1} = 0.1$ mg·ml^{-1} in 10 mM Sørensen's buffer

Calibration solutions

A series of N = 6 calibration solutions S_Ci were prepared using increasing volumes V_{S_1}i of stock solution S_1 and diluted to 10 ml with the 10 mM Sørensen's buffer.

—	$V_{S_1} \rightarrow S_C$i	$[ibu]_{S_C i}$
S_C1	0.00 ml	$[ibu]_{S_C 1} = 0.00$ µg·ml^{-1}
S_C2	0.75 ml	$[ibu]_{S_C 2} = 7.50$ µg·ml^{-1}
S_C3	1.00 ml	$[ibu]_{S_C 3} = 10.0$ µg·ml^{-1}
S_C4	1.50 ml	$[ibu]_{S_C 4} = 15.0$ µg·ml^{-1}
S_C5	2.00 ml	$[ibu]_{S_C 5} = 20.0$ µg·ml^{-1}
S_C6	2.50 ml	$[ibu]_{S_C 6} = 25.0$ µg·ml^{-1}

Once prepared, calibration solutions were stored at room temperature in the dark prior to analysis.

5.4.5.1.b Calculations

Using the method developed in Chapter 4 the analysis were conducted 5 times (p = 5) for each of the N standard solutions.

Pearson product-moment correlation coefficient

The Pearson correlation coefficient of this calibration is $\rho^2 = 0.998921$ proving a good correlation between the ibuprofen concentration in calibration solutions and the absorbance signal.

Homoscedasticity

The Bartlett's test gives $\chi^2_{OBS} = 2.5 < \chi^2_5 = 11.1$ proving that the calibration method is homoscedastic. As a consequence, the N standard deviations were merged in $S_0 = 16.16385510$ with a degree of freedom $\nu_0 = 24$.

Regression parameters

The regressions models for this calibration are:

For 1.WIC:

$Y = 64.73263358 \cdot X + 0.74581964401$

For 1.WOC:

$Y = 64.77373653 \cdot X$

For 2.WIC:

$Y = 23.90637051 \cdot X^2 + 58.40165929 \cdot X + 0.2500888374$

For 2.WOC:

$Y = 61.65434390 \cdot X^2 + 0.1543404903 \cdot X$

Significance of coefficients

The significance of the coefficients study gives:

Model	$t_{N-k-1}(0.95)$	$t_{OBS}(0.95)$	Result
1.WIC	$t_4(0.95) = 2.776$	$t_{OBS}(B_{1.WIC}) = 60.86$ $t_{OBS}(A_{1.WIC}) = 0.04$	significant not significant
1.WOC	$t_5(0.95) = 2.571$	$t_{OBS}(B_{1.WOC}) = 126.81$	significant
2.WIC	$t_3(0.95) = 3.182$	$t_{OBS}(C_{2.WIC}) = 4.25$ $t_{OBS}(B_{2.WIC}) = 37.47$ $t_{OBS}(A_{2.WIC}) = 2.67$	significant significant not significant
2.WOC	$t_4(0.95) = 2.776$	$t_{OBS}(C_{2.WOC}) = 2.07$ $t_{OBS}(B_{2.WOC}) = 39.71$	not significant significant

This reveals that only the 1.WOC coefficients are all significant.

Models validity

The validity of the models was finally tested, giving:

Model	F_{OBS}	$F_{\nu_1,\nu_2}(0.95)$	Result
1.WIC	$F_{OBS}(1.WIC) = 1.75$	$F_{4,24}(0.95) = 2.78$	valid
1.WOC	$F_{OBS}(1.WOC) = 1.40$	$F_{5,24}(0.95) = 2.62$	valid
2.WIC	$F_{OBS}(2.WIC) = 0.33$	$F_{3,24}(0.95) = 3.01$	valid
2.WOC	$F_{OBS}(2.WOC) = 0.84$	$F_{4,24}(0.95) = 2.78$	valid

The 4 models are valid. However, considering the significance of coefficients, only the 1.WOC model can be used for the quantification of the ibuprofen release.

5.4.5.2 Quantification procedure

5.4.5.2.a Ibuprofen concentration in the aliquot

For the quantification, the response of each aliquot was measured n = 6 times by HPLC, giving an average signal Y_i. According to the 1.WOC model, the corresponding ibuprofen concentration $[ibu]_i$ was calculated with the corresponding uncertainties $\delta[ibu]_i$ using the relations:

$$[ibu]_i = \frac{Y_i}{B_{1.WOC}} \tag{5.1}$$

And

$$\delta[ibu]_i = \frac{S_r(1.WOC) \cdot t_5(0.95)}{B_{1.WOC}} \cdot \sqrt{\frac{1}{N} + \frac{1}{n} + \frac{(Y - \overline{Y_{S_C i}})^2}{N \cdot B_{1.WOC}^2 \cdot \mathrm{Var}([ibu]_{S_c i})}} \tag{5.2}$$

5.4.5.2.b Cumulated ibuprofen release

The cumulated ibuprofen amount released $m_{ibu}i$ is defined as the sum of the ibuprofen amount in the cell plus the amount of ibuprofen removed after each sampling:

$$m_{ibu}i = V_{RS}\ [ibu]_i + V_a \sum_{j=1}^{i-1} [ibu]_j \tag{5.3}$$

The corresponding uncertainties were obtained by using the law of uncertainties propagation:

$$\Delta m_{ibu}i = \sqrt{\sum_{j=1}^{i} \left|\frac{\partial m_{ibu}i}{\partial [ibu]_j}\right|^2 \ |\delta[ibu]_j|^2} \tag{5.4}$$

5.4.6 Mathematical model

5.4.6.1 Problem description

The transport of drug in a membrane is governed by the Fick's second law of diffusion. In this study, the diffusion can be described by working with three diffusion domains which are the dM, the epidermis and the RS. The free release in solution is the same but without the epidermis domain. On the same time, the ibuprofen introduction in the dM is imposed by UV-induced photocleavage reaction that is considered arbitrarily as a first oder kinetic reaction [17].

In one dimension, this mathematical representation gives a system of partial differential equations (PDE) that describes the ibuprofen concentration profile in each domain in function of the drug release from the ChipM.

$$\begin{cases} \dfrac{d[ibu]_t}{dt} = -k_A\ [ibu]_t & x = 0 \\ \dfrac{\partial [ibu]_{x,t}}{\partial t} = D_{ibu.dM}\ \dfrac{\partial^2 [ibu]_{x,t}}{\partial x^2} & x \in \text{dM} \\ \dfrac{\partial [ibu]_{x,t}}{\partial t} = D_{ibu.epi}\ \dfrac{\partial^2 [ibu]_{x,t}}{\partial x^2} & x \in \text{epidermis} \\ \dfrac{\partial [ibu]_{x,t}}{\partial t} = D_{ibu.RS}\ \dfrac{\partial^2 [ibu]_{x,t}}{\partial x^2} & x \in \text{RS} \end{cases} \tag{5.5}$$

With $D_{ibu.y}$ the diffusion coefficient of ibuprofen in the domain y. Its value, expressed in $m^2 \cdot s^{-1}$, depends on the temperature of the diffusion layer y and on ibuprofen characteristics. However, the collecting of information describing the photocleavage characteristics from ChipM, the diffusion of the ibuprofen through a complex porous structure, the influence of dM and RS characteristics (viscosity, interactions with ibuprofen), etc. appeared difficult.

As a consequence, the model proposed only considers the kinetic aspect and not the spatial dimension. This approximation means an isotropic distribution of ibuprofen in each domain of the system:

$$\frac{\partial [ibu]_{x,t}}{\partial x} = 0 \tag{5.6}$$

However, by working with this condition, the Fick's equations cannot be solved. For this reason, the model developed is based on an analogy between diffusion phenomenon and chemical reaction kinetic equations.

5.4.6.2 Model proposal

The analogy proposed compares the passage of the ibuprofen between domains to a chemical reaction (Table 5.1). In a chemical reaction a substance A is converted to B and the kinetic of the reaction is characterized by a constant k_a. Considering a linear multistage reaction, B gives C which is finally transformed into D with the corresponding kinetic constants k_b and k_c.

Kinetic	A	$\xrightarrow{k_a}$	B	$\xrightarrow{k_b}$	C	$\xrightarrow{k_c}$	D
Diffusion model	ibu_{ChipM}	$\xrightarrow{k_1}$	ibu_{dM}	$\xrightarrow{k_2}$	ibu_{epi}	$\xrightarrow{k_3}$	ibu_{RS}

Table 5.1: Model Proposal

The release of ibuprofen from the surface of the pores into the dM is a photochemical reaction. In this model the same equations are applied to describe the passage of the ibuprofen from the dM to the epidermis and from the epidermis to the RS. As a consequence the ibuprofen bound to ChipM (ibu_{ChipM}) is converted to ibu_{dM} which gives ibu_{epi} and finally ibu_{RS}, with the corresponding constants k_1, k_2 and k_3.

Thus, by assuming only first order kinetic reactions, the system of equation becomes:

$$\begin{cases} \dfrac{d[ibu]_t^{ChipM}}{dt} = -k_1\ [ibu]_t^{ChipM} & \text{on ChipM surface} \\ \dfrac{d[ibu]_t^{dM}}{dt} = k_1\ [ibu]_t^{ChipM} - k_2\ [ibu]_t^{dM} & \text{in dM} \\ \dfrac{d[ibu]_t^{epi}}{dt} = k_2\ [ibu]_t^{dM} - k_2\ [ibu]_t^{epi} & \text{in epidermis} \end{cases} \tag{5.7}$$

$$\text{With} \quad \begin{cases} [ibu]_{t=0}^{ChipM} = ibu_0 \\ [ibu]_{t=0}^{dM} = 0 \\ [ibu]_{t=0}^{epi} = 0 \end{cases} \tag{5.8}$$

The resolution of this system gives:

$$\begin{cases} [ibu]_t^{ChipM} = ibu_0\ e^{-k_1\ t} \\ [ibu]_t^{dM} = \dfrac{ibu_0\ k_1}{k_2 - k_1}\left(e^{-k_1\ t} - e^{-k_2\ t}\right) \\ [ibu]_t^{epi} = \dfrac{ibu_0\ k_1\ k_2}{k_2 - k_1}\left(\dfrac{(e^{-k_1\ t} - e^{-k_3\ t})}{k_3 - k_1} - \dfrac{(e^{-k_2\ t} - e^{-k_3\ t})}{k_3 - k_2}\right) \end{cases} \tag{5.9}$$

Finally, the amount of ibuprofen released freely in solution is estimated by the equation $[\text{ibu}]_t^{RS} = \text{ibu}_0 - [\text{ibu}]_t^{ChipM} - [\text{ibu}]_t^{dM}$ since the ibuprofen does not cross the epidermis layer. In that case an accumulation of ibuprofen in RS is observed.

With the passage through the skin, the ibuprofen is first transferred from the ChipM to the , then through the epidermis to RS. In that case too an accumulation of the ibuprofen in RS should be observed. However, the low permeability of the epidermis should delay this accumulation compared to the free release in solution.

5.5 Bibliography

[1] Wagner, H., Kostka, K.-H., Lehr, C.-M. & Schaefer, U. F. Drug distribution in human skin using two different in vitro test systems: comparison with in vivo data. *Pharm. Res.* **17**, 1475-1481 (2000).

[2] Abdul Rasool, B. K., Abu-Gharbieh, E. F., Fahmy, S. A., Saad, H. S. & Khan, S. A. Development and evaluation of ibuprofen transdermal gel formulations. *Trop. J. Pharm. Res.* **9**, 355-363 (2010).

[3] Akhter, S. A. & Barry, B. W. Absorption through human skin of ibuprofen and flurbiprofen; effect of dose variation, deposited drug films, occlusion and the penetration enhancer N-methyl-2-pyrrolidone. *J. Pharm. Pharmacol.* **37**, 27-37 (1985).

[4] Luengo Contreras, J. E. (2007) *Human skin drug delivery using biodegradable PLGA-nanoparticles. Ph.D. Thesis. Universität des Saarlandes:DE.*

[5] Leveque, N., Makki, S., Hadgraft, J. & Humbert, P. Comparison of Franz cells and microdialysis for assessing salicylic acid penetration through human skin. *Int. J. Pharm.* **269**, 323-328 (2004).

[6] Viyoch, J., Patcharaworakulchai, P., Songmek, R., Pimsan, V. & Wittaya-Areekul, S. Formulation and development of a patch containing tamarind fruit extract by using the blended chitosan-starch as a rate-controlling matrix. *Int. J. Cosmet. Sci.* **25**, 113-125 (2003).

[7] Kunicher, N. *et al.* Characterization of factors that determine lentiviral vector tropism in skin tissue using an ex vivo model. *J. Gene Med.* **13**, 209-220 (2011).

[8] Harford, J. B. Preparation and Isolation of Cells In *Current Protocols in Cell Biology*, John Wiley & Sons, Inc., New York (2001).

[9] Kitano, Y. & Okada, N. Separation of the epidermal sheet by dispase. *Br. J. Dermatol.* **108**, 555-560 (1983).

[10] Aujard, I. *et al.* o-Nitrobenzyl photolabile protecting groups with red-shifted absorption: syntheses and uncaging cross-sections for one- and two-photon excitation. *Chem. Eur. J.* **12**, 6865-6879 (2006).

[11] Il'ichev, Y. V., Schwoerer, M. A. & Wirz, J. Photochemical Reaction Mechanisms of 2-Nitrobenzyl Compounds: Methyl Ethers and Caged ATP. *J. Am. Chem. Soc.* **126**, 4581-4595 (2004).

[12] Neugebauer, W., Williams, R. E., Barbier, J.-R., Brzezinski, R. & Willick, G. Peptide synthesis on chitin. *Int. J. Pept. Protein Res.* **47**, 269-275 (1996).

[13] Neugebauer, W. A., D'Orleans-Juste, P. & Bkaily, G. Peptide synthesis on chitosan/chitin. *Adv. Chitin Sci.* **4**, 411-416 (2000).

[14] Stahl, J., Niedorf, F. & Kietzmann, M. The correlation between epidermal lipid composition and morphologic skin characteristics with percutaneous permeation: an interspecies comparison of substances with different lipophilicity. *J. Vet. Pharmacol. Therapeut.* **34**, 502-507 (2011).

[15] McIlvaine, T. C. A buffer solution for colorimetric comparison. *J. Biol. Chem.* **49**, 183-186 (1921).

[16] Al-Saidan, S. M. Transdermal self-permeation enhancement of ibuprofen. *J. Control. Release* **100**, 199-209 (2004).

[17] Ast, T., Heine, N., Germeroth, L., Schneider-Mergener, J. & Wenschuh, H. Efficient assembly of peptomers on continuous surfaces. *Tetrahedron Lett.* **40**, 4317-4318 (1999).

Chapter 6

Prospectives for design and programming

Abstract: This last part is dedicated to the practical applications of the ATTS and includes proposals and potential uses. For this reasons, this chapter represents a substantial document for future studies as it concerns the design of the system but also the programming of the electronic support. Finally, it answers to the main specifications introduced at the beginning of this study by the creation of a tool which makes chronotherapies and polytherapies possible.

6.1 General remarks

The use of the intelligent transdermal technology proposed is based on time and power modulation of ChipM illumination and on the programming of an eS as the released amount is function of this illumination time.

Indeed, the eS contains a program which allows the control of illumination on different areas but also the control of moment and illumination time of the mS. This opens the way to personalized treatment by implementing polytherapies and chronotherapies on a single support. However, since the initial design of the ATTS is composed of mS embedded in an aS, several possibilities of design exist and deeper investigations are required. For these reasons a range of applications able to broaden the capacities of release were identified. Furthermore, to limit the cost of production resulting from personalized medications, the product described is an assembly based on a mosaic principle. This allows, from regular mass products, to obtain highly individualized assemblies.

As a consequence, the ATTS is made of detachable items. The items are assembled on an aS which combines everything together. Once the mS is empty, or the energy supply is finished, the part can be replaced, extending the life time of the device thus reducing the cost for the patient.

6.2 ATTS as tool for polytherapy

In a near future, the use of polytherapies may increase in a significant way. However, the lack of tools allowing a rigorous control of administration currently limits their use. Therefore, the ATTS developed represents an innovative solution to manage the release of several drugs from a single support.

6.2.1 Mode of use

Because of their structure, the ChipM, modified or not, can be used in different ways. In case of non modified structures, the matrices can complete the outfit of the existing passive TTS since the release of a medication happens by uncontrolled diffusion. On the contrary, the modified matrices can serve as a powerful tool to ameliorate the available devices.

Moreover, since the ATTS mS is based on the use of a porous structure, the diffusion phenomenon is really fast compared to a traditional TTS since the released molecules diffuse in liquid dM.

6.2.1.1 Passive use

The use of the patch in passive mode means that the release happens without control. This is the case for all the ChipM which do not have secondary couplings. Passive uses are presented here (Figure 6.1) to demonstrate potential uses of the the ATTS. In A, the ChipM is loaded with a basic dM such as a buffer solution. This kind of structure can be used as protective or wound healing. Indeed, if the initial ChipM is mainly dedicated to be used as a mS, the opposite can also be imagined with its use as a trap, for example for physiological liquids after injury.

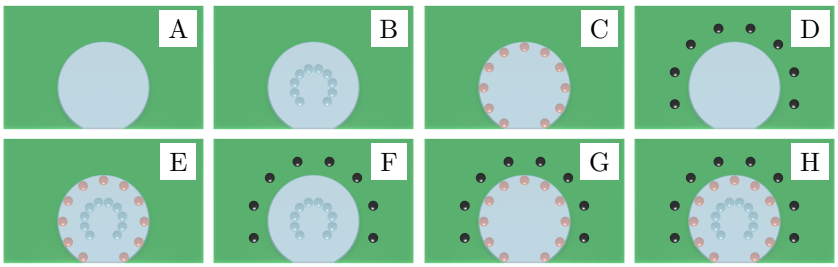

Figure 6.1: ChipM for use in passive mode
A: ChipM empty ; B: Drug loaded dM ;
C: Primary coupling on ChipM ; D: Doped ChipM ;
E, F, G, H: Combinations of A, B, C and D

Based on the same idea, the loading of the dM with an active molecule is presented in the matrix B. This active molecule is released without control and can be used to neutralize absorbed products. In release mode, this is a classical passive TTS. The matrix C, represents a ChipM whose surface has been modified by a primary coupling. This modification can help to stabilize the chitosan or, as for the matrix B, to neutralize absorbed molecules. In D, is presented a doped ChipM in which substances are incorporated in the structure of the material, here the chitosan. These agents can serve to improve the aesthetic appearance of the product but also to increase the mechanical properties. Matrices E, F, G and H are combinations of the previously described A, B, C and D.

6.2.1.2 Active use

The use of the ChipM in an active way depends of the presence of a stimuli responsive moiety as primary coupling. Indeed, as it is demonstrated in this study a controlled release is possible by submitting a photosensitive ChipM to light. Herein are proposed different possibilities of active uses with a photolinker as primary coupling (Figure 6.2).

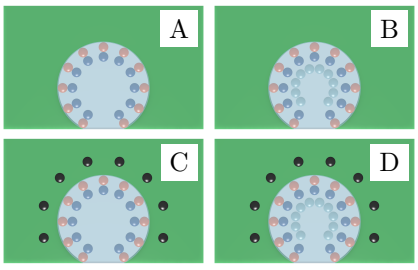

Figure 6.2: ChipM for use in active mode
A: Secondary coupling on ChipM ; B: Secondary coupling with drug loaded dM ;
C: Secondary coupling with doped ChipM ; D: Combination of B and C.

In A, an active agent is immobilized on a photolabile moiety and released while subjected to light. This corresponds to the structure used to demonstrate the proof of concept of the ATTS in Chapter 5. In B, the dM is loaded with an agent and released from the ChipM without control.

This free agent can be another drug, a permeation enhancer, a molecule able to reduce skin irritation, an ionic substance to improve the release rate by increasing the gradient, etc. In that case, the obtained TTS is both active and passive. This gives the possibility to indirectly control the release by working with highly concentrated drug loaded dM, the tuning is assured by controlled release of a permeation enhancer bound to the photolinker.

The matrix C is a doped ChipM. As for the doped matrix in passive mode, it can serve to modify the ChipM properties or appearance. However, in the case of photorelease, the doping also makes it possible to modify the response of the matrix to the light. Finally, in D, the ChipM is a mix of the three others.

6.2.2 Architecture

In addition to the mode of action, the design of the final ATTS is also as a way to personalize a treatment. For this reason, different architectures are suggested using a circular design. For each of the architecture investigated the theoretical drug loading using the values obtained in Chapter 4 were calculated and compared with commercially available products.

6.2.2.1 Patchwork geometry

For the architectures it is possible to use several mS on the same aS, each of them facing one LED (Figure 6.3). The architecture α_7 can be used for example as a "weekly TTS" with the release from one mS per day. This method presents the advantage to makes it possible the use of several independent mS loaded with different drugs.

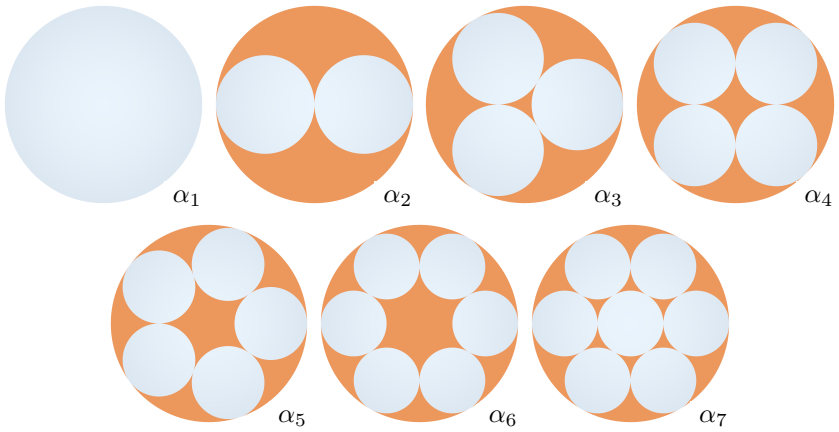

Figure 6.3: Architecture α_1 to α_7, mS in blue, aS in orange

As a consequence it induces a reduction of the production costs with the possibility to tune the ATTS by placing different mS. Moreover, this opens the way to reusable TTS since only the aS and the mS have to be replaced regularly, the eS remaining the same between usages.

6.2.2.2 Combinations of mS

Considering an industrial production of j different mS and using the architectures introduced previously, the amount of combinations that are possible to obtain for each architecture can be calculated by using the relation 6.1.

$$\aleph(\alpha_i; j) = \sum_{k=1}^{i} \binom{i-1}{k-1}\binom{j}{k} = \frac{\Gamma(i+j)}{\Gamma(j)\,\Gamma(i+1)} \tag{6.1}$$

$$\text{With } \Gamma(n) = (n-1)! \tag{6.2}$$

Until j = 7, the amount of combinations are listed in the table 6.1.

	α_1	α_2	α_3	α_4	α_5	α_6	α_7
j = 1	1	1	1	1	1	1	1
j = 2	2	3	4	5	6	7	8
j = 3	3	6	10	15	21	28	36
j = 4	4	10	20	35	56	84	120
j = 5	5	15	35	70	126	210	330
j = 6	6	21	56	126	252	462	792
j = 7	7	28	84	210	462	924	1716

Table 6.1: Combinations for ATTS architectures

The results clearly show the potential of the ATTS since the production of 7 different mS allows the assembly of 1716 different TTS by using the architecture α_7.

As an other example, if 18 different mS are commercially available, by using the architecture α_5, the potential combinations are $\aleph(\alpha_5; 18)$ = 26,334. The resort to biosimulation is a clear advantage for the study of interactions resulting from these combinations.

6.2.2.3 Theoretical drug loading

According to the geometric specifications of the project, the diameter of the aS is limited to the width of a credit card (5.398 cm from ISO/IEC 7810 ID-1 standard standard).

By working with a 1.988 cm thick mS and a drug loading of 168.99 µmol·g^{-1} of chitosan (Chapter 4), a surface loading of 0.6719 µmol·cm^{-2} can be reached. Using this value, the theoretical loading for each of the architectures was estimated.

6.2.2.3.a Architecture α_1

Unit mS radius	2.699 cm	Surface density	1.000
Unit mS surface	22.885 cm^2	Total mS surface	22.885 cm^2
Unit mS volume	4.549 cm^3	Total mS volume	4.549 cm^3
Unit chitosan mass	90.986 mg	Total chitosan mass	90.986 mg
Unit mS loading	15.376 µmol	Total mS loading	15.376 µmol

6.2.2.3.b Architecture α_2

Unit mS radius	1.350 cm	Surface density	0.500
Unit mS surface	5.721 cm^2	Total mS surface	11.443 cm^2
Unit mS volume	1.137 cm^3	Total mS volume	2.275 cm^3
Unit chitosan mass	22.746 mg	Total chitosan mass	45.493 mg
Unit mS loading	3.844 µmol	Total mS loading	7.688 µmol

6.2.2.3.c Architecture α_3

Unit mS radius	1.253 cm	Surface density	0.646
Unit mS surface	4.930 cm^2	Total mS surface	14.788 cm^2
Unit mS volume	0.980 cm^3	Total mS volume	2.940 cm^3
Unit chitosan mass	19.597 mg	Total chitosan mass	58.792 mg
Unit mS loading	3.312 µmol	Total mS loading	9.935 µmol

6.2.2.3.d Architecture α_4

Unit mS radius	1.118 cm	Surface density	0.686
Unit mS surface	3.926 cm^2	Total mS surface	15.706 cm^2
Unit mS volume	0.781 cm^3	Total mS volume	3.122 cm^3
Unit chitosan mass	15.611 mg	Total chitosan mass	62.443 mg
Unit mS loading	2.638 µmol	Total mS loading	10.552 µmol

6.2.2.3.e Architecture α_5

Unit mS radius	0.999 cm	Surface density	0.685
Unit mS surface	3.136 cm^2	Total mS surface	15.681 cm^2
Unit mS volume	0.623 cm^3	Total mS volume	3.117 cm^3
Unit chitosan mass	12.469 mg	Total chitosan mass	62.344 mg
Unit mS loading	2.107 µmol	Total mS loading	10.536 µmol

6.2.2.3.f Architecture α_6

Unit mS radius	0.900 cm	Surface density	0.667
Unit mS surface	2.543 cm^2	Total mS surface	15.257 cm^2
Unit mS volume	0.505 cm^3	Total mS volume	3.033 cm^3
Unit chitosan mass	10.110 mg	Total chitosan mass	60.657 mg
Unit mS loading	1.708 µmol	Total mS loading	10.250 µmol

6.2.2.3.g Architecture α_7

Unit mS radius	0.900 cm	Surface density	0.778
Unit mS surface	2.543 cm^2	Total mS surface	17.800 cm^2
Unit mS volume	0.505 cm^3	Total mS volume	3.538 cm^3
Unit chitosan mass	10.110 mg	Total chitosan mass	70.767 mg
Unit mS loading	1.708 µmol	Total mS loading	11.959 µmol

It appears from these calculations that, except the architecture α_1, the α_7 is the designs which presents the highest coupling capacity as more than 75% of the surface of the ATTS is occupied by mS.

6.2.2.4 Comparison with existing products

By comparing these values with commercially available passive TTS, calculations give:

Mylan estradiol (Mylan)	15.50 cm^2 Estradiol (1.94 mg) Mw = 273.3820 $g{\cdot}mol^{-1}$	125.16 $\mu g{\cdot}cm^{-2}$ 0.46 $\mu mol{\cdot}cm^{-2}$	$<$ to ATTS
Catapress TTS (Boehringer Ingelheim)	7.00 cm^2 Clonidine (5.00 mg) Mw = 230.0939 $g{\cdot}mol^{-1}$	714.29 $\mu g{\cdot}cm^{-2}$ 3.10 $\mu mol{\cdot}cm^{-2}$	$>$ to ATTS
Watson fentanyl (Watson)	30.00 cm^2 Fentanyl (7.50 mg) Mw = 336.4705 $g{\cdot}mol^{-1}$	250.00 $\mu g{\cdot}cm^{-2}$ 0.74 $\mu mol{\cdot}cm^{-2}$	$\approx$ to ATTS

Comparisons clearly highlight that the ATTS is close to commercial products. However, since the coupling capacity of the ChipM is not optimized (Chapter 4), higher values are expected.

6.3 ATTS as tool for chronotherapy

6.3.1 Notion of response curve and response time

As introduced in Chapter 5, the release of a compound from a ChipM can be model as a series of diffusion phenomena after the initial photocleavage reaction. As a consequence each of the ChipM can be characterized by a response curve and a response time. The response curve is defined as the amount of drug in dM after the photo triggered release and is function of the amount of drug present on the support. Since this amount varies with time, the rate of release changes after each new illumination.

For this reason, the idea of response curve is introduced as a relation between the amount that is released in function of the remaining amount and the time of illumination (Figure 6.4). These curves are determined experimentally as in Chapter 5, or by *in-silico* extrapolations.

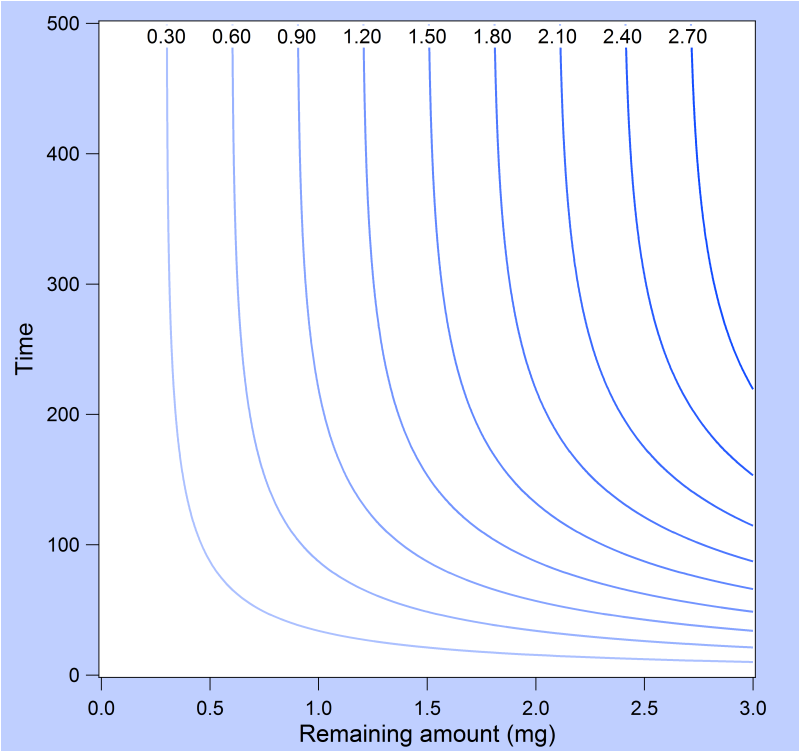

Figure 6.4: Example of a response curve

Once in the dM, a molecule needs a certain time to reach the circulatory system of the patient. This time corresponds to the time of response and mainly depends on the structure of the ChipM and the composition of the dM.

For this reason, each ChipM formulation is also characterized by its time of response. Its value is obtained by mathematical modeling or experimentally. Finally, using the response curve and the time of response, the amount of drug administrated to a patient can be estimated.

6.3.2 Programming of the ATTS

A dedicated software can be used to manage the drug release from an ATTS. After the establishment of the posology, the doctor transfers to the software three data which are the kind of drug (Figure 6.5a, in that case drugs A, B, E and I), the amount and the time of administration.

By consultation of a database made of response curves and times of response for each drug loaded ChipM, an algorithm proposes different architectures and combinations that correspond to the posology (Figure 6.5b).

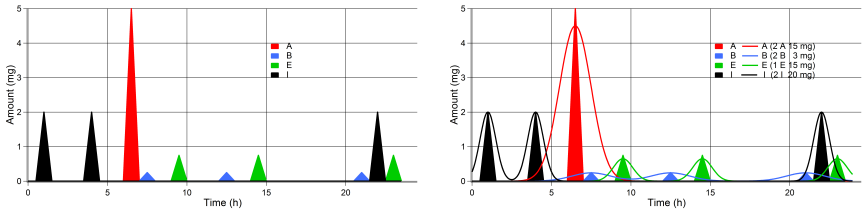

(a) Posology according to the prescription

(b) Estimated release from response curve

Figure 6.5: Comparison between posology and estimated release

The algorithm predicts the correct time of illumination to release the proper amount of drug, the energy consumption for the eS and also the correlation with the posology for each proposition.

After selection of the best proposal by the doctor, the software returns the distribution of the different drug loaded ChipM (Figure 6.6a) and also the time of illumination of the corresponding LED according to the position of the drug on the architecture (Figure 6.6b).

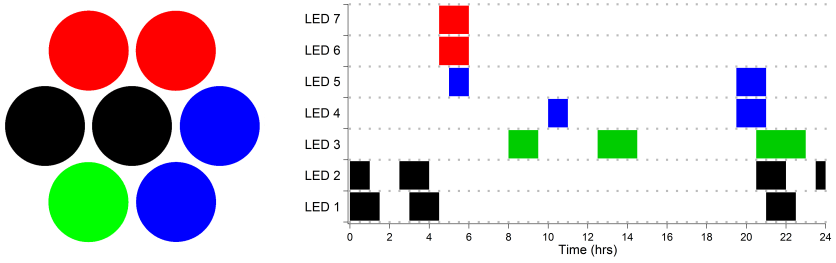

(a) Architecture distribution

(b) Corresponding time of illumination

Figure 6.6: Relation between the architecture and the programming

The prescription is then transmitted to the pharmacist for the assembling and the programming of the eS. The programing software tree structure is presented in figure 6.7.

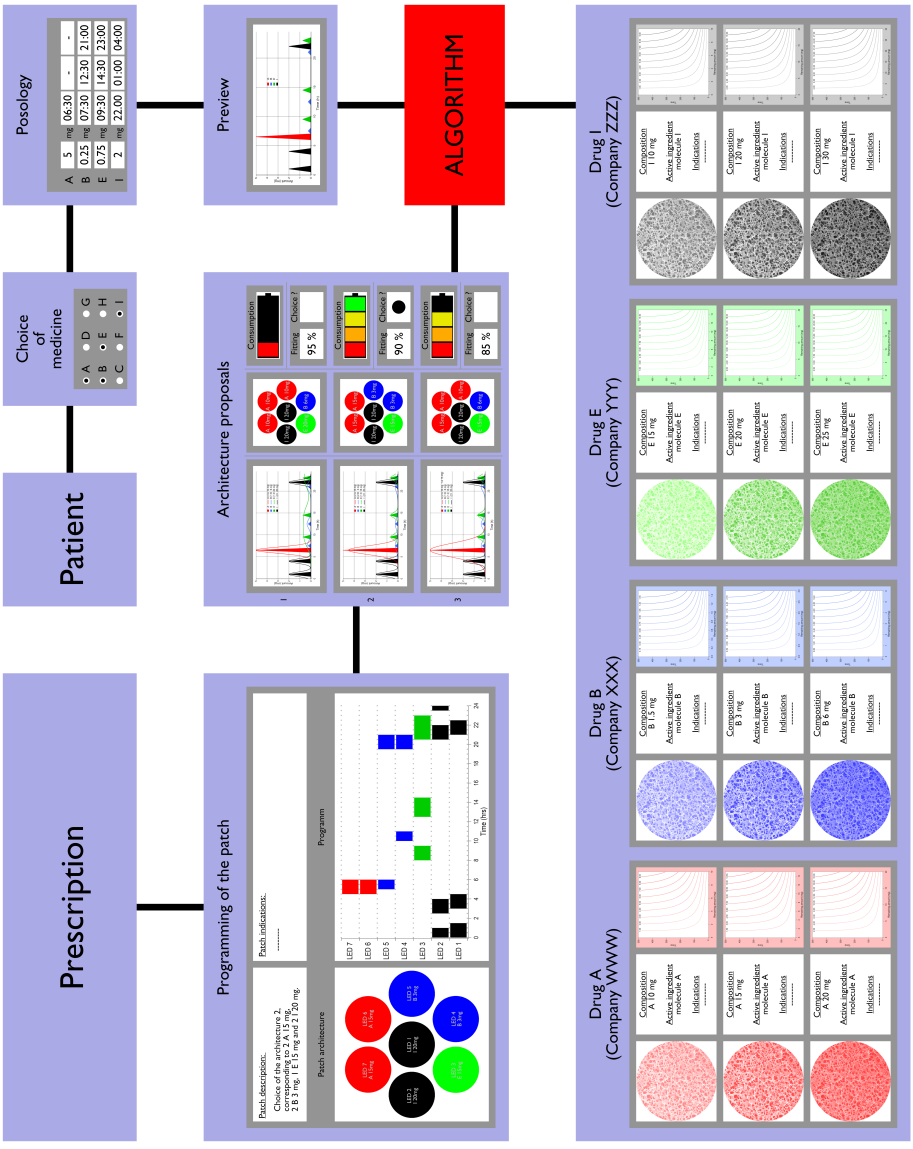

Figure 6.7: Example of programming software tree structure for the ATTS

Chapter 7

– Conclusion and perspectives –

In the last years, therapies based on transdermal delivery have extensively increased their number. This phenomenon can be correlated to two main factors which are a better match with the patient compliance and the design of commercially available devices able to control the release kinetics. This thesis describes a new transdermal drug delivery strategy designing surface modified porous scaffolds able to control the release of drug. The delivery of drug with time and dose control is becoming a crucial point in the development of new therapies for chronic diseases.

Herein photochemistry was chosen as good candidate for the control of the release and the first step consisted to synthesize a photocleavable traceless linker to allow the design of a photo induced release device. Then, a polymer matrix with the associated surface modification chemistry was developed to support the photolinker. Finally, the proof of concept was demonstrated by the release of ibuprofen on demand by an *in-vitro* study on human epidermis.

The Chapter 2 presents the synthesis of the photolinker. The reaction is considered as efficient as the overall yield is higher than 75%. However, some improvements are still possible for the recrystallization, so it can be assumed that it is possible to obtain a better yield by using different parameters. On the same time further studies should complete the understanding of the cleavage mechanism and kinetic from a polymer support.

Chapter 3 describes the procedure to obtain highly porous chitosan matrices using the TIPS method. Modifications of the freezing parameters makes it possible to influence the structure of the final material. Analysis were conducted to determine in which extent the freezing properties interfere with the phase change of the solution.

It appeared that the freezing step is of critical importance since ice crystal size, shape and distribution are strongly related with material characteristics such as pores size distribution and interconnection of the pores. However, the control of the ice crystal morphology is difficult and remains a major challenge. Investigations revealed that their formation is highly dependent of heat exchanges and more precisely on the evacuation of the latent heat released in the solution during the phase change. As a consequence, a mathematical model based on FEM was proposed to predict the heat exchanges.

With these results, a dedicated apparatus, the POMAP, using Peltier effect to manage the freezing conditions, has been built and makes it possible to considerably improve the quality of the materials produced by the method. Using the POMAP, obtained ChipM show a homogeneous structure made of uniform pores and the reproducibility is better.

In the Chapter 4, an innovative and effective method is presented for the production of ibuprofen loaded ChipM. Using the solid phase peptide synthesis method, different couplings on highly porous chitosan microstructures were realized. The procedures are particularly of interest as they allow an easy surface modification in a minimum of steps and in one solvent, which is crucial for reactions on porous materials.

A first coupling was made with the photolinkers PL1. The use of its protected equivalent PL1-Fmoc allowed the determination of surface loading by the quantification of DBF after the deprotection step. The quantitation method developed allows a really precise estimation of the ChipM coupling capacity. This quantitative study gives encouraging results as a surface loading of 168.99 µmol·g^{-1} of chitosan could be obtained.

As a consequence the use of the Fmoc protected PL1 photolinker represents an interesting way to optimize the coupling conditions. Indeed, since the loading is influenced by several parameters such as the temperature, the concentration of reagents or the diffusion in the pores, a better control of these factors should allow a significant improvement of the loading. In a second time, the attachment of ibuprofen on ChipM·PL2 was realized and the obtained matrices were used to demonstrate the proof of concept.

Finally, the possibility to obtain chitin porous structures by acetylation of the ChipM was also proved. This opens the way to the production of a new type of passive TTS by impregnation with a drug loaded solution. This is of great interest as the release from this kind of system should be faster than in a classical TTS.

In the Chapter 5 the photo-induced ibuprofen release from drug loaded ChipM was investigated using FD-C system and human epidermis. Using a very precise method for the quantification of low concentrations, this study can be considered as a real success because the proof of concept is established by significant drug release.

To describe the release from the ChipM and its diffusion through the porous structure and through the skin, a mathematical model is suggested. This model is based on kinetic equations instead of the Fick's second law of diffusion. However, the predicted results are in adequacy with experimental results and it clearly appears that the skin is the limiting factor for transdermal drug delivery. Moreover, the obtaining of diffusion rate curves in a separate way for transport in and in skin allows a better understanding of molecular diffusion in complex structures and gives access to information which remain difficult to obtain experimentally. Considering the similarities between the heat equation and the Fick's law, the use of the model developed in Chapter 3 for heat exchanges should allows a finer description of the molecular transport involved in the ATTS.

Finally, the establishment of a drug concentration profile in function of all the involved parameters, such as the time of illumination, the initial amount of drug, the viscosity of the and the presence or not of permeation enhancer will allow the programming of the eS using the curves obtained by study of FD-C or predictions from the model.

The Chapter 6 describes drug combinations on the ATTS. The resulting product is a fully personalized system by combining standardized modified matrices. This gives a huge advantage in terms of industrial production as only normal modified matrices have to be produced. Depending of the needs, the pharmacist, the doctor or the patient can build their system by combining drug loaded units.

The ATTS answers to the specifications proposed in this study. Indeed, it groups on a single support a tool for polymedication and chronotherapy with a fine control in time and in quantity of the treatment administered to a patient, even for a complex mixture. Moreover, the study of synergies, using *in-silico* biosimulation, should help to identify new synergies between drugs giving, in theory, an infinity of drug combinations.

The tools and methods developed in this study are also destined to interesting future applications. In particular the researches are now focused on the development of the POMAP, with the production of additional modules, and on the surface modification for the improvement of the drug loading.

As an example of module for the POMAP, the addition of pumps should increase the production possibilities. In case of liquid pumps, different liquids can be pumped through the production cell such as solvents (for washing, surface modification, etc.) or biological liquids (for cell culture on the scaffold). The main advantage of the pump module is that the full production is isolated from the outside giving a perfect control of the working conditions (temperature, sterile conditions, anaerobic conditions, etc.). In a first time, the use of a vacuum pump module should simplify the freeze drying.

The addition of a supercritical CO_2 module makes the obtaining of highly porous structures like, for example silica aerogels, possible. In that case, the average pore size is too small to support a classical freeze drying and the supercritical extraction is the only way to get a dry polymer structure. This also opens the way to the production of materials with double porosity. As an example, a ChipM obtained by a normal TIPS method can be used as template for a sol-gel process. The chitosan template is then removed by dissolution and the resulting structure is dried with supercritical CO_2. This method would allow the obtaining of highly permeable silica aerogels with two different porosities: one from the template structure and a second one from the aerogel.

Other modules are also under study, such as tunable PM architectures giving the possibility to use various molds shapes (curves, spheres, etc.) or to apply different cooling rates on a single mold to induce different porosities on the same scaffold. Finally, an electrodeposition module is now under development to allow the deposition of metal on a classical polymer scaffold, and the obtaining of porous metal scaffold.

Concerning the surface modifications, reaction conditions have to be optimized in term of reagents concentrations, temperature and soaking methods in order to improve the drug loading. However, another way is currently explored and consists in the use of drug loaded nanoparticles. Using this method the drug loading of a matrix should be increased to a great extent and the nanoparticle also acts as permeation enhancer. Another advantage of this method is that all drug molecules can be used on the same photolinker. Several suggestions are presented in Appendix C using PLGA nanoparticles as drug carrier. This increases again the release capacities of the ATTS.

Appendix A

Raw product analysis

A.1 Apocycin

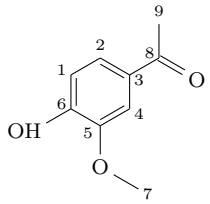

Figure A.1: Apocynin

^{1}H-NMR (200 MHz, DMSO-*d6* δ) 2.49 (s, 3H, H_9), 3.83 (s, 3H, H_7), 6.88 (d, J = 8.2 Hz, 1H, H_1), 7.45 (d, J = 2.0 Hz, 1H, H_4), 7.51 (dd, J = 8.2 Hz, J = 2.0 Hz, 1H, H_2), 9.97 (s, 1H, OH).

^{13}C-NMR (200 MHz, DMSO-*d6* δ) 26.15 (C_9), 55.57 (C_7), 111.15 (C_4), 114.86 (C_1), 123.33 (C_2), 128.86 (C_3), 147.46 (C_6), 151.65 (C_5), 151.65 (C_8).

A.2 Ethyl-4-bromobutyrate

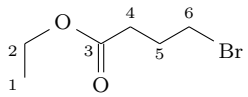

Figure A.2: Ethyl-4-bromobutyrate

^{1}H-NMR (200 MHz, DMSO-*d6* δ) 1.19 (t, J = 7.1 Hz, 3H, H_1), 2.00 (dt, J = 6.6 Hz, J = 7.3 Hz, 2H, H_5), 2.44 (t, J = 7.3 Hz, 2H, H_4), 3.55 (t, J = 6.6 Hz, 2H, H_6), 4.01 (quad., J = 7.1 Hz, 2H, H_2).

^{13}C-NMR (200 MHz, DMSO-*d6* δ) 14.04 (C_1), 27.68 (C_5), 31.99 (C_4), 33.89 (C_6), 59.93 (C_2), 171.92 (C_3).

Appendix B

pH calculations

B.1 Lactic acid solution

For a weak acid, the acid dissociation constant is expressed as:

$$K_a = \frac{[A^-]\ [H_3O^+]}{[AH]} \tag{B.1}$$

where

$[A^-]$	Concentration of conjugated base ions
$[H_3O^+]$	Concentration of $[H_3O^+]$ ions
[AH]	Concentration of undissociated acid molecules

As the solution stays neutral $[H_3O^+] = [A^-]$

If C_{A0} is the initial concentration of lactic acid then $[A^-] = C_{A0} - [H_3O^+]$

Finally, by replacing in the K_a equation:

$$[H_3O^+]^2 + K_a\ [H_3O^+] - K_a\ C_{A0} = 0 \tag{B.2}$$

By solving this equation:

$$[H_3O^+] = \frac{1}{2}\left(-K_a + \sqrt{K_a^2 + 4\ K_a\ C_{A0}}\right) \tag{B.3}$$

$$\text{With } C_{A0} = \frac{m}{Mw\ V} \tag{B.4}$$

where

m	The mass of lactic acid in solution
Mw	The molecular weight of lactic acid
V	The volume of the solution

Finally, as $pH = -\log[H_3O^+]$ so:

$$pH = -log\left(\frac{1}{2}\left(-10^{-pK_a} + \sqrt{10^{-2\ pK_a} + \frac{4\ m\ 10^{-pK_a}}{Mw\ V}}\right)\right) \tag{B.5}$$

Using the same equation, the uncertainties on the expected value for the pH are calculated using the relation:

$$\delta pH = \sqrt{\left|\frac{\partial pH}{\partial pK_a}\right|^2 |\delta pK_a|^2 + \left|\frac{\partial pH}{\partial m}\right|^2 |\delta m|^2 + \left|\frac{\partial pH}{\partial V}\right|^2 |\delta V|^2}$$

B.2 Ammonia solution

For a weak base, the acid dissociation constant is expressed as:

$$K_b = \frac{[BH^+]\ [HO^-]}{[B]} \tag{B.6}$$

where

$[BH^+]$	Concentration of conjugated acid ions
$[HO^-]$	Concentration of $[HO^-]$ ions
[B]	Concentration of undissociated basic molecules

As the solution stays neutral $[HO^-] = [BH^+]$. If C_{B0} is the initial concentration of ammmonium hydroxide then $[B] = C_{B0} - [HO^-]$

Finally, by replacing in the K_b equation:

$$[HO^-]^2 + K_b\ [HO^-] - K_b\ C_{B0} = 0 \tag{B.7}$$

By solving this equation:

$$[HO^-] = \frac{1}{2}\left(-K_b + \sqrt{K_b^2 + 4\ K_b\ C_{B0}}\right) \tag{B.8}$$

$$\text{With } C_{B0} = \frac{C_0\ V_0}{V_{B0}} \tag{B.9}$$

where

C_0	The concentration of commercial ammonia solution
V_0	The volume of initial ammonia solution transfered
V_{B0}	The volume of the final solution

Finally, as $pH = 14 - \log[HO^-]$ so:

$$pH = 14 - log\left(\frac{1}{2}\left(-10^{-pK_b} + \sqrt{10^{-2\ pK_b} + \frac{4\ C_0\ V_0\ 10^{-pK_b}}{V_{B0}}}\right)\right) \tag{B.10}$$

Using the same equation, the uncertainties on the expected value for the pH are calculated using the relation:

$$\delta pH = \sqrt{\left|\frac{\partial pH}{\partial pK_b}\right|^2 |\delta pK_b|^2 + \left|\frac{\partial pH}{\partial C_0}\right|^2 |\delta C_0|^2 + \left|\frac{\partial pH}{\partial V_0}\right|^2 |\delta V_0|^2 + \left|\frac{\partial pH}{\partial V_{B0}}\right|^2 |\delta V_{B0}|^2}$$

Appendix C

Nomenclature

The possibilities that are resulting from the creation of the ATTS for polytherapies and chronotherapies require the introduction of a tool able to describe in a simple way the structure of the mS. Considering the amount of parameters involved a nomenclature is proposed to characterize the ChipM produced using the POMAP.

C.1 Non-modified ChipM

The complete dissolution of chitosan is dependent on the acid concentration. Therefore, the full dissolution of chitosan is considered as total when all GlcNH units are protonated. As a consequence, the concentration of acid is directly in relation with the amount of amine moieties on chitosan. For this reason, the mass of chitosan that is possible to dissolve in a X%(v:v) solution of lactic acid (LA) is given by the relation:

$$m_{chitosan} = \frac{m_{LA}\ Mw_{chitosan}}{Mw_{LA}\ DDA\ DP} \tag{C.1}$$

$$\text{With } DP = \frac{Mw_{chitosan} - Mw_{H_2O}}{DDA\ Mw_{GlcNH} + (1 - DDA)\ Mw_{GlcNAc} - Mw_{H_2O}} \tag{C.2}$$

$Mw_{chitosan} \in$ [190,000;310,000] g·mol^{-1} and DDA = 0.818

Lactic acid concentration		$m_{chitosan}$(g)	$m_{chitosan}$ retained (g)
0.25%(w:v)	27.7538 mM	[0.57277;0.57279]	0.5 g
0.50%(w:v)	55.5075 mM	[1.14555;1.14559]	1.0 g
0.75%(w:v)	83.2613 mM	[1.71832;1.71838]	1.5 g
1.00%(w:v)	111.0150 mM	[2.29109;2.29118]	2.0 g
1.25%(w:v)	138.7688 mM	[2.86387;2.86397]	2.5 g
1.50%(w:v)	166.5225 mM	[3.43664;3.43677]	3.0 g
1.75%(w:v)	194.2763 mM	[4.00941;4.00956]	3.5 g
2.00%(w:v)	222.0300 mM	[4.58219;4.58236]	4.0 g
2.25%(w:v)	249.7838 mM	[5.15496;5.15515]	4.5 g
2.50%(w:v)	277.5376 mM	[5.72773;5.72794]	5.0 g

The nomenclature (Figure C.1) for non-modified ChipM finally consists to describe each matrix by three parameters which are the concentration in chitosan, the concentration in acid and the cooling rate used to produce it. As exposed above, the dissolution of the chitosan depends on the concentration in acid. This explains the "stairs" shape of the nomenclature. In this nomenclature, the concentration of lactic acid used to dissolve the polymer is described by the green scale.

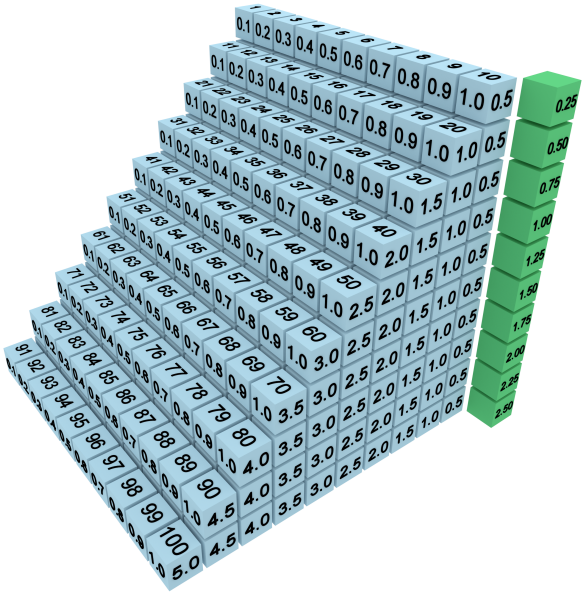

Figure C.1: Nomenclature for the non-modified ChipM

The blue part represents the chitosan concentration (from 0.5 to 5.0 g per 100 ml of acid solution) and the cooling rate imposed by the POMAP (from 0.1 to 1.0 °C·min^{-1}). Finally the intersection of a blue column with a green level allows a perfect description of the ChipM. The matrix is finally characterized by the number of the column and the number of the level.

A matrix is written $\binom{W}{acid}|X)\cdot$ChipM, with W the level on green scale, X the column and the name of the acid.

C.2 Modified ChipM

The nomenclature suggested allows a precise description of a matrix after its modification. As presented in Chapter 4, these modifications can consist out of several designs.

C.2.1 Conventions of writing

C.2.1.1 Major rules

- Primary coupling: The agents Y covalently bound in a permanent way are written to the right. In case of several primary couplings on the same ChipM they are separated by a vertical bar and the order is not considered ;

Example: $\binom{W}{acid}|X)\cdot$ChipM·Y or $\binom{W}{acid}|X)\cdot$ChipM·$Y_1|Y_2$

- Secondary coupling: The agents Z covalently bound in a non permanent way are written to the right between parentheses (Z). In case of several secondary couplings on the same ChipM they are separated by a vertical bar and the order is not considered ;

Example: $\binom{W}{acid}|X)\cdot$ChipM$\cdot$(Z) or $\binom{W}{acid}|X)\cdot$ChipM$\cdot$(Z$_1$|Z$_2$)

- Diffusion media: Considering the possibility to use a dM loaded with actives, for passive release, the loading is written to the right between braces {lo}. In case of multi-loading on the same dM, they are separated by a vertical bar and the order is not considered ;

Example: $\binom{W}{acid}|X)\cdot$ChipM$\cdot${lo} or $\binom{W}{acid}|X)\cdot$ChipM$\cdot${lo$_1$|lo$_2$}

- Doped matrix: The ChipM structure can also be doped during its production by incorporating an agent in the initial chitosan solution. This doping agent can be used to modify the physicochemical characteristics of the ChipM but it can also be released. In that case the doped ChipM acts as a passive delivery system. The doping agent is written to the left between parenthesis (do). In case of multi-doping on the same ChipM, they are separated by a vertical bar and the order is not considered ;

Example: (do)$\cdot\binom{W}{acid}|X)\cdot$ChipM or (do$_1$|do$_2$)$\cdot\binom{W}{acid}|X)\cdot$ChipM

C.2.1.2 Minor rules

- If the agent is an active molecule, this is specified by the addition of the letter A as subscript ;

Example: $\binom{W}{acid}|X)\cdot$ChipM$\cdot$(Z$_A$), $\binom{W}{acid}|X)\cdot$ChipM$\cdot${lo$_A$}

and (do$_A$)$\cdot\binom{W}{acid}|X)\cdot$ChipM

- If the agent is a particle, this is specified by the addition of the letter P as subscript ;

Example: $\binom{W}{acid}|X)\cdot$ChipM$\cdot$(Z$_P$), $\binom{W}{acid}|X)\cdot$ChipM$\cdot${lo$_P$}

and (do$_P$)$\cdot\binom{W}{acid}|X)\cdot$ChipM

- If the agent is a permeation enhancer, this is specified by the addition of the letter E as subscript ;

Example: $\binom{W}{acid}|X)\cdot$ChipM$\cdot$(Z$_E$), $\binom{W}{acid}|X)\cdot$ChipM$\cdot${lo$_E$}

and (do$_E$)$\cdot\binom{W}{acid}|X)\cdot$ChipM

- If the agent does not have any particular role, it is only described by the major rules.

C.2.2 Rules of priority

- A primary coupling has priority on a secondary coupling ;

Example: $\binom{W}{acid}|X)\cdot$ChipM$\cdot$Y$\cdot$(Z), $\binom{W}{acid}|X)\cdot$ChipM$\cdot$Y$_1|$Y$_2\cdot$(Z)

$\binom{W}{acid}|X)\cdot$ChipM$\cdot$Y$\cdot$(Z$_1|$Z$_2$)

and $\binom{W}{acid}|X)\cdot$ChipM$\cdot$Y$_1|$Y$_2\cdot$(Z$_1|$Z$_2$)

- A secondary coupling has priority on a loaded dM ;

Example: $\binom{W}{acid}|X)\cdot$ChipM$\cdot$(Z)$\cdot\{$lo$\}$,

$\binom{W}{acid}|X)\cdot$ChipM$\cdot$(Z$_1|$Z$_2$)$\cdot\{$lo$\}$, $\binom{W}{acid}|X)\cdot$ChipM$\cdot$(Z)$\cdot\{$lo$_1|$lo$_2\}$

and $\binom{W}{acid}|X)\cdot$ChipM$\cdot$Y$\cdot$(Z)$\cdot\{$lo$\}$

C.3 Examples

Several examples, used in this project or not are presented below.

C.3.1 Primary coupling

C.3.1.1 Acetylation as primary coupling

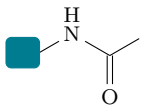

Figure C.2: Primary coupling example with acetylation

$\binom{W}{acid}|X)\cdot$ChipM$\cdot$OAc

C.3.1.2 PL1 as primary coupling

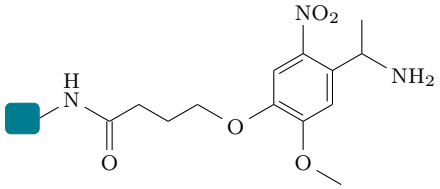

Figure C.3: Primary coupling example with PL1

$\binom{W}{acid}|X)\cdot$ChipM$\cdot$PL1

C.3.1.3 PL2 as primary coupling

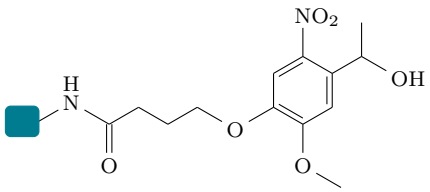

Figure C.4: Primary coupling example with PL2

$$\binom{W}{acid}|X)\cdot\text{ChipM}\cdot\text{PL2}$$

C.3.2 Secondary coupling

C.3.2.1 Amide bound on PL1

This coupling is obtained by an amide bound formation on PL1 using a carboxylic acid. The released molecule is an amide.

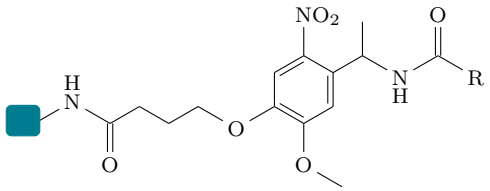

Figure C.5: Secondary coupling example on PL1

$$\binom{W}{acid}|X)\cdot\text{ChipM}\cdot\text{PL1}\cdot(\text{RCOOH})$$

- Amide bound with PLGA nanoparticles: The use of drug loaded PLGA nanoparticles (PLGA_P), allows the release of molecules without functional group but also to reach a higher drug loading. In that case the reaction has to be conducted in water to avoid PLGA dissolution. The amide PLGA is released.

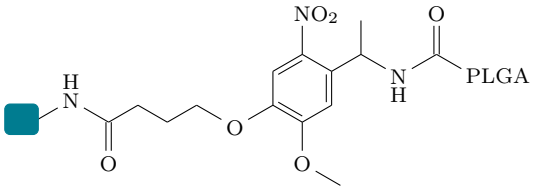

Figure C.6: Secondary coupling example on PL1 with a PLGA nanoparticle

$$\binom{W}{acid}|X)\cdot\text{ChipM}\cdot\text{PL1}\cdot(\text{PLGA}_P)$$

- Amide bound with amino acid and nanoparticles: To avoid the release of lactic amide or glycolic amide by direct coupling on PL1, a possibility is to introduce an amino-acid between the photolinker and the nanoparticle. Since the toxicity of several amino amide is known to be almost inexistent, this allows the release of a drug without any disadvantages induced by the presence of amides.

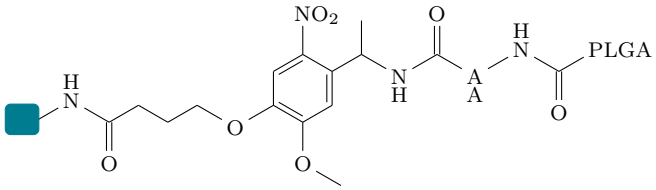

Figure C.7: Secondary coupling example on PL1 with a PLGA nanoparticle and an amino acid

$$\binom{W}{acid}|X)\cdot\mathrm{ChipM}\cdot\mathrm{PL1}\cdot(\mathrm{AA}|\mathrm{PLGA}_P)$$

C.3.2.2 Ester bound on PL2

Contrary to PL1, the photolinker PL2 makes the release of carboxylic acids possible.

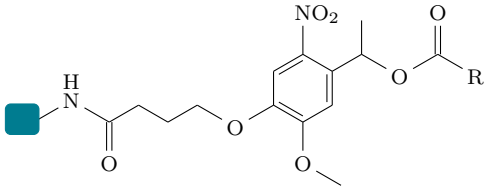

Figure C.8: Secondary coupling example on PL2

$$\binom{W}{acid}|X)\cdot\mathrm{ChipM}\cdot\mathrm{PL2}\cdot(\mathrm{RCOOH})$$

- Ester bound with amino acid and nanoparticles: As for PL1, the introduction of PLGA nanoparticles is possible, in that case without release of amides.

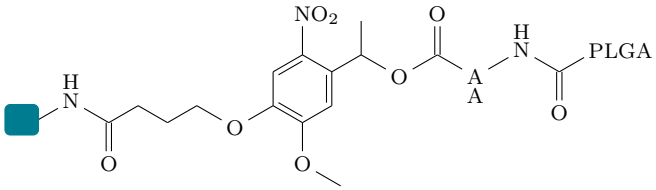

Figure C.9: Secondary coupling example on PL2 with a PLGA nanoparticle and an amino acid

$$\binom{W}{acid}|X)\cdot\mathrm{ChipM}\cdot\mathrm{PL2}\cdot(\mathrm{AA}|\mathrm{PLGA}_P)$$

C.3.2.3 Carbonate bound on PL2

The introduction of *p*-NPCF, which is a good leaving group, is a good way to obtain carbonates and carbamate bounds on PL2.

- Carbonate on PL2: Upon UV illumination, the carbonate PL2 releases an alcohol and CO_2.

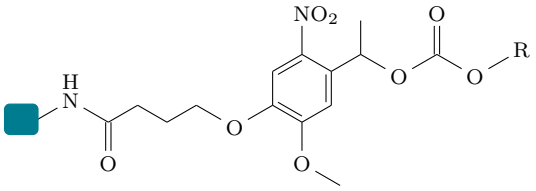

Figure C.10: Secondary coupling example on PL2 with an alcohol

$$\left({}^{W}_{acid}|X\right)\text{-ChipM-PL2-(ROH)}$$

- Carbamate on PL2: Upon UV illumination, the carbamate PL2 releases an amine and CO_2.

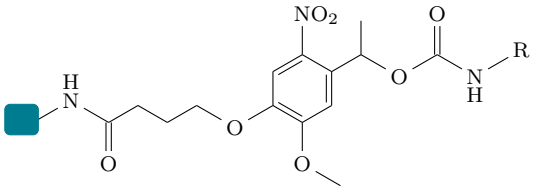

Figure C.11: Secondary coupling example on PL2 with an amine

$$\left({}^{W}_{acid}|X\right)\text{-ChipM-PL2-}(RNH_2)$$

Curriculum Vitæ

Jean-Baptiste Sauvet
13.01.1985
In Evry, France
Nationality: French

5, croisée des Lys
68 300 Saint Louis (FR)
jb.sauvet@gmail.com
+33 (0)677 999 862

EDUCATION

2009/2013 **Ph.D. Thesis in Physical Chemistry**
University of Basel/Department of chemistry - Basel - CH

2005/2009 **French Grande Ecole in Chemistry and Chemical Engineering (M.S.)**
ESCOM - Cergy Pontoise - FR

2003/2005 **Preparatory Classes for Grandes Ecoles (Physics and Chemistry)**
Lycée François 1er - Fontainebleau - FR

WORK EXPERIENCE

2009/2013 **Ph.D. student**
Design, development, and in vitro evaluation of an intelligent transdermal therapeutic system.
FHNW/University of Basel - Basel - CH

2008 **Research engineer**
*Temporal following by quantitative NMR of extraction and transformation of pigment compounds from saffron (*Crocus Sativus L.*) in aqueous solution under temperature gradient.*
INRA/AgroParisTech - Laboratory of molecular gastronomy - Paris - FR

2007 **Research engineer**
Synthesis and biological evaluation of cytotoxic agents and tumors selective bioreductive prodrugs.
Institute of Cancer Therapeutics - Bradford - UK

2006 **Research technician**
Thermodynamic study by GC/Rolsi of the methanol (inhibitor of gases hydrates formation) distribution in distillation units of natural gas.
École des Mines de Paris - Fontainebleau - FR

SELECTED SKILLS AND TECHNIQUES

Chemistry	Organic and inorganic synthesis
	Solid phase synthesis
	Purification
	Characterization
Analysis	Analysis methods: NMR, UV, IR, GC, HPLC, MS, Raman
	Electron microscopy: SE2, Inlens and EDX detectors
	BET measurement
	Nanomaterials characterization
Computer skills	LaTeX/OpenOffice/Microsoft Office, GIMP, ChemDraw, Blender
	Mathematical modeling and calculation: Igor Pro, Maple, COMSOL, R
	Computer languages: Python and script shell
	Operating systems: Linux, Windows
Language	French: Native language
	English: Fluent
	German: Notions

SCIENTIFIC PUBLICATIONS AND PRESENTATIONS

Publications in progress:

- Kinetic analysis using multivariate regression: Application to surface color changes.

- Mathematical model of the thermodynamic behavior of a polymer solution during the freezing: Application to the production of scaffolds.

- Mathematical model of molecular diffusion through a complex system.

- Porous polymeric scaffolds production via thermally induced phase separation.

Patents:

- Faupel, M. D., Bischoff, S., George, F. & Stark, P. Transdermal device for the controlled administration of at least one active ingredient to a patient. WO2013114011A1 (2013).

- Faupel, M. D., Sauvet, J. -B., D., Bischoff, S., George, F. & Stark, P. New process for production of porous material using a dedicated device. (In progress)

Conference talk:

- “Médecine personnalisée: Nanomatériaux et photoniques dans un nouveau système thérapeutique”

French-German Research Institute of Saint-Louis (ISL) - Saint Louis FR (2009)

Authors: Michel Faupel , Renaud Greget and Jean Baptiste Sauvet

- “Applications of Artificial Intelligence on Silicon and Data Processing Algorithms”

French-German Research Institute of Saint-Louis (ISL) - Saint Louis FR (2013)

Authors: Michel Faupel , Renaud Greget and Jean Baptiste Sauvet

Awards:

- EUREKA SUCCESS STORY Eurostars 4349 ALTHERAS

“The memory patch that could revolutionize Alzheimer treatment”

- Winner at the French “Worldwide Innovation Challenge” (2014)

Category “personnalized medecine”

Acknowledgements

The workload which a thesis implies is an “Aesop’s tongue” experience. It offers on the same time a wonderful and exiting opportunity to create, play and discover but on the same time it is a tortuous way that would have been difficult to follow alone. For these reasons, I would like to extend my thanks to people who contribute to this study.

I first would like to thank Prof. Dr. Uwe Pieles, from the FHNW. I’m grateful to him to have trusted me and, throughout my entire Ph.D., for the freedom he let me to work on my rhythm.

This work was directed by Prof. Dr. Wolfgang Meier at the university of Basel. I thank him for the support and for his patience.

Special thanks to Dr. Serge Bischoff, Dr. Michel Faupel, Peter Stark, Dr. Florence Keller, Dr. Florian George, Dr. Renaud Greget, Pierre Borsotto and more generally to the Rhenovia’s and PIAG’s teams. The task would have been impossible without their confidence and their help. Michel, thank you for having allowed me to lead this project.

I would like to thank Dr. Joachim Koeser to have made me discover the chitosan. Thanks also for our scientific discussions (among others). The complete edition will soon be published in 24 volumes, paperback version, on original “chiffon de lin vergé” paper.

Thanks to Dr. Fabiola Porta, for her patience and diplomacy during the correction of this manuscript and for discussions to liberate the humanity from the Cargo cult science. This day will come.

I also would like to thank my colleagues from the FHNW and from the BZM. In particular, thanks to Olivera Scheuber, Prof. Dr. Georgios Imanidis, Käthy Wenger, Roger Lièvre and Georg Hasler.

Finally, my warmest thanks to Alvarium, the “Snoopy’s house”, aGkuraka, Laurie, Marlène, Béranger, Hélène, Maxime, who all supported me, in spite of my recurring bad mood.